

Fabrication of lipid bilayer giga-ohm seals on silicon-based microelectrodes

Md. Mashiur Rahman

Doctor of Philosophy

Department of Structural Molecular Science
School of Mathematical and Physical Science
The graduate University of Advanced Studies

2005

Abstract

Ion channels play key roles in functions and dysfunctions of all cells. Single channel recording methods using planar (black) lipid membranes (BLM) and patch clamp techniques are widely used at present, but they are not suited for automation and miniaturization. Therefore, in order to develop electrophysiology library arrays, several groups have recently reported on wafer-based devices that can replace the more traditional glass pipettes and Teflon partitions that are employed for investigating ion channels activities in cells and artificial membrane. The supported planar lipid bilayer (SPLB) is a lipid bilayer supported on solid surfaces. Concerning the ion-channel biosensors, single ion channel recording has been succeeded in suspended membranes made by the painting method on micro-machined supports. In the case of the suspended membrane, it is not easy to make a single bilayer with a small pore diameter (several μm), which is necessary for high speed recording and low noises. In the SPLBs made by vesicle fusion however, single channel recording have not yet been reported. The SPLB on the silicon based microelectrode are extremely attractive since small pore can be easily made, thus it has a potential of high stability, high sensitivity and high density of integration. It is considered that a major challenge in the production of tightly sealed bilayers to reduce leakage currents to the levels found in the suspended membrane, and most likely, this will require the reduction of the substrate surface roughness and the elimination of edge effects. The efforts to get high resistivity in the tethered supported membrane on Au surface have been done by several groups. Recently, the tethered lipid bilayers with a high electrical resistance of $\sim 130\text{ M}\Omega$ and the subsequent detection of only a few synthetic ligand-gated ion channels incorporated in the tethered lipid bilayer, have been reported. [S. Terrettaz et al. *Langmuir* 19 (2003) 5567] In spite of these efforts, it is clear that a much higher resistivity ($\text{G}\Omega$ seal) is required to realize a supported membrane biosensor which can be applied to the single ion channel recording.

In the present thesis, based on these backgrounds, I have developed several elementary processes to realize an ideal SPLB with $\text{G}\Omega$ resistance on Si-based microelectrodes. I have developed the techniques to fabricate a hole (well) with a diameter of about $1\ \mu\text{m}$ for microelectrodes on a $\text{SiO}_2/\text{CoSi}_2/\text{Si}$ substrate, while maintaining the SiO_2 surface roughness at less than $1\ \text{nm}$ using a femtosecond laser microfabrication technique and synchrotron radiation etching. The SPLB membrane

was formed on the surface of a microelectrode area by the fusion of giant unilamellar vesicles. I have characterized the stability, electrical resistance, capacitance, and current noise of the bilayers.

After the deposition of Co on the Si(100) surface, the SiO₂ thin film consists of spin on glass (SOG) (400 nm thickness) and sputtered SiO₂ (200 nm thickness) was formed on the Co/Si. Then by annealing at 540°C for 10min, the Co/Si layer was changed to CoSi₂ keeping the SiO₂ surface roughness less than 1 nm. A 300 nm of Co layer was deposited on the SiO₂ surface by sputtering as an etching contact mask and circular patterns were made on the Co mask using the femto-second laser ablation. The SR etching of the SiO₂ layer to make the wells on the electrode was carried out at the beam line 4A2 of the SR facility (UVSOR) at the Institute for Molecular Science, using a mixture of SF₆ (0.05 Torr) and O₂ (0.002 Torr) as an etching gas. The SR etching results in a vertical wall and completely stops at the surface of the CoSi₂/Si(100). SR was used because of its unique features such as high spatial resolution, extremely high material selectivity between CoSi₂ and SiO₂, anisotropic etching, low damage, and clean etching atmosphere. Finally the Co contact mask was removed without damaging the substrate by immersion into 0.1 M HNO₃ aq. AFM images of the SiO₂ surface after the removal of the Co mask showed that the surface was very flat ($R_a=0.8$ nm), which is essential for the formation of the defect-free SPLB on the surface.

Ag (50 nm) was deposited by electroplating on the surface of CoSi₂ which was exposed at the bottom of the etched well. Then the surface of the Ag was changed into AgCl also by electroplating. The giant unilamellar vesicles were prepared by adding a buffer solution (10 mM KCl, pH = 6.6) to vacuum-dried films of dipalmitoylphosphatidylcholine (DPPC) and 1-palmitoyl-2-oleoyl-sn-3-phosphor-L-Serin (POPS) (9:1, w/w) and agitating at RT. Mixing of negatively charged lipid POPS to neutral lipid DPPC was essentially effective to form unilamellar giant vesicles without aggregation. Formation of SPLB covering the well-type electrode by the rapture of the giant vesicle was confirmed by fluorescence microscope. When substrates are immersed in an aqueous solution of lipid vesicles, the vesicles adhere to the surface, rupture, and spread to form a bilayer on hydrophilic surfaces of SiO₂. It has been suggested that a thin water layer approximately 1-2 nm is trapped between the support and the headgroups of the lower leaflet of the bilayer. [Bayerl, T. M.; Bloom, M. Biophysical Journal, 58 (1990) 357]

Fluorescence microscopy images showed that the diameter of the SPLB formed on the SiO₂/Si(100) surface by the rapture of the giant vesicles was typically about 150 ~ 300 μm, large enough to cover the electrode area (10 μm ~ 30 μm diameter). AFM images of the bilayer showed that the thickness of the SPLB membrane was 4.5 nm, corresponding to the height of a single bilayer. The electric characteristics were measured by a patch clamp amplifier through the AgCl/Ag electrode. The resistances before and after the lipid bilayer formation were 10±3 MΩ and 1.2 GΩ, respectively. This confirmed the GΩ seal formation of SPLB on the microelectrodes. The capacitance of the bilayer measured by using a patch clamp amplifier was 10.7 pF. These values were observed with extremely good reproducibility during our experiments for more than 5 hours.

Although the resistance value fulfills the condition required for the measurement of single channel measurements, even then it is much smaller than those (> 30 GΩ) realized in the planer or suspended membranes. This may be due to the edge leak current. Therefore, by depressing the edge leak current, much higher resistance of lipid bilayer is expected to be obtained.

I have considered to use the hydrophobic self-assembled monolayers (SAM) as a “guard ring” to reduce the edge leak current of SPLB. I have developed a patterning method of octadecyltrichlorosilane (OTS) SAM by photo-lithography and UV ashing. OTS-SAM were formed on the sputtered SiO₂ surface by immersing the sample into a 1.0 mM solution of OTS in toluene for 10 s at 22°C. Then negative resist (7μm height) pattern was made with lithography technique. After 30 min of UV ashing, resist pattern was removed with remover. The OTS-SAM on the open area, which was not covered with the resist, were completely removed by UV ashing, while no change was observed in the OTS-SAM on the area covered with the resist. The height of the OTS-SAM was ~2.5 nm and the roughness of the SiO₂ surface without OTS-SAM was R_a=0.8 nm. SPLB was formed on this patterned OTS-SAM by rapture of giant unilamellar vesicles. AFM and fluorescence microscopy images have shown that SPLB forms bilayer on hydrophilic SiO₂ surfaces and a monolayer on OTS-SAM hydrophobic surfaces. This technique has been considered to use for the formation of tightly sealed bilayers to reduce leakage current of the SPLB.

Outline

1	Introduction	3
1.1	Background of supported membrane biosensor	3
1.2	Electrical properties of lipid bilayer	4
1.2.1	Planer membrane	6
1.2.2	Suspended membrane	7
1.2.3	Supported membrane	8
1.3	Purpose of the present study	10
1.4	Outline of this thesis	10
	Reference	12
2	Experimental.....	14
2.1	Fabrication of SiO ₂ layer	14
2.1.1	Thermally oxidation	15
2.1.2	Sputtering deposition.....	16
2.1.3	Spin-on-Glass	20
2.2	Patterning technique	24
2.2.1	Lithography	24
2.2.2	Femtosecond laser patterning.....	29
2.3	Synchrotron Radiation etching	33
2.4	Ag and AgCl electrode formation	38
2.5	Lipid bilayer formation by giant vesicle fusion	43
	Reference	50
3	Shrinking of Spin-on-Glass Films Induced by Synchrotron Radiation and Its Application to Three-Dimensional Microfabrications	53
	Abstract.....	53
3.1	Introduction	54
3.2	Experimental.....	55
3.3	Results and Discussion	57
3.3.1	SR-induced etching and shrinkage of SOG.....	57
3.3.2	Change in IR absorption spectrum induced by SR.....	62
3.4	Conclusion.....	64

Reference	65
4 Giant Vesicle Fusion on Microelectrodes Fabricated by Femtosecond Laser	
Ablation Followed by Synchrotron Radiation Etching	66
Abstract.....	66
4.1 Introduction	67
4.2 Experiment	68
4.3 Results and Discussion	71
Reference.....	77
5 Formation of supported planer lipid bilayer by vesicle fusion on patterned	
octadecyltrichlorosilane self-assembled monolayer for reducing the edge leak current	78
Abstract.....	78
5.1 Introduction	79
5.2 Experiment	82
5.2.1 Deposition and patterning of OTS-SAM.....	82
5.2.2 Preparation of giant vesicles and formation of SPLB	84
5.3 Results and discussion	86
5.3.1 Patterning of OTS-SAM.....	86
5.3.2 Formation of lipid bilayers on patterned OTS/SiO ₂ surface	90
5.4 Conclusion.....	92
Reference.....	93
6 Summery.....	94
7 List of publications	97

Chapter 1

1 Introduction

1.1 Background of supported membrane biosensor

A biosensor is a device which allows a direct transduction of the concentration of (bio) chemical species into an electrical signal. Biosensor technology has potential applications in various fields such as pharmacology, biochemistry, protein chemistry, electronics, and physics, e.g., it may be used for diagnosis of diseases, monitoring of clinic or environmental samples and testing of pharmaceutical or food products. To date, however, the most successful commercial application of biosensors have been enzyme-based biosensors, particularly on disposable electrodes. Recently, a new type of biosensor known as ion-channel biosensor has attracted much interest.

Ion channels play key roles in functions and dysfunctions of all cells; they are gates in the cell membrane that generate electrical signals. Numerous biochemical receptors give rise to an electrical current through the cell membrane by direct or indirect interaction with ion channels. Monitoring the current of single ionotropic receptors with automated biosensor devices may result in new classes of highly sensitive screening tools. However, measurements using ion channel gating still require a rather sophisticated and delicate laboratory setup. To turn ion channel sensors into a tool more easy and practical to use, while providing reliable and reproducible performance, the problem of suspending the host lipid bilayer membrane on a suitable substrate must be addressed. Functional studies of single ion channel proteins require the reduction of electrical background noise to 10^{-13} – 10^{-12} A and consequently a high electrical insulation of the surrounding membrane patch ($R > 10^9 \Omega$, “Giga-ohm seal”).

1.2 Electrical properties of lipid bilayer

Today, lipid bilayer related work is a matured field of research as a result of applications of many elegant techniques including spectroscopy, membrane bioelectrochemistry, patch-clamp, acoustics, and membrane reconstitution. Most of these works are closely related to the electrical properties of the bilayer. An unmodified bilayer displays a high D.C. resistance and low permeability for ions. The electrical properties of the bilayer are usually measured under direct current. A small voltage is induced across the bilayer separating two aqueous solutions via a pair of reversible electrodes. Figure 1.1 shows a schematic drawing of a sampling unit to apply the technique developed by Montal & Müller, a very basic electrical equivalent of the same system is a circuit of a parallel capacitor and a resistor (Fig. 1.1).[1] The resistor (R_m) reflects the pure electrical conductance of the bilayer. The conductance of the pure lipid membrane is very low, but not negligible in experiments with current in pA order. In a circuit more realistically equivalent to the simple bilayer system itself, at least the resistors made up by the electrodes and aqueous phases must be added.

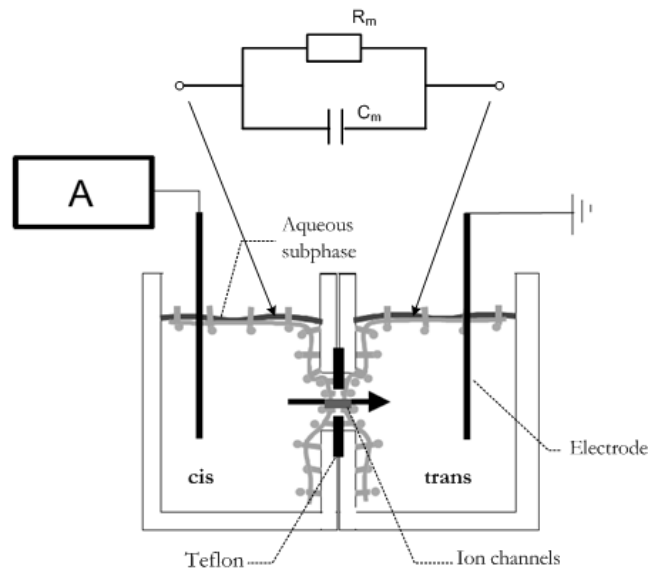


Figure 1.1: Schematic drawing of planer lipid bilayer and the most simple electrical equivalent circuit of such a bilayer, consisting of a resistor (R_m) and a capacitor (C_m) in parallel. The lipids are put onto an aqueous subphase in both sides of the chamber and raised to cover a small aperture in a Teflon film. Inserted ion channels allow the ion flux (arrow) which can be registered with the electrodes. The left electrode is connected to the amplifier (A). This side is called *cis* side and the other chamber is grounded and called *trans* side.

1.2.1 Planer membrane

Figure 1.1 shows the representative arrangement of the measurement system of the planer membrane. The work with planer membranes began with Rudin and his group in 1959-1963.[2] They first investigated lipid monolayers and multilayers of the Langmuir-Blodgett (LB) type. Planer membrane provided the opportunity to study the relation between the structure and function of biomembranes such as transport phenomena via reconstituting membrane proteins into the lipid bilayer. Since then investigations on the potential use of ion channels in biosensor devices have been carried out. The first example of a single-molecule was conducted over 35 years ago: the observation of current flow through a single ion-conducting channel formed by the peptide antibiotic gramicidin in a planar lipid bilayer.[3]

Such planer membranes are also known as Black or Bilayer Lipid Membrane (BLM).[4] These membranes need a frame with apertures or pores for both their stabilization and manufacturing. Teflon is a well-suited polymer for this application because it is chemically stable, it has good electrical properties (high resistivity, low dielectric constant, and low dielectric loss[5]), and it supports planer membranes that are stable for several hours.[6] There are several methods to make pores such as mechanical punching, drilling, or indentation, combined with shaving away material from the opposite side of the sheet until the indentation is intersected.[7] Pores are also prepared using a high voltage pulse to burn holes through thin polymer sheets.[6] In general it is difficult to generate pores with diameters below tens μm with these methods,[7] and difficult to create a single bilayer over a small pore of a diameter of several μm which is necessary for high speed recording and low noises.

1.2.2 Suspended membrane

Recently a new type of planer membrane on small apertures ($\sim\mu\text{m}$) was developed which is known as suspended membrane [Fig. 1.2(a)]. Eray *et al* demonstrated that such suspended membranes can be formed on $40\ \mu\text{m}$ diameter microfabricated polyimide apertures and that the activity of alamethicin and acetylcholine receptor could be tested.[8] Yaling Cheng *et al.* introduced a micromachined support for suspended membrane, consisting of a $128\ \mu\text{m}$ diameter aperture on gold/SU8 surface suspended over a small aqueous reservoir. Single-channel activities of gramicidin and alamethicin were observed in these systems. Firtig *et al.* have utilized ion-milled glass substrate for measuring macroscopic ion channel activities in whole-cell mode.[9]

In order to develop electrophysiology library arrays, several groups have recently reported on wafer-based devices[10-14] that can replace the more traditional glass pipettes and Teflon partitions that are employed for investigating ion channels activities in cells and artificial membrane. Penttoja *et al.* [15] reported on utilizing silicon devices for investigatin the activity of single channel proteins supported in suspended bilayers. Wilk *et al.*[16] formed $8.5\ \sim 16.7\ \text{G}\Omega$ of suspended membrane on $150\ \mu\text{m}$ diameter apertures of silicon fabricated Teflon coated aperture and measured OmpF porin ion channel proteins. Mayer *et al.* fabricated $\leq 40\ \mu\text{m}$ in films of amorphous Teflon and recorded single ion channel of alamethicin which was stable for 4 h.[12] In these works suspended membranes created made by employing a painting method or Langmuir-Blodgett deposition of lipid films. These membranes were however not stable over a long period of time (several hours). Supported membranes have potential of higher stability and controllability than suspended membrane.

1.2.3 Supported membrane

The supported planer lipid bilayer (SPLB) is a lipid bilayer supported on solid surfaces [Fig. 1.2(b)]. The preparation of protein-incorporating SPLB by vesicle fusion on solid supports was pioneered by the group of McConnell for studying cell-cell interaction processes.[17] Since the SPLBs have the advantage of long-term and high mechanical stability compared with suspended membranes,[18] they have been used not only in the *in vitro* basic researches of cell membrane relating phenomena such as cell-cell recognition in the immune system,[19-25] but also in the applied researches of biosensors and biochips.[10, 11, 26-33] Promising applications potentials of the later lie in the diagnosis of diseases as well as the use in drug screening assays. Creating SPLB on silicon based microelectrodes is extremely attractive since small pores can be easily made, thus this approach has a potential of high stability, high sensitivity and high density of integration. Single channel recording has however not yet been reported in the SPLB made by vesicle fusions because of several difficulties. These are described in the following section.

Table 1.1: Comparison between planer, suspended and supported membrane

Membrane type	Scale	Leak current	Controllability	Stability
Planer membrane	mm ~ several tens μm	no	Depend on nature	Less stable
Suspended membrane	$\sim 10 \mu\text{m}$	no	Depend on nature	Potential of high stability (if small pore is realized)
Supported membrane	$\mu\text{m} \sim \text{nm}$	Edge leak current	Potential of high controllability	Potential of high stability

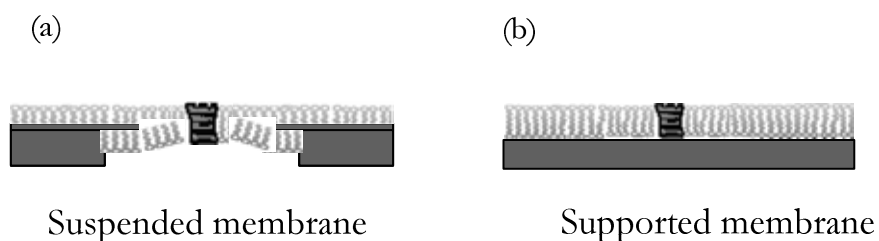


Figure 1.2: Schematic drawing of suspended (a) and supported (b) membrane. A suspended membrane is a single bilayer formed in a small hole, whereas a supported membrane is a single lipid bilayer supported on a solid surface.

There are two origins of current leakage; one is defects in the membrane; another is a circumferential leak from the edge of the SPLB. The common methods of SPLB assemble on surfaces are monolayer transfer by the LB technique and vesicle fusion method. LB films are a mechanically assembled arrays of amphiphilic molecules upon a water surface. Once the molecules are compressed to the desired organization, the film can then be transferred to a solid support. Although SPLBs formed by LB technique have some advantages such as the thickness and molecular arrangement are controllability at the molecular level, they usually contain pinholes.[34] Whereas, SPLBs formed by vesicle fusion method are suitable for defect free membranes.[35] The vesicle fusion method is a feasible and prevalent technique to form supported membranes on solid surfaces.[19] When substrates are immersed into an aqueous solution of lipid vesicles, the vesicles adhere to the surface, rupture, and subsequently spread to form a bilayer on hydrophilic surfaces and a monolayer on hydrophobic surfaces.[36]

It is considered that a major challenge in the fabrication of the ideal (sufficiently high resistance) supported membranes is the production of tightly sealed bilayers to reduce leakage currents to the levels found in suspended membranes. For this purpose, a reduction of the substrate surface roughness and the elimination of edge effects are required. The efforts to obtain a high resistivity in the tethered supported membrane on Au surface have been undertaken by several groups. [26, 37, 38] Recently, tethered lipid bilayers with a high electrical resistance of $\sim 130 \text{ M}\Omega$,

and the subsequent detection of multichannel current of a ligand-gated channel protein incorporated in the tethered lipid bilayer have been reported.[27]

It is clear that a much higher resistivity ($G\Omega$ seal) is required to realize a supported membrane biosensor which can be used for single ion channel recording. Otherwise the noise level would be too high.

1.3 Purpose of the present study

In the present thesis, based on these backgrounds, I have developed several elementary processes to realize an ideal SPLB with $G\Omega$ resistance on Si-based microelectrodes. While a large aperture size was used in many laboratories, it would be very interesting to reduce the size of the bilayer area, both to reduce noise and increase the mechanical stability.[39] I suppose that a nanometer-sized ion channel protein does not need a large bilayer area for insertion. Emphasis was put on the fabrication of a very flat substrate surface, which is a necessary prerequisite to form a defect free membrane. Since the surface of SiO_2/Si is very flat ($Ra < 0.2$ nm) and SiO_2 is an excellent insulator, it was chosen as substrate to create a defect free SPLB.

1.4 Outline of this thesis

I have developed a technique to fabricate the hole (well) with about $1 \mu m$ diameter for the microelectrode on the surface of SiO_2/Si substrate. The circular pattern was made on the Co thin film by using femtosecond laser ablation, and the hole was made by synchrotron radiation etching using this Co pattern as a contact-mask. This process enabled the fabrication of the electrode hole while maintaining the original nano-level flatness ($Ra \sim 0.8$ nm) of the Si substrate. A single planar lipid bilayer, deposited on these microelectrodes by the rupture of giant unilamellar vesicles, showed a high resistivity ($1.2 G\Omega$) necessary for the single channel recordings. Although the

resistance value fulfills the condition required for the measurement of single channel measurements, even then it is much smaller than those ($> 100 \text{ G}\Omega$) realized in the planer or suspended membranes. This may be due to the edge leak current. Therefore, by depressing the edge leak current, much higher resistance of lipid bilayer is expected to be obtained. I have considered using hydrophobic self-assembled monolayers (SAM) as the “guard ring” to reduce the edge leak current of SPLB.

In chapter 2, the techniques and instruments (SiO_2 deposition technique: Thermal oxidation, sputtering deposition, Spin-on-glass (SOG); patterning technique: photo-lithography, femtosecond laser patterning; synchrotron radiation etching; lipid bilayer formation by giant vesicle fusion) are described. In the SR etching of SOG, I have found that the indirect exposure to SR caused shrinkage of this layer under the Co mask. In chapter 3, the shrinkage phenomenon of SOG will be discussed. In chapter 4, formation of SPLB on the microelectrode, which is the core of this thesis, will be discussed. I have characterized the stability, electrical resistance, capacitance, and current noise of the SPLB. In chapter 5, an octadecyltrichlorosilane (OTS) SAM patterning technique by photo-lithography and ultraviolet light (UV) ashing will be discussed. Chapter 6, contains the summary of this thesis.

Reference

1. M. Montal and P. Mueller, Proceedings of the National Academy of Sciences of the United States of America, **69** (1972) 3561-3566.
2. R.D. Mueller P, Nature, **213** (1967 Feb 11) 603.
3. S.B. Hladky and D.A. Haydon, Nature, **225** (1970) 451-3.
4. H.T. Tien and A. Ottova-Leitmannova, *Planar lipid bilayers (BLMs) and their applications*. Membrane science and technology series ; 7. 2003, Amsterdam ; London: Elsevier. x, 1034.
5. B. Sakmann and E. Neher, *Single-channel recording*. 2nd ed ed. 1995, New York ; London: Plenum. xxii, 700 , [2] of col. plates.
6. W. Hanke and W.R. Schlue, *Planar lipid bilayers*. Biological techniques series. 1993, London: Academic Press. x, 133.
7. W.F. Wonderlin, A. Finkel, and R.J. French, Biophys J, **58** (1990) 289-297.
8. M. Eray, N.S. Dogan, L.J. Liu, A.R. Koch, D.F. Moffett, M. Silber, and B.J. Vanwie, Biosens Bioelectron, **9** (1994) 343-351.
9. N. Fertig, C. Meyer, R.H. Blick, C. Trautmann, and J.C. Behrends, Phys Rev E, **6404** (2001) art. no.-040901.
10. C. Schmidt, M. Mayer, and H. Vogel, Angew Chem Int Edit, **39** (2000) 3137-3140.
11. Y.L. Cheng, R.J. Bushby, S.D. Evans, P.F. Knowles, R.E. Miles, and S.D. Ogier, Langmuir, **17** (2001) 1240-1242.
12. M. Mayer, J.K. Kriebel, M.T. Tosteson, and G.M. Whitesides, Biophys J, **85** (2003) 2684-2695.
13. N. Fertig, M. Klau, M. George, R.H. Blick, and J.C. Behrends, Applied Physics Letters, **81** (2002) 4865-4867.
14. N. Fertig, A. Tilke, R.H. Blick, J.P. Kotthaus, J.C. Behrends, and G. ten Bruggencate, Applied Physics Letters, **77** (2000) 1218-1220.
15. R. Pantoja, D. Sigg, R. Blunck, F. Bezanilla, and J.R. Heath, Biophys J, **81** (2001) 2389-2394.
16. S.J. Wilk, M. Goryll, G.M. Laws, S.M. Goodnick, T.J. Thornton, M. Saraniti, J. Tang, and R.S. Eisenberg, Appl Phys Lett, **85** (2004) 3307-3309.
17. H.M. McConnell, L.K. Tamm, and R.M. Weis, Proceedings of the National Academy of Sciences of the United States of America-Physical Sciences, **81** (1984) 3249-3253.
18. Z.V. Leonenko, A. Carnini, and D.T. Cramb, Biochim Biophys Acta, **1509** (2000) 131-47.
19. H.M. McConnell, T.H. Watts, R.M. Weis, and A.A. Brian, Biochimica Et Biophysica Acta, **864** (1986) 95-106.
20. M. Stelzle and E. Sackmann, Biochimica Et Biophysica Acta, **981** (1989) 135-142.
21. A. Sonnleitner, G.J. Schutz, and T. Schmidt, Biophysical Journal, **77** (1999) 2638-2642.
22. E. Kalb, J. Engel, and L.K. Tamm, Biochemistry, **29** (1990) 1607-1613.
23. A. Schmidt, J. Spinke, T. Bayerl, E. Sackmann, and W. Knoll, Biophysical Journal, **63** (1992) 1385-1392.
24. J.J. Ramsden and P. Schneider, Biochemistry, **32** (1993) 523-529.
25. K.H. Pearce, R.G. Hiskey, and N.L. Thompson, Biochemistry, **31** (1992) 5983-5995.
26. S.M. Schiller, R. Naumann, K. Lovejoy, H. Kunz, and W. Knoll, Angewandte Chemie-International Edition, **42** (2003) 208-211.
27. S. Terrettaz, M. Mayer, and H. Vogel, Langmuir, **19** (2003) 5567-5569.
28. J.T. Groves, N. Ulman, and S.G. Boxer, Science, **275** (1997) 651-653.
29. B.A. Cornell, V.L.B. BraachMaksvytis, L.G. King, P.D.J. Osman, B. Raguse, L. Wiczorek, and R.J. Pace, Nature, **387** (1997) 580-583.
30. H. Bayley and P.S. Cremer, Nature, **413** (2001) 226-230.
31. Y. Fang, A.G. Frutos, and J. Lahiri, J. Am. Chem. Soc., **124** (2002) 2394-2395.
32. K. Morigaki, H. Schonherr, C.W. Frank, and W. Knoll, Langmuir, **19** (2003) 6994-7002.

33. A.T.A. Jenkins, R.J. Bushby, S.D. Evans, W. Knoll, A. Offenhausser, and S.D. Ogier, *Langmuir*, **18** (2002) 3176-3180.
34. T.D. Osborn and P. Yager, *Langmuir*, **11** (1995) 8-12.
35. G. Cevc and H. Richardsen, *Advanced Drug Delivery Reviews*, **38** (1999) 207-232.
36. R. Tero, M. Takizawa, Y.J. Li, M. Yamazaki, and T. Urisu, *Langmuir*, **20** (2004) 7526-7531.
37. U. Radier, J. Mack, N. Persike, G. Jung, and R. Tampe, *Biophysical Journal*, **79** (2000) 3144-3152.
38. A.T.A. Jenkins, R.J. Bushby, N. Boden, S.D. Evans, P.F. Knowles, Q.Y. Liu, R.E. Miles, and S.D. Ogier, *Langmuir*, **14** (1998) 4675-4678.
39. R.A. Levis and J.L. Rae, *Ion Channels, Pt B*, **293** (1998) 218-266.

Chapter 2

2 Experimental

2.1 Fabrication of SiO₂ layer

SiO₂ is an excellent insulator with excellent interface properties in connection with silicon substrates. It is thus the most common insulator in semiconductor device technology particularly in silicon MOS/CMOS where it is used as a gate oxide.[1, 2] SiO₂ films with characteristics of high quality of thickness controls, high flatness, low defect and high density films can be obtained by following techniques:

1. Thermally oxidation
2. Sputtering deposition
3. Physical vapor deposition (PVD)
4. Chemical vapor deposition (CVD)
5. Electro deposition
6. Physical deposition
 - Spin-on-glass
 - Sol-gel
 - Screen printing

Thermal oxidation, sputtering deposition, and spin-on-glass are adapted to form SiO₂ layer in my experiments. In this chapter, the details of these techniques are described.

2.1.1 Thermally oxidation

Thermally oxidized SiO₂ layer is grown by annealing a cleaned Si wafer into an oxygen rich atmosphere at high temperature (usually > 1000°C).[3] The thickness d of the growth layer with respect to growth time t is governed by the reaction rate at the surface and Fick's diffusion law: [2]

$$d = \frac{A}{2} \left(1 + \frac{t + \tau}{A^2 / 4B} \right)^{1/2} - \frac{A}{2}$$

A, B, and τ are constants dependent on temperature, partial oxygen pressure and the presence of water vapor. Water vapor increases the growth rate, at a cost of lower film density. However post-annealing in an inert atmosphere can improve the film properties close to those of a dry grown oxide. For short growth time $(t + \tau) \ll A^2 / 4B$ the reaction controlled term B/A dominates and the growth is linear. For longer growth times the thickness is limited by diffusion and so growth is parabolic and given by $d \approx \sqrt{Bt}$.

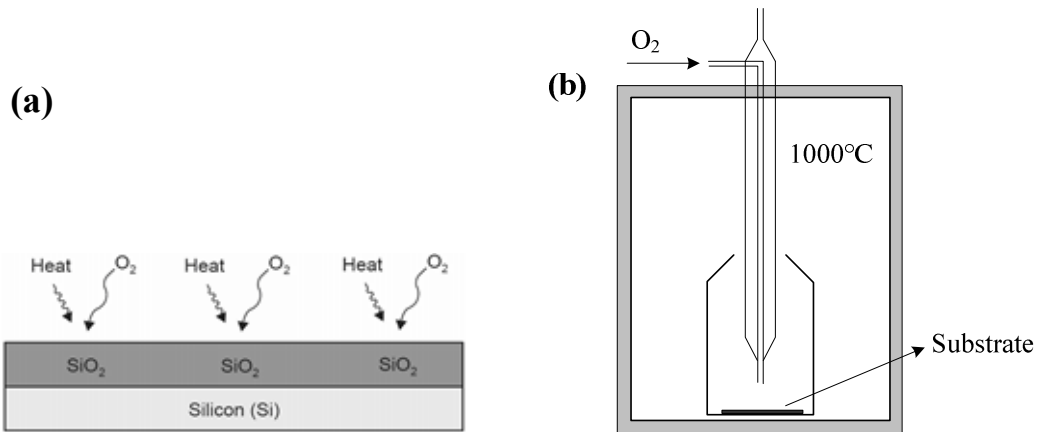


Figure 2.1.1: (a) Thermal silicon oxidation process. (b) Schematic drawing of the electric furnace system.

Growth rate of thermally oxidized SiO₂ and it's surface roughness

Oxidation of Si wafers was performed in an electric furnace KDF S-100 (Denken Co., Ltd.). The growth rate of thermally oxidized SiO₂ at 900°C and 1000°C was measured as a function of time under a oxygen gas flow of 1.0 liter min⁻¹ [Fig. 2.1.2(a)]. The average growth rate at 900°C and 1000°C were 11.2 nmh⁻¹ and 26.6 nmh⁻¹, respectively. The film thickness of SiO₂ increases with the annealing temperature. One of the most important qualities of thermal oxidized SiO₂ film is its low surface roughness. The AFM image shows that the thermal oxidized SiO₂ surface is very

flat [Fig. 2.1.2(b)]. At 900°C and 1000°C annealing temperature the value of surface roughness $R_a = 0.13$ nm and 0.11 nm, respectively.

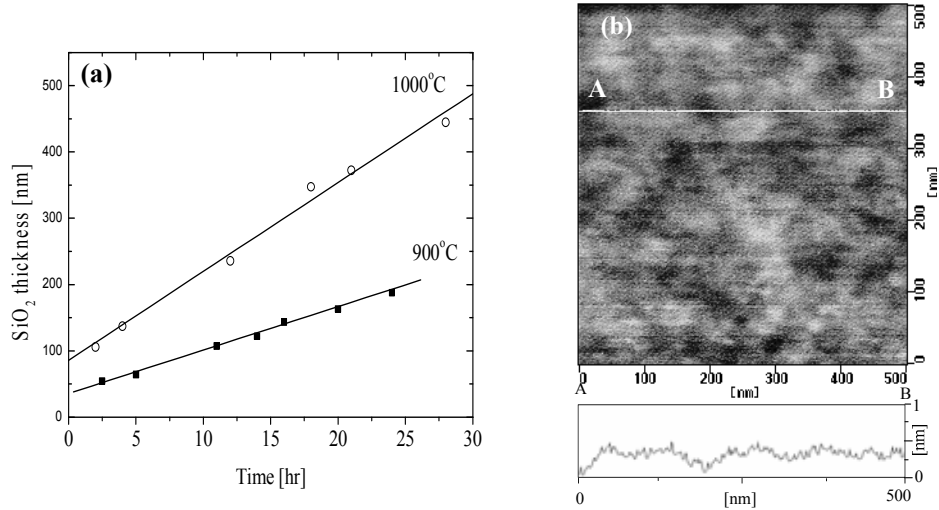


Figure 2.1.2: (a) Thermally oxidized SiO₂ film thickness as a function of oxidation time. Annealing temperature was 900°C and 1000°C. (b) AFM topography of SiO₂ (235nm) formed on the freshly cleaned Si surface by annealing at 1000°C for 12 h in a dry oxygen atmosphere. The cross sectional profile in line with A-B is given.

2.1.2 Sputtering deposition

Sputtering is a vacuum process used to deposit very thin films on substrates for a wide variety of commercial and scientific purposes.[3-5] The process of "sputtering" has come a long way since it was first used to silver the backs of mirrors in the late 19th century. This process offers the advantage of a homogeneous large area coating in the final production. It is performed by applying a high voltage across a low-pressure gas (usually argon at about 10⁻⁵ of Torr) to create a "plasma," which consists of electrons and gas ions in a high-energy state. This is sometimes called a "glow discharge" process because the plasma emits a colorful halo of light. The material to be sputtered is in the form of a thin plate called the target. The target is mounted in a chamber filled with argon gas at low pressure (typically 10⁻⁵ of Torr). When the target is connected to negative high voltage, a glowing plasma forms just above the target surface, much like the glow in a neon sign. Positive argon ions produced in the plasma by collisions of electrons with argon atoms are accelerated toward the negatively-charged target. When the fast-moving ions collide with the target, free atoms of target material are expelled. The object to be coated (called the substrate) is mounted

in front of the target, and some of the free atoms land on the substrate, building a thin film [Fig. 2.1.3(a)].

Modern sputtering machine uses magnetron sources, where an artfully arranged magnetic field strongly constricts the movement of the plasma electrons to tight cycloidal paths. This decreases electron leakages from the plasma, so that each electron produces many ions, making the rate of sputtering practical for production.

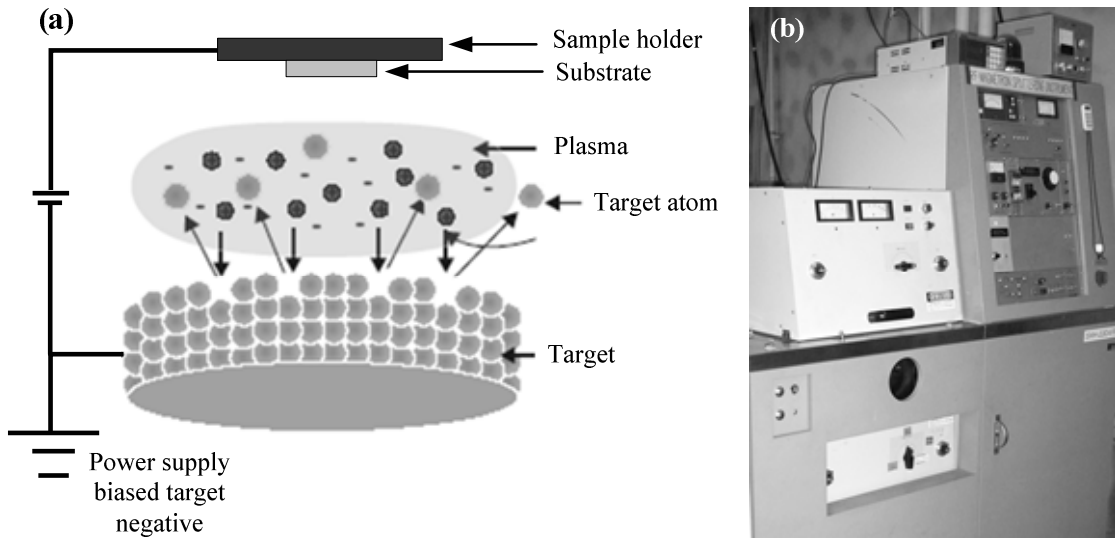


Figure 2.1.3: (a) Schematic drawing of sputtering process, and (b) Rf magnetron sputtering machine (SMH -2304 RE, Ulvac Co. Ltd.) used in the experiments.

Characteristics of sputtering

Advantages of the sputtering deposition are: precise thickness control, high density, composition reproducibility, and good step coverage. Many kinds of materials, including pure metals alloys and compounds, can be sputtered. Sputtering deposition is preferred over evaporation because sputtering will transfer the target material to the substrate in roughly the same composition. In the evaporation method, the deposition rate highly depends on the vapor pressure of elements, so the deposited film composition does not always match that of the evaporation source.

The disadvantages of the sputtering deposition are the higher equipment and materials costs, and the lower deposition rates. Moreover, the “lift-off process” becomes difficult in photolithography because of the greater packing density (high adhesion) of the sputtered materials.

Sputtering rate

The Sputtering rate is affected by target bias voltage, argon pressure, chamber temperature and chamber pressure. Higher target bias voltage releases more sputtered atoms. A Rf magnetron sputtering machine [Figure 2.1.3(b), SMH -2304 RE, Ulvac] has been used for the present experiments. For deposition of the SiO₂, Ag, Co, and Pt on Si wafers by sputtering we usually follow the conditions shown in Table 2.1.

Table 2.1: Experimental conditions of sputtering deposition

Target bias voltage	200 W
Chamber pressure	
Before argon insert	2×10^{-6} Torr
After argon insert	2×10^{-5} Torr
Argon supply	8.0 sccm (standard cubic centimeters per minute)
Chamber temperature	RT (Not controlled)

It is essential to evaluate the sputtering rate for a particular target of a sputter machine. Figure 2.1.4 shows the sputtering rate of Co, Ag, SiO₂ and Pt at the conditions shown in Table 2.1.

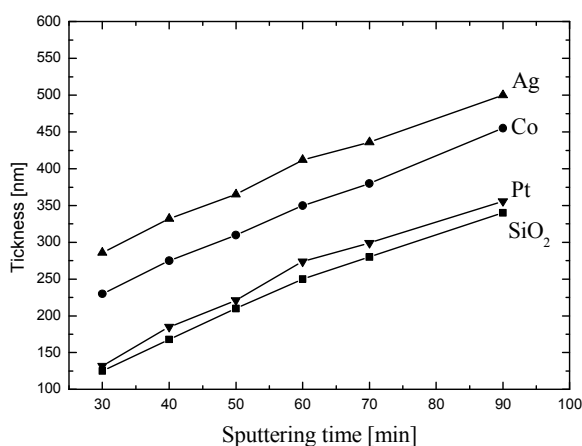


Figure 2.1.4: Sputtered film thickness as a function of sputtering time.

Surface roughness

Surface roughness is one of the key factors for fabrication of flat surface. In this thesis emphasis was put on fabricating of a very flat substrate surface (<1.0 nm), necessary to form a defect free supported planer lipid bilayer. One of the advantages of sputtering is that the sputtered surface is very flat. This could be confirmed with AFM observations using a SPI3800 scanning probe microscopy system (Seiko Instrument Inc.) in the dynamic-force mode (tapping mode). A Si cantilever was used. Figure 2.1.5 shows the AFM topographic images of SiO_2 , Ag, Co, and Pt deposited (100 nm each) on Si(100) by sputtering and the values of surface roughness R_a are 0.29, 0.81, 0.46 and 0.98 nm, respectively. It shows that SiO_2 has better flat surface compare to Ag, Co and Pt

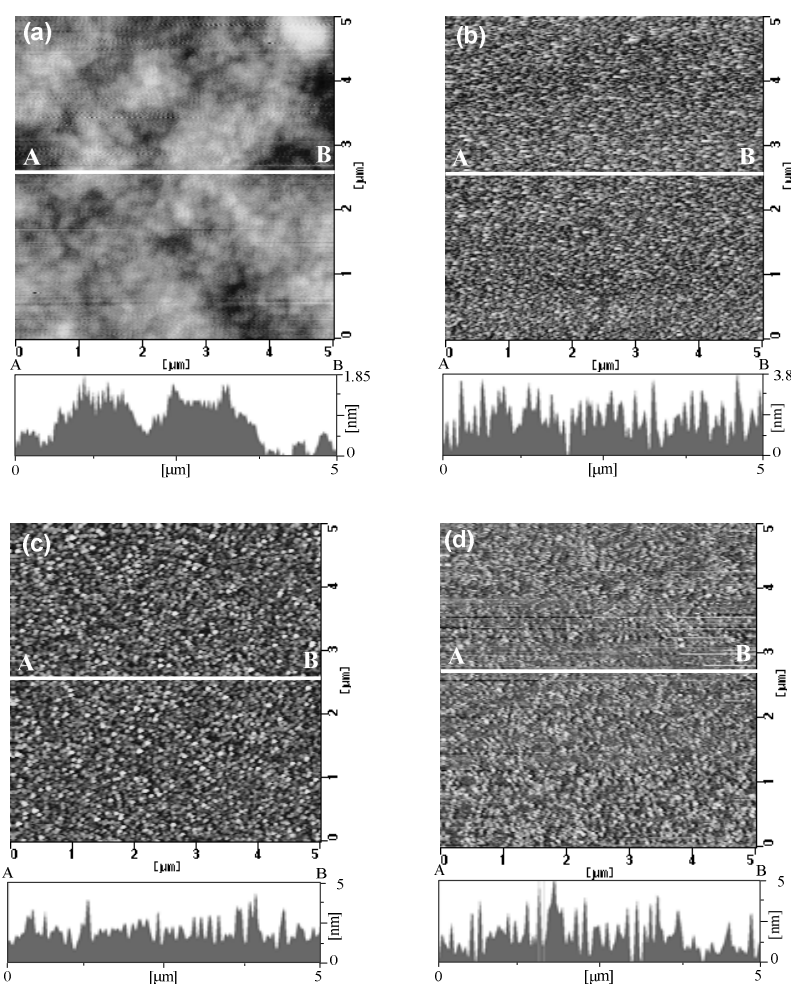


Figure 2.1.5: AFM images ($5 \times 5 \mu\text{m}^2$) of (a) SiO_2 (b) Ag (c) Co and (d) Pt film deposited on a Si(100) surface by sputtering deposition. The thickness of the film is 100 nm. The cross sectional profile in line A-B is given.

2.1.3 Spin-on-Glass

Spin-on-Glass (SOG) has been widely used in semiconductor processes in the past for flattening interlevel dielectrics.[6, 7] The properties of annealed SOG are comparable to those of SiO₂ from chemical vapor deposition, which is widely used in very-large-scale integrated technology. The dielectric constant of SOG is 3.1, whereas SiO₂ has a dielectric constant of 3.9.[8] This shows that SOG is the better intermetal dielectric insulator. The starting material is liquid and capable of being dispensed and spun on the wafer to fill gaps and deep trenches. It is usually cured by heating to high temperatures (for examples at 400-500°C) in the last stage of the processes. This step reduces the thickness of the SOG larger. SOG films exposed to elevated temperatures will decrease in their thickness as time progresses. The time dependence of the film thickness is approximately exponential and can be described by the equation:

$$T = T_f + ae^{-t/\tau}$$

Where, T_f is the final thickness of the film, $T_f + a$ the initial thickness, t the curing time, and τ a constant with the dimension of time. [8]

Careful handling of the deposition and curing process is essential for SOG, as it is prone to contamination, cracking of the dielectric layer, and poor adhesion. Several investigations have shown that SOG could outgas and create problems in the subsequent layers during device processing.[9] The major component of the out gassed materials is water. SOG retains water for the following reasons: (1) The temperatures at which SOGs are cured are generally below 450°C, which is too low to completely remove the water, (2) SOG can take in moisture during the storage period between baking and the next step, (3) SOG can absorb water during immersion in water, which is usually performed after the via etching process. [9]

A commercial siloxane-type SOG (Accuglass 512B, Rasa Industries, Ltd.) was used in the present experiments to make thick (400 nm) SiO₂ insulator layer on the Co/Si surface. It is composed primarily of siloxane which contains CH₃ (15% organic content) as illustrated in Fig. 2.1.6.

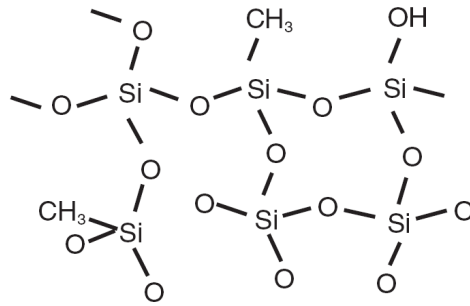


Figure 2.1.6: Structure of Accuglass 512B, composed mainly of siloxane.

Deposition process of SOG

SOG needs to be stored in a refrigerator and must be at room temperature before applying it to the substrate. Deposition and curing techniques of SOG films are similar to photoresist processing, and their etching closely resembles the methods employed for those of other SiO₂ films. The process of deposition SOG is schematically depicted in Fig. 2.1.7. First SOG liquid was spin-coated on substrate at 3000 rpm for 10 s [Fig. 2.1.7(a)]. Immediately after the spin-coating, the film was subjected to three stages of soft baking on hot plates at 80°C, 150°C and 250°C for 1 min at each temperature [Fig. 2.1.7(b)]. The final curing was performed at 425°C for 30 min under a nitrogen gas flow of 1.0 liter min⁻¹[Fig. 2. 1.7(c)]. At this process the SOG film was converted by the crosslinking reaction induced by heat treatment to the dielectric film, SiO₂. After these curing processes, the thickness of the SOG film on the substrate was 350~600 nm. The thickness of the SOG film can be adjusted by the amount of SOG deposited and spin coating speed. The SOG film thickness was measured as a function of SOG amount [Fig. 2. 1.8(a)]. The SOG was deposited on the Co/Si(100) layer on a wafer, which was 14×14 mm² in size, the Co thickness being about 20nm. One of the advantages of the SOG film is its high surface flatness. Figure 4.1.8(b) shows the AFM image of SOG, proving that the surface is very flat and the value of surface roughness $R_a = 0.25$ nm.

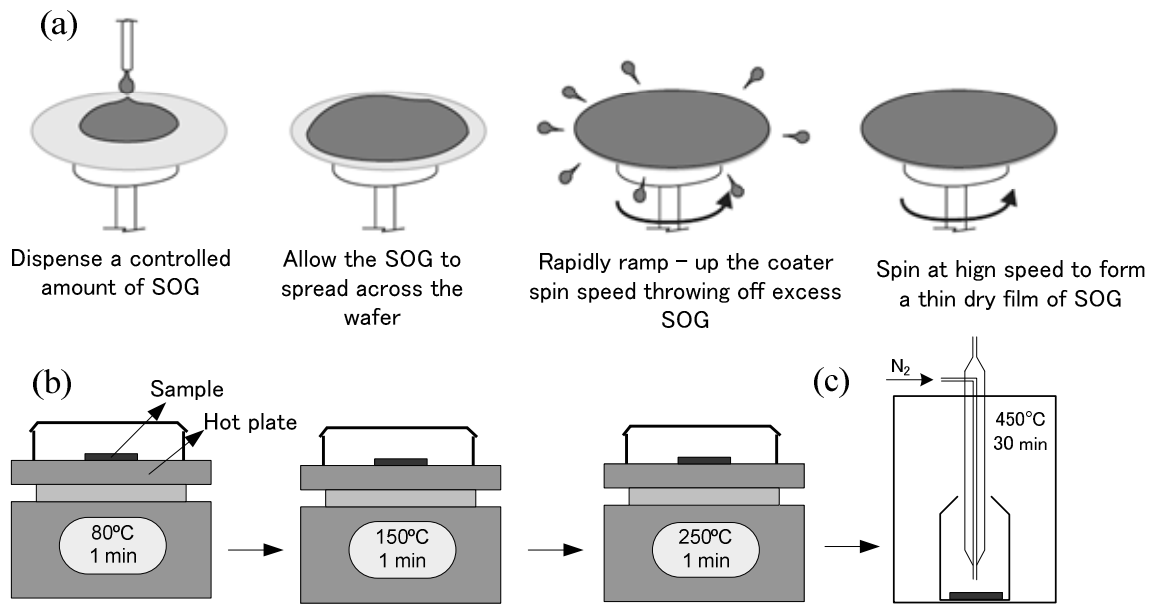


Fig. 2.1.7: Deposition process of SOG. (a) spin coating of SOG on substrate (b) baking on hot plate (c) curing in electric furnace.

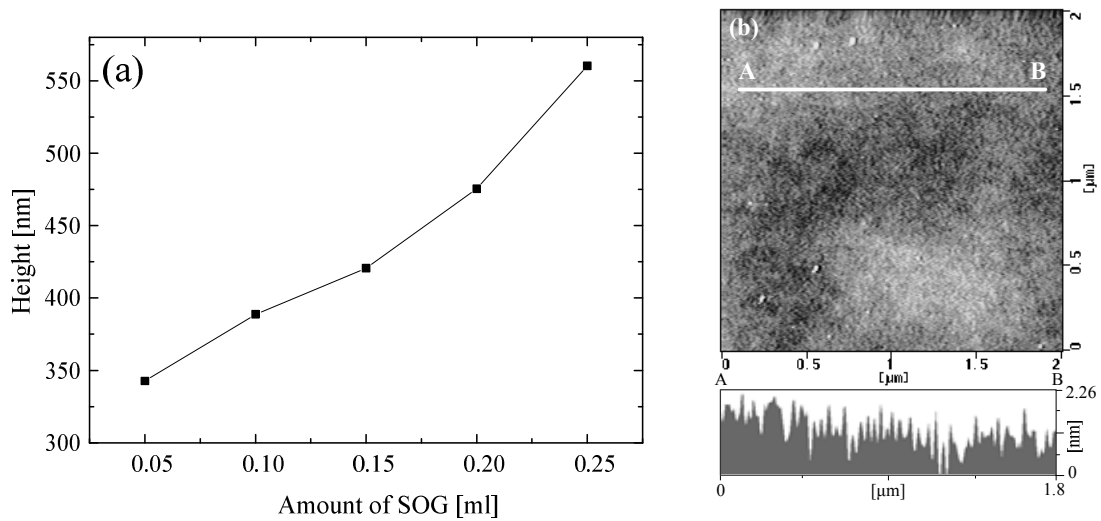


Figure 2.1.8: (a) SiO₂ film thickness as a function of SOG liquid amount on Co/Si substrate. The sample was 14×14 mm² in size and spin-coated at 3000rpm for 10 s. (b) AFM image (2×2 μm²) of SOG surface after the curing process. The cross sectional profile in line with A-B is given.

SR curing process

For the fabrication of microelectrodes, SOG was etched by the SR etching technique (details will be described in 2.3 section) using a Co thin film as an etching mask and a mixture of SF₆ (0.05 Torr) and O₂ (0.002 Torr) as an etching gas. It was found that after the SR etching the Co mask (200 nm thickness) was swelled by the SR irradiation (10000 mA min doze) as shows in Fig. 2.1.9 (a) and (b). For thicker Co mask (300 nm) same type of swelled surface was found after the SR etching [Fig. 2.1.9(c)]. This confirms the existence of residual gas in annealed SOG film that got outside at the SR etching process and caused a peeling away of the Co mask. A previous IR study showed that the SOG film can be densified at higher temperatures, typically at 800-900°C, and that a sullenly- and water-free film is obtained.[10] The SOG/Co/Si substrate was also baked at 700°C for 20 min in my experiment, but the SOG was cracked at this high temperature, which was confirmed by microscope observation.

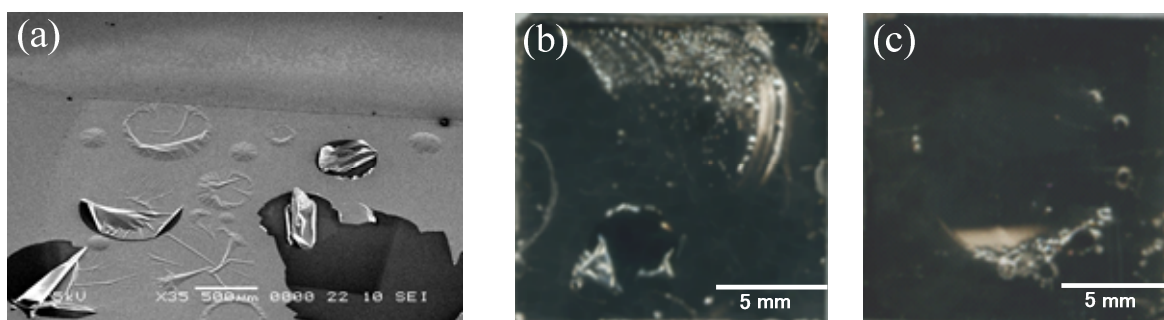


Figure 2.1.9: (a) SEM image and (b, c) CCD images of swelled Co/SOG/Si surface after SR etching. Co mask thickness was (a,b) 200 nm and (c) 300 nm. Sample size was $15 \times 15 \text{ mm}^2$.

I found that in order to prevent the peeling away of the Co mask, the SOG film can be degassed by direct SR irradiation onto the SOG surface prior to the Co mask deposition. We call this process “SR curing” hereafter. Earlier studies have shown that SR exposure causes a shrinkage of the SOG film. [11] After the SOG deposition on Co/Si substrate, the sample was SR cured at 10000 mA min doze. AFM images showed that the SOG surface after the SR curing is as flat ($R_a = 0.19 \text{ nm}$) as that before the SR curing [Fig. 2.1.10(a)]. Then Co contact mask (300 nm) was deposited on SOG by sputtering and SR etching was carried out. Now SR etching can be performed with no peeling away of the Co layers, which was confirmed by SEM and microscope. Finally, the Co mask was removed by immersion into 0.1 M HNO₃ aq. Figure 2.1.10(b) shows the topography image of SOG surface after the Co removal, the value of surface roughness R_a is 0.27 nm. I conclude that the SR curing process significantly removes the residual gas from the SOG and makes a defect free SOG. In this thesis, all the SOG samples was cured with SR.

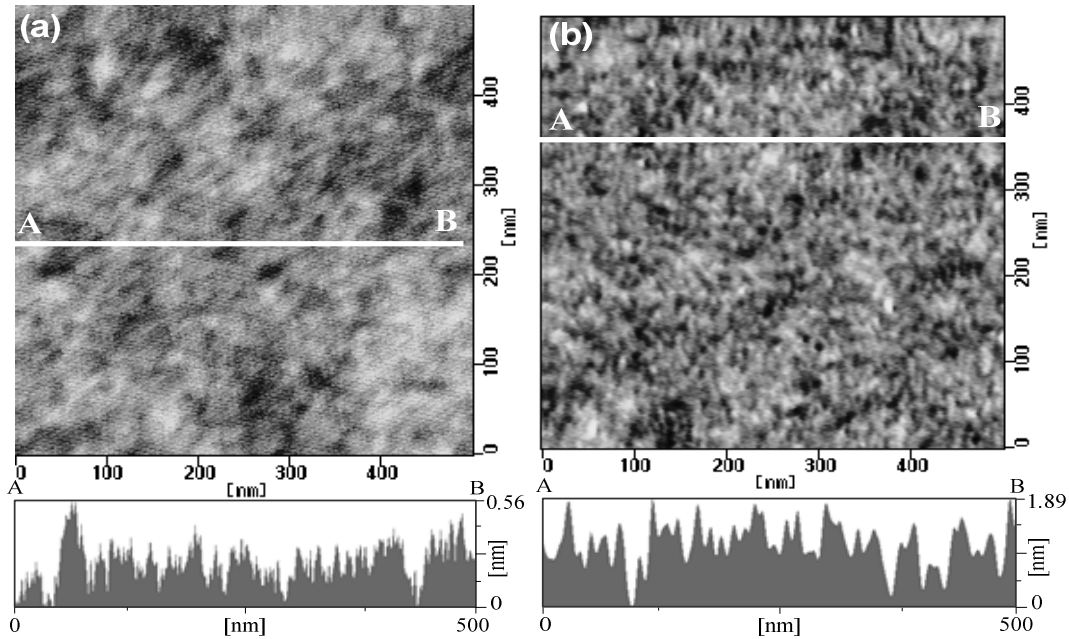


Figure 2.1.10: AFM topography images of SOG surfaces (a) after SR curing and (b) after SR curing followed by Co mask removing. The surface roughness R_a are 0.19 and 0.27 nm for (a) and (b), respectively.

2.2 Patterning technique

There are several patterning techniques such as lithography, focused ion beam, femtosecond laser patterning, electron beam lithography, in Si-wafer fabrication processes. In the experiments I have used lithography and femtosecond laser patterning for the patterning of Co contact mask. In this section, the details of these techniques are described.

2.2.1 Lithography

Lithography is a process of transferring geometric shapes on a mask to the surface of a silicon wafer.[12-30] These shapes make up the parts of the circuit, such as gate electrode, contact window, metal interconnections, and so on. Although most lithography techniques used today were developed in the past 20 years, the process was actually invented in 1798; in this first process, the pattern, or image, was transferred from a stone plate (lithos). [31]

In the lithographic process, a photosensitive polymer film is applied to the silicon wafer (known as resist or photoresist), dried, and then exposed to ultraviolet (UV) light or other radiation

through a mask (called photomask) with a proper pattern. After the exposure, the wafer is soaked in a solution that develops the images in the photosensitive material. Either the exposed or the non-exposed areas of the resist film are removed in the developing process depending on the type of resist used. If the exposed area is dissolved by the developer and the unexposed region is resilient (the mask pattern is reproduced on the resist), the material is called a positive resist. If the exposed material is resilient to the developer and the unexposed region is etched away (the mask pattern is inverted on the resist), it is called a negative resist. Fig 2.2.1(a) shows these two types of resist. In combination with this a patterning process, a lift-off technique can be used.

A lift-off technique allows the metallization after resist exposure and development. [32, 33] Metal can be evaporated over the entire surface, and a discontinuity is maintained between the metal on the substrate and the metal over the resist. During removal of the resist in a suitable solvent (known as resist remover), the metal over the resist is also removed and a clean and faithful reproduction of the image is obtained on the metal film as shown in Fig. 2.2.1(b). An important feature of this lift-off processes is that the side wall profile of the resist must be vertical or with an overhang. This causes a break in the deposited metal film and ensures easy lift-off. An additional advantage of the lift-off technique is that multilevel metal structures can be formed and in fact any material or combination of materials that can be evaporated can be used.

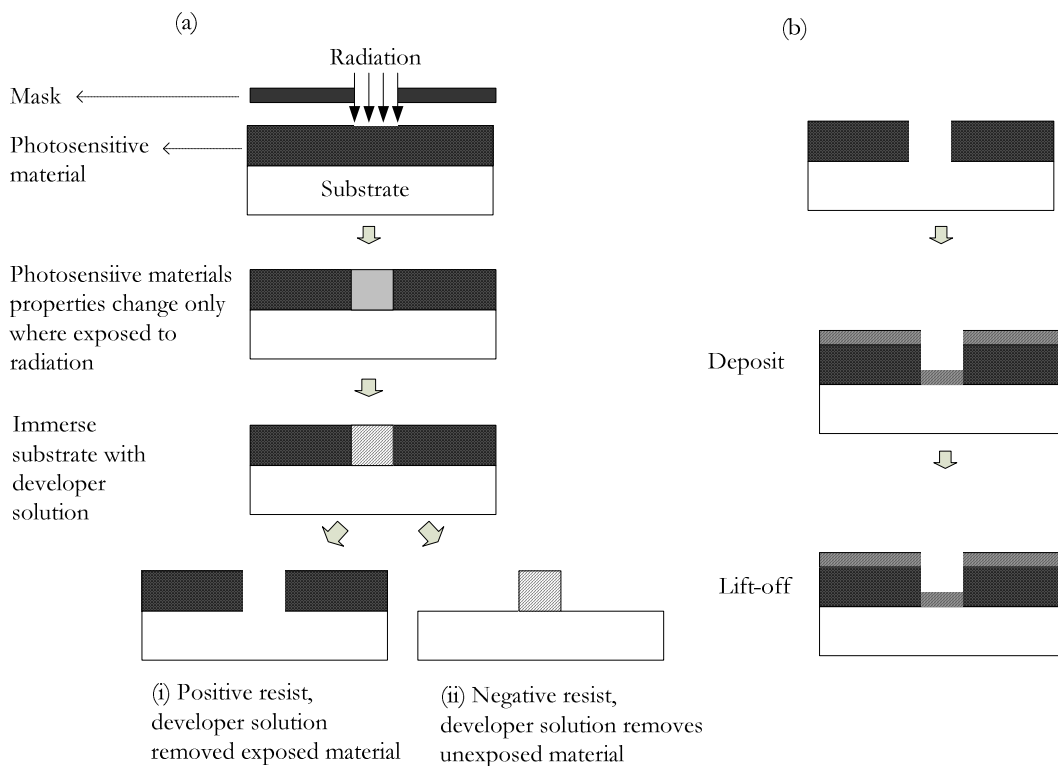


Figure 2.2.1: (a) Pattern definition in (i) positive resist (ii) negative resist. (b) Pattern transfer from patterned resist to overlying layer by lift-off.

Aligner

The exposure instrument for the lithography process is called *aligner*. Aligners do several jobs. First, they rigidly hold the wafer and mask in place after the mask pattern is aligned to a previous pattern already processed into the wafer. Second, they provide a source of exposing radiation for the resist. Some exposure tools, such as the e-beam machine, provide a third function; they allow the wafer to be exposed directly without requiring a mask. Exposure tools performance can be evaluated by three parameters: resolution, registration, and throughput. *Resolution* is defined in terms of the minimum feature that can be repeatedly exposed. *Registration* is a measure of how closely successive mask levels can be overlaid, and *throughput* is defined as the number of silicon wafers that can be exposed per hour. [34]

The majority of very large scale integration (VLSI) exposure tools used in IC production are optical systems that use UV light. They are capable of less than 200 nm resolution, $\pm 0.2 \mu\text{m}$ registration, and up to 100 exposures per hour. Electron beam exposure systems can produce IC features with a resolutions of less than approximately $0.5 \mu\text{m}$ with $\pm 0.2 \mu\text{m}$ registration.[35] The e-beam systems are primarily used to produce photomasks; relatively few are dedicated to direct wafer exposure. [36] X-ray lithographic systems have approximately $0.5 \mu\text{m}$ resolution and $\pm 0.5 \mu\text{m}$ registration but are not yet used to produce ICs in volume. [37-39]

Lithography process

The following process is followed for lithography as schematically shown is Fig. 2.2.2.

Coating: The wafer is held on a vacuum spindle of coater. Then a small amount of resist (2-3 ml) is dispensed onto the center of the wafer and spun at high speed to produce a uniform thin film in two steps [Fig. 2.2.2(a)]. First the substrate is spun at 1000 rpm for 10 sec to throw off excess resist and then spun at 3000 rpm for 10 sec to form a unify resist on the substrate. After the coating process the thickness is $1.5\sim 2.5 \mu\text{m}$ and $2\sim 4 \mu\text{m}$ for positive and negative resists, respectively. Note that, negative resist is stickier than the positive resist. The thickness of the resist can be adjusted by the amount of resist and spin coating speed. The thickness of the resulting resist film is proportional to the percent solids in the resist and inversely proportional to the square root of the spin speed.[40] Negative resists usually have poorer resolution capability than positive resists, but are very sensitive and permit a large number of wafers to be exposed in an hour. In the experiments the following resists were used:

Positive resist: S1813 purchased from Okada Kagaku Co., Ltd

Negative resist: N-HC 600 purchased from Tokyo Ohka Kogyo Co., Ltd.

Pre-bake: After coating, the wafer is given a pre-bake at 80°C for 30 min to remove the

resist solvent, stabilize the film and increase the resist adhesion to the wafer [Fig. 2.2.2(b)]. In the experiments electric oven was used for the pre-bake.

Exposure: The wafer and the appropriate mask pattern are subsequently exposed to UV light [Fig. 2.2.2(c)] for 20s and 15s for positive and negative resist, respectively. A positive resist usually requires more exposure energy (longer exposure times) than a negative resist to form resist images.[41] A mask aligner (K-309PW95, Kyowariken Co., Ltd.) was used for the exposure in the experiments.

Developing: In the developing process the sample was immersed in the developer solution for 2~3 min and rinsed with pure water and dried under flowing N₂. In the experiments the following developers were used:

For positive resist: MF CD-26 purchased from Okada Kagaku Co., Ltd

For negative resist: N-AS purchased from Tokyo Ohka Kogyo Co., Ltd.

Post-bake: It is often desirable to bake the sample once again after development. Baking improves chemical resistance and adhesion properties of the resist. For post bake, the sample was baked on hot plate at 80°C for 10 min. Note that usually the post-bake makes the resist coat harder and the lift-off process becomes more difficult.

Sputtering: For the lift-off process Co, Pt or Ag layer was deposited by sputtering (see section 2.1.2).

Resist removal: Finally to remove the resist, the sample was immersed in a commercial resist removing solution for 2-3 min to completely remove the resist.

Positive resist remover: 1112A purchased from Okada Kagaku Co., Ltd

Negative resist remover: NS purchased from Tokyo Ohka Kogyo Co., Ltd.

Figure 2.2.3(a) shows the SEM image of the patterned negative resist in the above process. The SEM image shows that the side wall of the resist is indeed vertical, which is essential for an easy lift off. The resist height was determined with a step profiler (Dektak3, ST) to 2.2 μm. Figure 2.2.3(b) shows the SEM image of the patterned Co (200 nm thickness) on Si(100) created by lithography and lift-off technique.

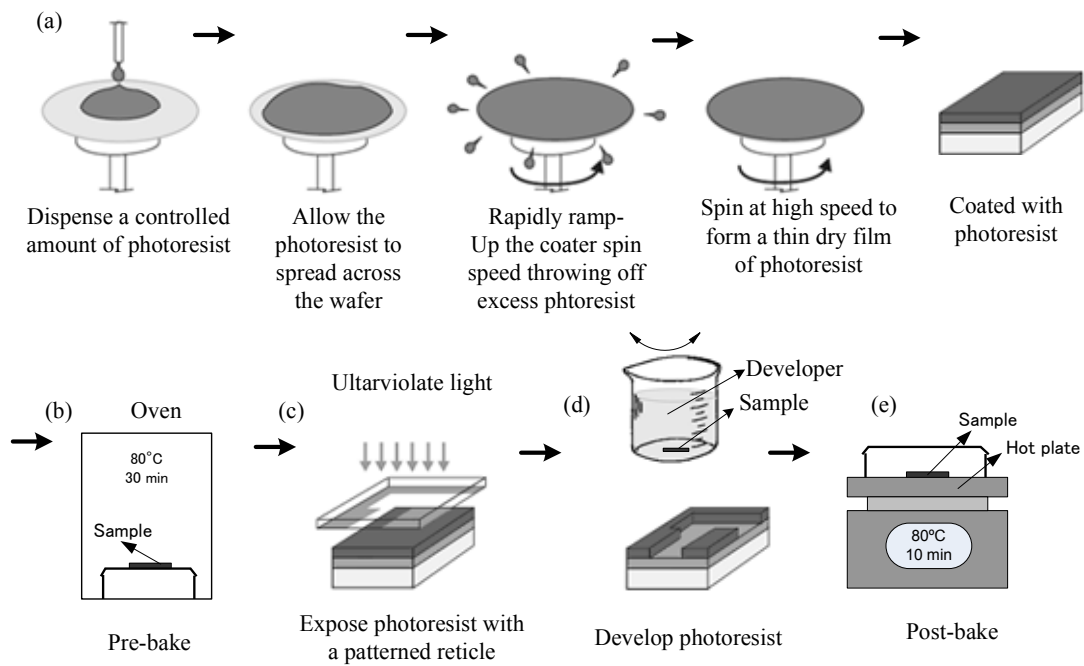


Figure 2.2.2: Lithography process: (a) coat with resist (b) pre-bake (c) exposure (d) develop and (e) post-bake.

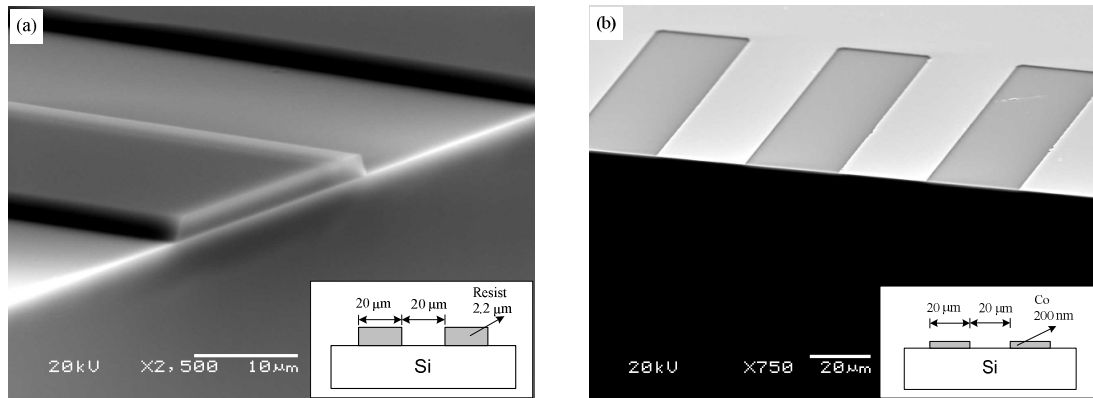


Figure 2.2.3: (a) SEM image of the patterned resist after lithography, where the resist height is 2.2 μm (b) SEM image of the patterned Co (200 nm thickness) on the Si. The brighter area is the Co film. The insertions show the schematic drawing of the cross sectional structure of the substrate

2.2.2 Femtosecond laser patterning

Laser machining

Laser machining is a process that uses a focused optical light beam to selectively remove materials from a substrate to create a desired feature on the substrate by ablation process. [42-48] This process is non-contact yet it has high spatial confinement. Laser increase the sample temperature less than other mechanical techniques. The process is generally based on the linear optical absorption and plasma formation mechanisms. However, conventional laser machining can not create micron-sized structures because linear optical absorption of the materials often lead to heat deposition and micro-cracks, so small collateral damage to the surrounding is unavoidable. Femto-second laser ablation process can overcome these demerits.

Femtosecond laser

Femtosecond laser produces pulses shorter than a pico second. It utilizes the ultrashort laser pulse properties to achieve an unprecedented degree of control in sculpting the desired microstructures internal to the materials without collateral damage to the surroundings. Using femtosecond rather than pico-second or nanosecond light pulses, laser energy is deposited into small volumes by multi-photon nonlinear optical absorption followed by an avalanche ionization. Typical heat diffusion time is in the order of nanosecond to microsecond time scale whereas the electron-phonon coupling time of most materials is in the pico-second to nanosecond. Therefore when laser energy is deposited at a time scale much shorter than both the heat transport and the electron-phonon coupling, the interaction process between light and material is essentially frozen in time. The extremely short time duration of a femtosecond pulse gives enormous peak powers and power densities. The affected zone can be altered from solid to vapor phase and to plasma formation almost instantaneously. Unlike conventional laser machining, femtosecond laser machining reduces collateral damages to the surroundings. Because the machining process is not dependent on the linear absorption at the laser wavelength, virtually any dielectric, metals, and mechanically hard materials can be machined by the same laser beam.

Femtosecond lasers are being used in a rapidly growing number of applications, including ultrafast photochemistry, photo-physics, photo-ablation, micromachining, imaging condensed matter, semiconductor device physics, and other areas.

Patterning of contact mask using femtosecond laser ablation

Femtosecond laser ablation was used for the patterning of the Co mask. This Co mask was used as a contact mask at synchrotron radiation etching process to remove the SiO₂ and made the microelectrodes (see chapter 4). The diameter of the electrode hole was about 1 μm. To maintain a flat surface, it was important to control the irradiation power of the femtosecond laser such that only the Co film is removed with ignorable damage to the lower SiO₂ layer. If the SiO₂ layer is also sputtered by the laser, debris (composition is unknown) of 100 ~ 200 nm diameter, which are difficult to remove by the usual etching solution such as HF, HCl, H₂SO₄, and HNO₃, were deposited around the wells. The experiments of femtosecond laser ablation were conducted at Aishin Seiki Co., Ltd in Karia city, Aichi.

The suitable conditions for femtosecond laser ablation

Several experiments were conducted to find out the suitable conditions for the patterning of the Co mask with femtosecond laser ablation, as schematically depicted in Fig. 2.2.4. Two Si substrates (14x14 mm²) (samples A and B) were cleaned [Fig. 2.2.4(a)] and the Co (10 nm thick) for the electrode was deposited on the mirror polished Si(100) surface by sputtering (see section 2.1.2) [Fig. 2.2.4(b)]. SiO₂ film (600 nm thickness) consisting of spin-on-glass (400 nm thickness) and sputtered SiO₂ (200 nm thickness) were deposited [Fig. 2.2.4(c)] (see section 2.13 and 2.12 respectively). The Co thin film for the etching contact-mask (300 nm) was deposited on the SiO₂ surface by sputtering deposition [Fig. 2.2.4(d)]. The mask patterns were made by femtosecond laser ablation under different conditions [Fig. 2.2.4(e)]. One sample (sample A) was made with a higher power (500 mW) with long irradiation time (8 msec), whereas another sample (sample B) was made with lower power (250 mW) with small irradiation time (2 msec). For both samples, SiO₂ was subsequently removed by SR etching (see section 2.3) (SR doze=20000 mA min) using a mixture of SF₆ (0.05 Torr) and O₂ (0.002 Torr) as etching gas [Fig. 2.2.4(f)]. Finally the Co contact mask was removed by immersion into 0.1 M HNO₃ aq. [Fig. 2.2.4(g)].

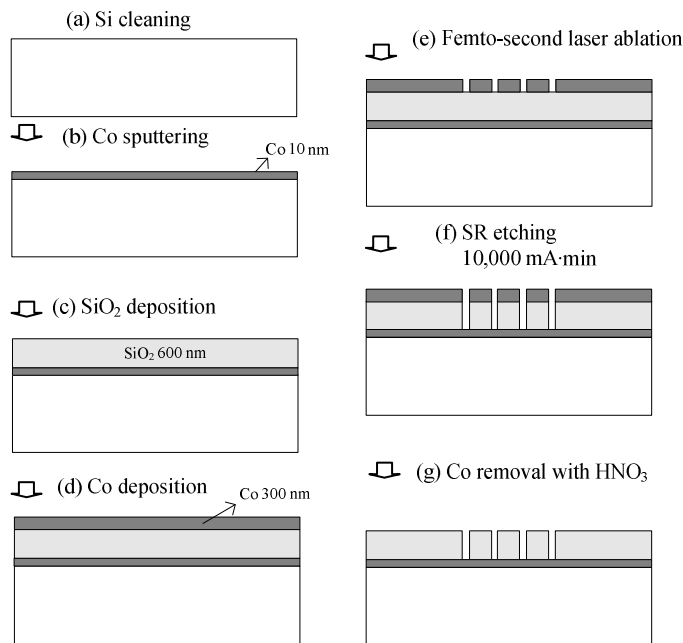


Figure 2.2.4: Schematic drawing of the Co contact mask patterning process by femtosecond laser ablation

The AFM images of the Co mask patterned by femtosecond laser ablation show that owing to a height of 58 nm and 27 nm consisting of sputtered particles is formed around the hole areas for the samples A and B, respectively [Fig. 2.2.5(a) and Fig. 2.2.6(a)]. The AFM image after the SR etching followed by Co removal show that 198 nm heights of debris were formed around the hole for the sample A [Fig. 2.2.5(b)]. Whereas, for the sample B no debris were found around the hole [Fig. 2.2.6(b)]. To remove the debris of sample A, the sample was immersed into HF (5%), HCl (10%) and H₂SO₄ (10%) aq. for 10 min each, but the debris particles could not be removed with this treatment.

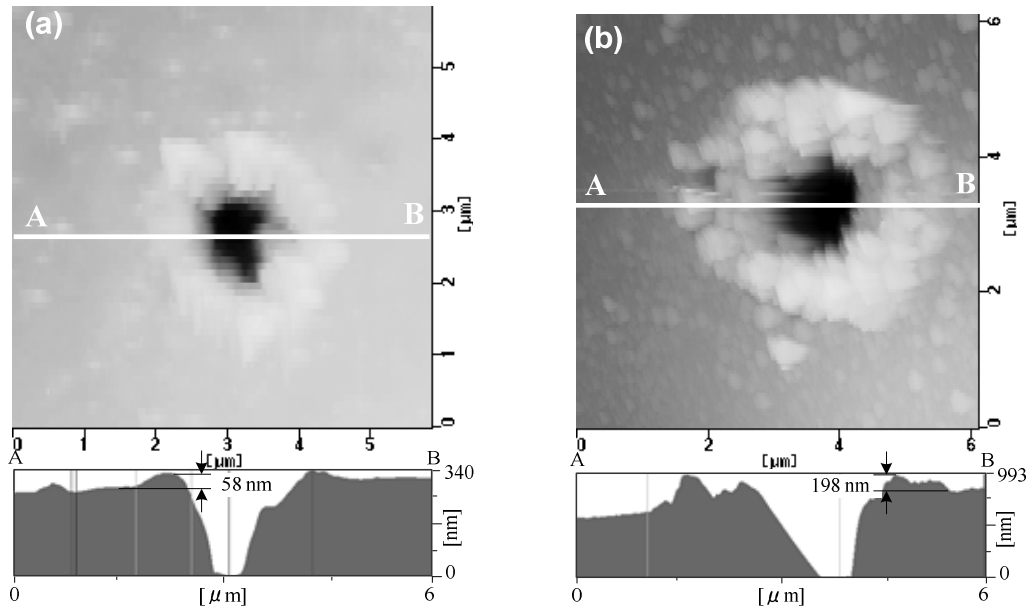


Figure 2.2.5: AFM images of sample A (a) after the patterning of Co contact mask by high power (500 mW) and with long irradiation time (8m sec), and (b) the same area after the Co mask was removed by HNO_3 .

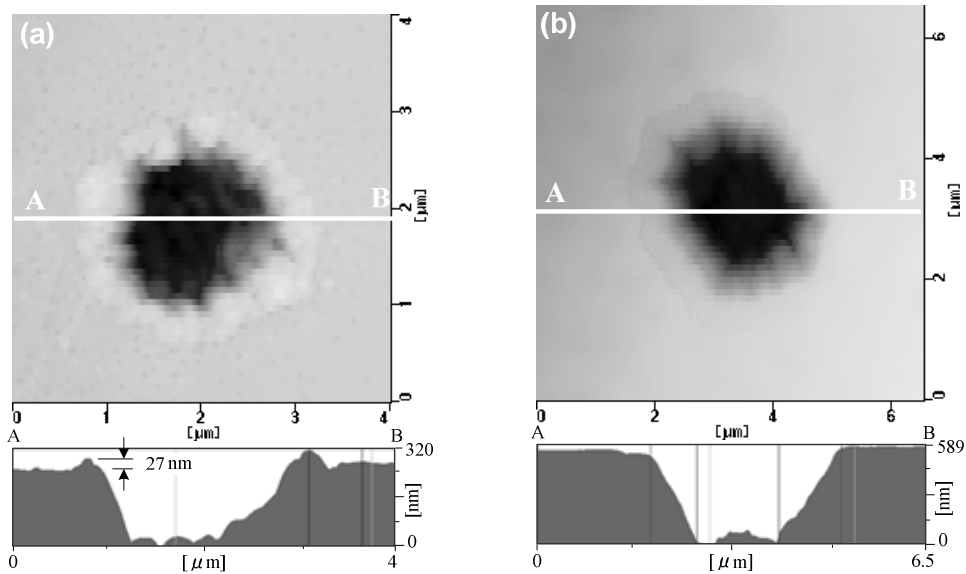


Figure 2.2.6: AFM images of sample B (a) after the patterning of Co contact mask by low power (250 mW) and with small irradiation time (2 msec), and (b) the same area after the SR etching of SiO_2 and followed by Co mask removal.

I concluded that following parameters are the best conditions for the patterning of Co mask with femtosecond laser ablation as shown in Table 2.2.2.

Table 2.2.2: Best conditions for the patterning of Co mask by femtosecond laser ablation process.

Laser wavelength (λ)	1,560 nm
Average power	250 mW
Frequency	258 KHz
Pulse width	900 fs
Irradiation time	2 msec

2.3 Synchrotron Radiation etching

SR stimulated semiconductor processes have attracted considerable attention from the view point of developing new surface technologies.[49-52] Applications of the synchrotron radiation (SR) stimulated photochemical reactions to material processes, such as SR stimulated etching and chemical vapor deposition (CVD) was first demonstrated in 1991 [53] and since then many experimental studies have been carried out. These SR stimulated processes demonstrate several unique characteristics such as low temperature, low damage, low contamination, high spatial resolution owing to the short wavelength of the radiation, and reaction selectivity via excitation energy tuning. The combination of these features using SR is anticipated to realize novel nano-process technology in the future. Studies in the past decade have succeeded in demonstrating the potential merits of SR photochemical reactions applied to semiconductor processes such as etching, CVD, surface cleaning or modification, and epitaxial growth.[50, 54, 55] The interesting phenomenon of material selectivity in surface reactions is considered to be unique to core electron excitations, although the mechanism is not yet fully understood. The disadvantages of the SR process are also becoming clearer. The rather low reaction rate is considered in making it difficult to apply this technique to conventional larger-scale integrated circuit (LSI) manufacture although perhaps it is suitable for the nano processes.

In the present work, for the fabrication of the electrode, spin-on-glass (SOG) was deposited on the CoSi₂ layer as a thick insulator and finally SOG was etched by the SR etching. Earlier study have shown the SOG can be etched by SR etching similar to SiO₂ layers prepared by thermal oxidation, CVD, etc. [11]

SiO₂ etching mechanism with SR

When a SR beam irradiates to a SiO₂ film, the valence and core electrons of both Si and O atoms are excited. SR induced Si-O bond breaking and the photo-stimulated oxygen atom or ion desorption takes place on the oxide surface. High Si-content regions are formed as a result of oxygen desorption from the oxide surface. In the SiO₂, SR also forms numbers of defects such as nono-bonding oxygen (Si-O), peroxy bridges (Si-O-O-Si), peroxy radicals (Si-O-O), and Si dangling bonds in the SiO₂ film. By heating the sample, these unstable Si-O and O-O bonds dissociate and oxygen, and volatile SiO molecules desorb from the SR irradiated area.

Co layer as a contact mask

An etching mask of SR etching should have several characteristics: (1) a large absorption coefficient around the excitation energy of the substrate materials, ~100eV for SiO₂ because the photo decomposition is induced by the excitation of Si 2p core electron, (2) a larger resistivity against the SR irradiation and etching process, (3) having a suitable process to efficiently dissolve the mask material without damaging the surface, (4) small grain sizes in the film which are necessary for the fine patterning. Considering these demands and referring to the absorption coefficient of metals, Co has been demonstrated to be one of the most satisfactory candidate for the SiO₂ etching mask material.[56, 57] The absorption coefficient of Co is shown in Fig. 2.3.1. At the end of the process the Co mask can be removed by immersion into 0.1 M HNO₃ aq.

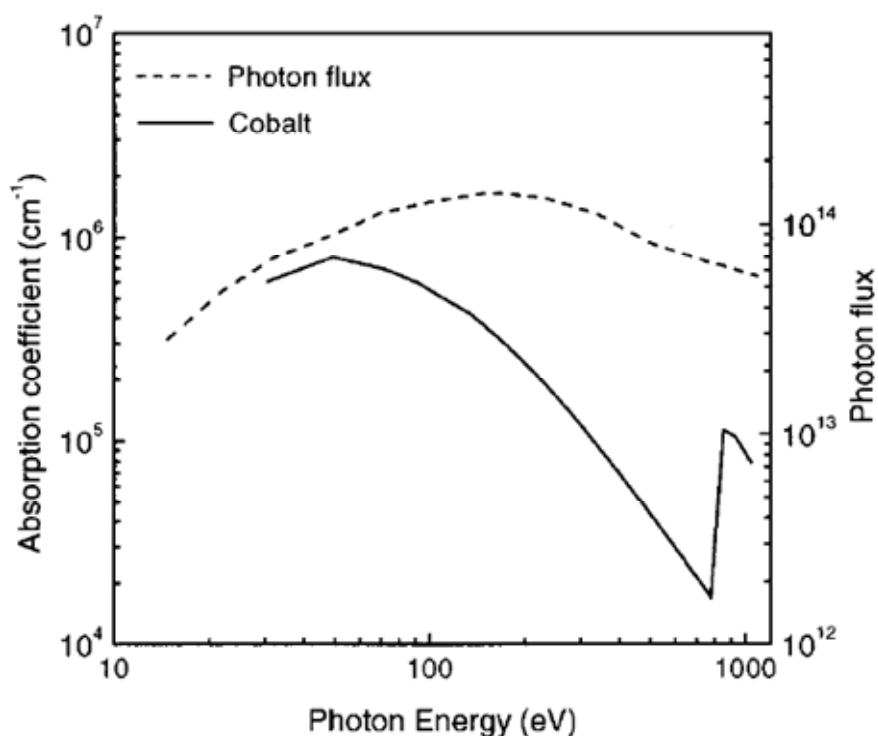


Figure 2.3.1: Calculated absorption coefficients of the Co thin film in the vacuum ultraviolet region and the photon flux (photons/s mrad 0.1λ 100 mA) of the beamline 4A2 in UVSOR.[56]

SR etching chamber

SR etching of $\text{SiO}_2/\text{Si}(100)$ substrates was conducted at the beam line 4A2 of the SR facility (UVSOR) in the Institute for Molecular Science (Fig. 2.3.2). The emitted beam from the storage ring is reflected and focused by the elliptically bent cylindrical mirror with a grazing incident angle of 2° . The beam line is equipped with another mirror for branching. The beam line irradiates the substrate surface without monochromatization in order to obtain a high photon flux. The electron beam energy was about 0.75 MeV. A large pressure difference between the etching chamber and the beam line was sustained by using a differential vacuum pumping system. No window is inserted between the storage ring and the sample chamber, and the SR lights irradiates the sample surface directly. The beam diameter on the sample surface was about 9 mm and the calculated total photon flux was 4.2×10^{16} photons/s for the 100 mA ring current. [56] The calculated spectrum distribution of the beam is shown in Fig. 2.3.1.

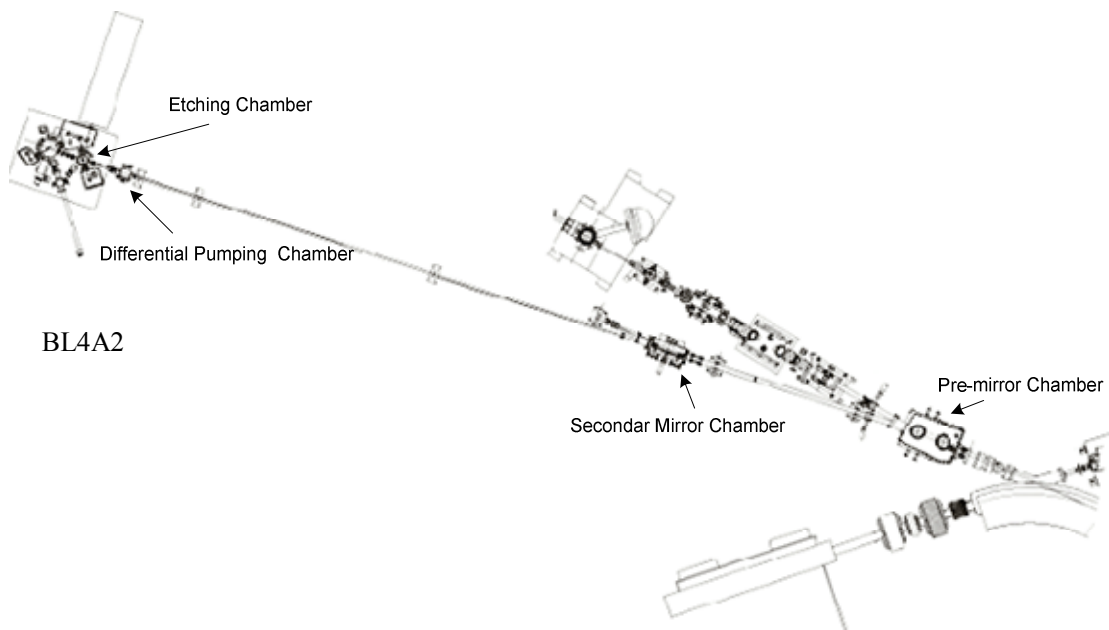


Figure 2.3.2: Schematic drawing of the BL4A2 beam line with a etching chamber

Etching of SOG with SR etching process:

The process of SOG deposition and SR etching is schematically depicted in Fig. 2.3.3. A single-crystal Si (100) wafer (p type, 80–120 Ω cm) covered by native oxide was first pre-cleaned in acetone, ethanol, and de-ionized water with an ultrasonic bath for 5 min, respectively, then immersed into a solution of concentrated H_2SO_4 and 30% H_2O_2 (70:30 v/v) at 110 $^\circ\text{C}$ for 10 min, and finally treated with 2.5% HF solution for 2 min to remove the native oxide [Fig. 2.3.3(a)]. The SOG thin film was deposited on the freshly cleaned Si surface [Fig. 2.3.3(b)]. The thickness of the SOG film measured with a step profile meter (Dektak 3, ST) was about 470 ± 10 nm. The thickness of the SOG layer can be controlled by the amount of the SOG solution and the spinning rate. (see section 2.1.3) AFM images show that the SOG surface is flat like a mirror-polished silicon wafer [Fig. 2.3.5(a)] The Co mask was fabricated on the SOG surface [Fig. 2.3.3(c)] by using photolithography and a lift-off technique. The thickness of the Co mask measured with a step profile meter was about 250 ± 10 nm [Fig. 2.3.4(a)].

The SR etching of SOG/Si(100) was conducted using a mixture of SF_6 (0.05 Torr) and O_2 (0.002 Torr) as the reaction gas at room temperature [Fig. 2.3.3(d)]. The sample was set normal to the incident SR beam. The beam current of the storage ring was 350~100 mA. The irradiation dose of the SR beam was 20000 mA min.

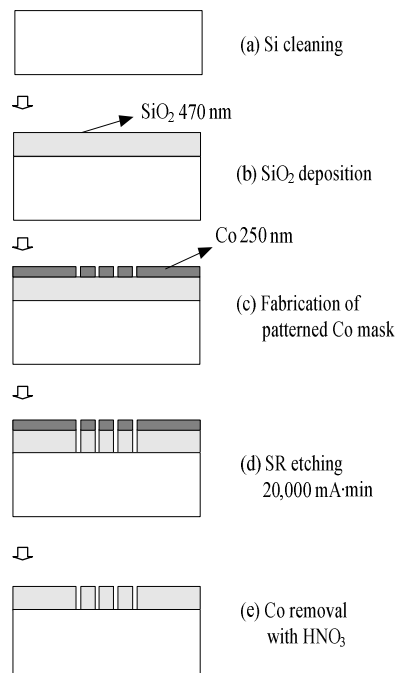


Figure 2.3.3: Schematic drawing of SR etching process.

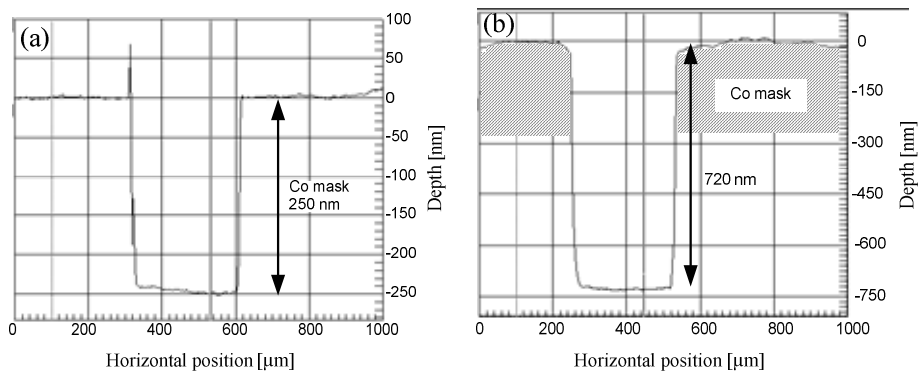


Figure 2.3.4: Step profiles of the Co/SOG/Si surface (a) before and (b) after the SR etching.

Figure 2.3.4(b) shows the step profile of the patterned area on the Co/SOG/Si surface after the SR etching, where the depth became 720 nm. This confirms that the SOG layer (470 nm) was almost completely etched by the SR radiation under SR₆ + O₂. The etching took place only in the SR-irradiated area and proceeded into the direction of the incident beam.[58] Another important characteristic was the etching selectivity between Si and SiO₂. The etching process stopped just at the interface of SiO₂/Si if O₂ was added to the reaction gas.[58] After the SR etching, the Co mask could be easily removed without damaging the substrate by immersion into 0.1 M HNO₃ aq. for 5 min.

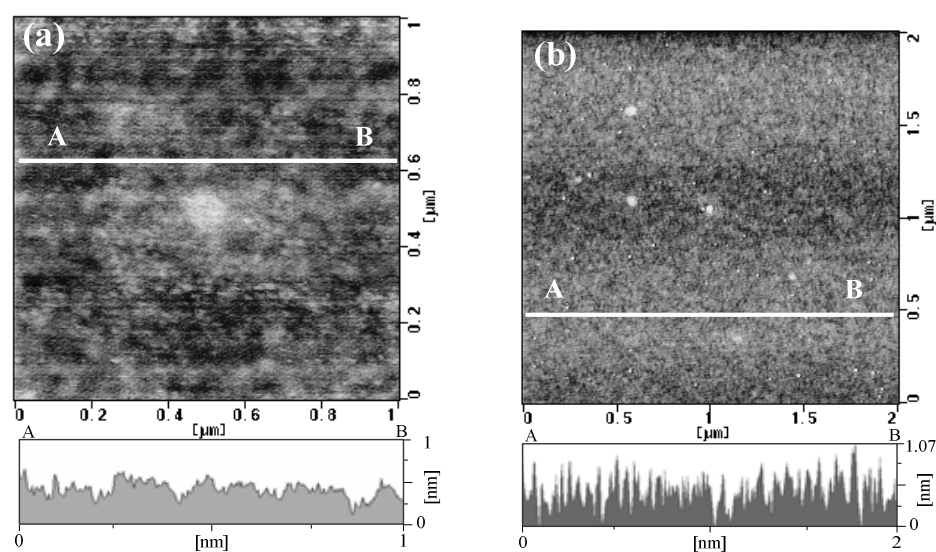


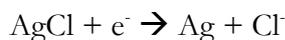
Figure 2.3.5: AFM topography images of SOG (a) before the Co mask deposition (b) after the SR etching followed by Co removal. The cross sectional profile in line A-B is given.

Figure 2.3.5(b) shows the AFM image of SOG surface after the Co removal, where the value of the surface roughness R_a is 0.54 nm. Before the SR etching and the Co mask deposition this value was 0.1 nm [Fig. 2.3.5(a)]. This confirms that the SR etching process is suitable for the etching of SOG while maintaining the surface flat. Co was demonstrated to be an ideal material as a SR etching mask, showing large resistivity for SR irradiation and being easily removed by dilute acid. The etching stopped completely at the SOG/Si interface. However, it is described in details in chapter 3.

2.4 Ag and AgCl electrode formation

A reference electrode is necessary to measure the electrical properties of supported membranes. The purpose of the reference electrode is to complete the measuring circuit and provide a stable and reproducible potential against which the indicator electrode is compared.[59] Silver chloride/silver (or AgCl/Ag) is widely used as a reference electrode in electrochemical fields because it is simple, inexpensive, very stable, non-toxic and has a superior temperature range (usable even above 130 °C). [60, 61] The contact is made through a liquid junction that allows the reference electrolyte to contact the sample. A salt bridge is formed from the sample through the electrolyte to the AgCl/Ag reference element. A direct metal contact to the solution would also complete the circuit but it would not provide a reproducible potential from one solution to the next.

The reference electrode is thus designed to produce the an identical, stable potential no matter in what solution it is placed.



The electrode consists of a silver layer that is coated with a thin layer of silver chloride either by electroplating or by dipping the wire in molten silver chloride. The solubility of silver chloride in water is about 10^{-5} M at 25°C and in saturate KCl solution increases to about 6×10^{-3} M. When the electrode is placed in a saturated potassium chloride solution it develops a potential of 199 mV vs the standard hydrogen electrode. The potential developed is determined by the chloride concentration of the solution, as defined by the Nernst equation.[62]

$$E_{cell} = E_{cell}^o - \frac{RT}{nF} \ln Q$$

Here,

R = gas constant

T = temperature in Kelvins

Q = thermodynamic reaction quotient

F = Faraday's constant

n = number of electrons transferred

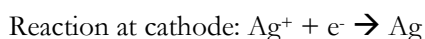
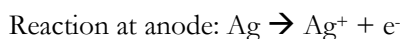
The potential of the electrode remains constant as long as the chloride concentration remains constant. The AgCl/Ag reference electrode develops a potential proportional to the chloride concentration, whether it is sodium chloride, potassium chloride, ammonium chloride or some other chloride salt. The concentration of chloride in the reference electrolyte determines the potential of the reference element. Potassium chloride is the most widely used electrolyte because it does not generally interfere with pH measurements and the mobilities of the potassium and chloride ions are nearly equal. This equal transference minimizes the junction potentials since the (+) potassium and (-) chloride ions move at the same rate. These ions provide the conductive path between the reference element and the sample, commonly referred to as a salt bridge. Usually saturated potassium chloride is used as electrolyte, but lower concentrations such as 1 M potassium chloride are also possible. Note that changing the electrolyte concentration changes the potential. Silver chloride is slightly soluble in strong potassium chloride solutions, so it is sometimes recommended the potassium chloride be saturated with silver chloride to avoid stripping the silver chloride off the silver wire. Most of reference electrodes use a saturated KCl solution with an excess of KCl crystals. This extra KCl dissolves into the electrolyte as the potassium and chloride ions diffuse out through the liquid junction in normal use. Thus this extra buffer of KCl extends the time before the reference cell starts to drift due to the depletion of chloride ions in the electrolyte.

In this thesis, I have fabricated a supported planer lipid bilayer (SPLB) on the SiO₂ surface with a well structure of 1 μm diameter with AgCl/Ag electrodes at their bottoms. First the well

structure was made on SiO₂/CoSi₂/Si by using a Co contact mask and SR etching. Then the Co mask was removed with 0.1 M HNO₃ aq. The fabrication process is described in details in chapter 4. Ag (about 50 nm) was deposited by electroplating on the CoSi₂ surface of which was exposed at the bottom of the etched well. Then the surface of the Ag was changed to AgCl also by electroplating. Subsequently the AgCl/Ag electrode was used as a reference electrode to measure the electrical properties of SPLB membrane.

Formation of Ag layer on CoSi₂ surface by electroplating

The process used in electroplating is called electrodeposition.[63, 64] It is an electrochemical process by which metal (Ag) is deposited on the substrate (CoSi₂) by passing a current through the bath.[65-69] Fabrication of CoSi₂/Si microelectrode is described in Chapter 4. Usually there is an anode (positive charger electrode), which is the source of the material to be deposited; the electrochemistry which is the medium through which metal ions are exchanged and transferred to the substrate to be coated; and a cathode which is the substrate (the negative charged electrode) to be coated. As the current is applied, positive metal ions from the solution are attracted to the negatively charged cathode and deposit on the cathode. As replenishment for these deposited ions, the metal from the anode is dissolved and goes into the solution and balances the ionic potential. For the Ag deposition on CoSi₂ surface, [Ag(S₂O₃)₂]³⁻ was used as electrolyte.



Preparation method of [Ag(S₂O₃)₂]³⁻ electrolyte solution for Ag electroplating

1. Dissolve AgNO₃ 10.2 g (0.06 mol) to 600 ml of H₂O
2. Dissolve KBr 71.4 g (0.6 mol) to 600 ml of H₂O
3. Mix these two (1+2) solution: $\text{AgNO}_3 + \text{KBr} \rightarrow \text{AgBr} \downarrow + \text{KNO}_3$
4. Filter the AgBr sediment
5. Dissolve Na₂S₂O₃•5H₂O 40 g (0.161 mol) to 200 ml of H₂O
6. Put the AgBr (3) into (5) solution:

$$\text{AgBr} + 2 \text{Na}_2\text{S}_2\text{O}_3 \rightarrow 4 \text{Na}^+ + \text{Ag}(\text{S}_2\text{O}_3)_2^{3-} + \text{Br}^-$$
7. Dilute the (6) solution to 300 ml H₂O to obtain 0.2 mol/l of [Ag(S₂O₃)₂]³⁻ solution

Experiment procedure

Figure 2.4.1 shows the schematic drawing of the electroplating system. A $[\text{Ag}(\text{S}_2\text{O}_3)_2]^{3-}$ solution, Ag wire (99.99% purity, 0.8 mm diameter), CoSi_2/Si substrate (see Chapter 4) were used as electrolyte, anode and cathode, respectively. A patch clamp amplifier (CEZ-2400, Nihon-Kodes Co., Japan) was used as current source.

For the confirmation of Ag formation and estimation of the current flow value, a larger current flow of electroplating was conducted. A SiO_2 thin film consist of spin-on-glass (SOG) (400 nm thickness) (see section 2.1.3) and sputtered SiO_2 (200 nm thickness) was deposited on the CoSi_2/Si surface. The Ag/ CoSi_2 electrode was formed on the opposite site of the Si substrate by sputtering and annealing the substrate. The Co layer (300 nm) etching contact mask was deposited on the SiO_2 surface by sputtering. The hole patterns were made by Focused Ion Beam (JFIB-2300, Jeol Ltd., Japan) where the hole size was about $1 \times 1 \mu\text{m}^2$. The SR etching (20000 mA min) of the SiO_2 layer to make the wells on the CoSi_2 was carried out, using a mixture of SF_6 and O_2 as the etching gas. The SR etching provides a vertical side wall and completely stops at the CoSi_2 surface. The Co mask was removed by immersion into 0.1 M HNO_3 aq. for 5 min. The detail about the SR etching is described in section 2.3. Figures 2.4.2 (a) and (b) show the AFM images of the patterned area and the schematic drawing of the substrate, respectively. Square wells of show the well areas of $1 \times 1 \mu\text{m}^2$ were successfully fabricated and the thickness of the SiO_2 layer was 540 nm.

Ag was deposited on CoSi_2 electrode surface by electroplating, where 200 pA of current was supplied for 5 min. Figure 2.4.2c depicts the AFM topography image of electrode areas after the electroplating, where 858 and 1161 nm of Ag was formed on the hole. Ag was deposited on CoSi_2 and further current flow filled the well and made hill on the well. This experiment confirms that:

1. SiO_2 is a good insulator and there is no leak current around the well area, as no Ag layer was found in the surrounding areas.
2. SR etching process completely removes the SiO_2 and stops at CoSi_2 surface. If a SiO_2 layer remains on the CoSi_2 surface the current will not flow and electroplating cannot be proceeded.

I estimated the electroplating rate from the excess Ag hills shown in Fig. 2.4.2(c). A current flow of 10 pA for 5 min is sufficient to deposit 50 nm of Ag layer at the bottom of the well-structure electrode. Thus this value was used for the membrane substrates.

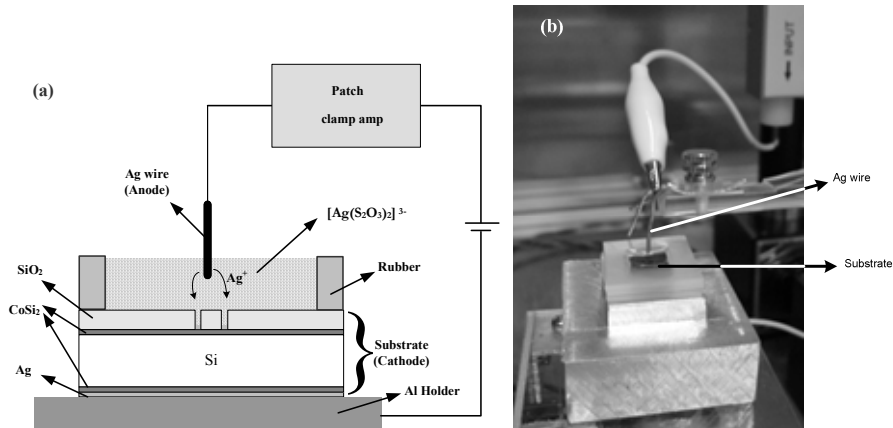


Figure 2.4.1: (a) Schematic drawing of the electroplating system (b) picture of the electroplating system.

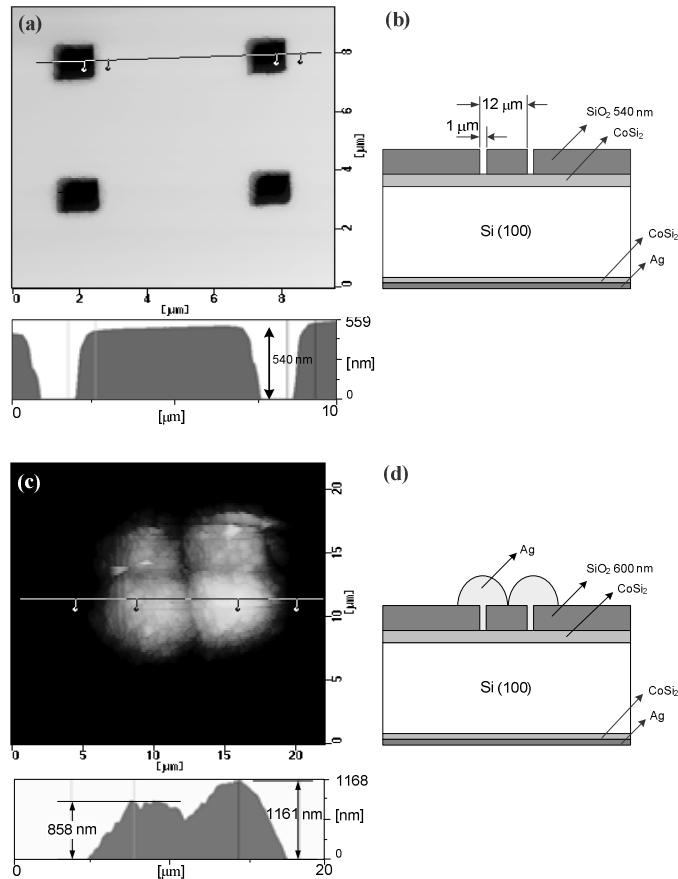


Figure 2.4.2: (a) AFM image around the well area before the electroplating, (b) Symmetric drawing of the cross sectional structure of the substrate. (c) AFM image around the well area after the electroplating of Ag at 200 pA for 5 min, (d) Schematic drawing of the cross sectional structure of the substrate.

of the bilayer, which preserve the intrinsic fluidity as well as the bilayer structure.[74-77] Vesicle fusion is the mixing of lipids between vesicles to form a larger, product vesicle and vesicle rupture is the conversion of a vesicle to a supported bilayer disk. In this thesis "vesicle fusion" is used to denote fusion events, while "vesicle rupture" is used to represent the conversion to a bilayer disk.

According to the size, the vesicles are classified into three types; small vesicle (<100 nm), large vesicle (0.1 to 1 μm), and giant vesicle (1 to 100 μm). Giant vesicles, especially, have received much attention to study the cell physiology as a model membrane due to the following advantages.

- Self-organization
- Stability in an aqueous medium
- Easy observation by optical methods
- Extent of visual information including morphological behavior to the small vesicles
- Various applications as a micro reaction environments for enzymatic reactions

Although small vesicles are easy to transform to SPLB, Giant vesicles were used in order to cover the 10-30 μm electrode area. In the present, I have fabricated well-structures of 1 μm diameter for the microelectrode on the surface of SiO_2/Si substrates, and deposited the SPLB membrane on the surface of the microelectrode area by the rupture of giant unilamellar vesicles. Since the electrode area is small (10~30 μm), the suspension of giant unilamellar vesicles (150~300 μm) was dialyzed to remove smaller vesicles from the suspension.

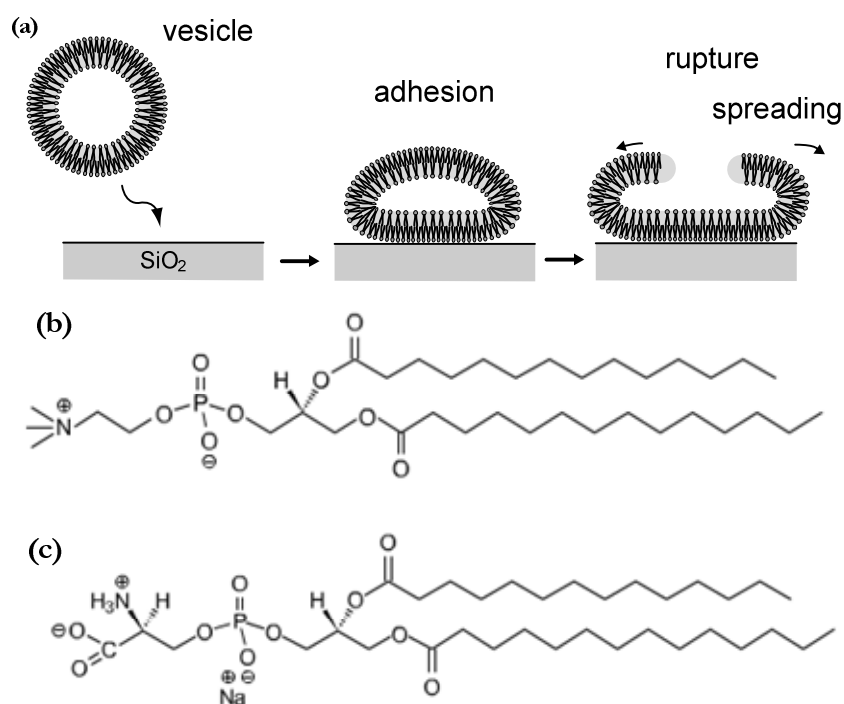


Figure 2.5.1: (a) Formation of bilayer on SiO_2 surface by rupture of vesicle. The molecular structure of (b) DPPC and (c) POPS.

Protocol of unilamellar giant vesicles preparation and formation of SPLB on a substrate

Figure 2.5.2 shows the protocol of vesicle preparation and formation of SPLB on a substrate.

01. Prepare 10 mg/ml lipid solution (DPPC:POPS:Rb = 89.5:10:0.5 weight ratio) in chloroform and methanol (2:1) [Fig.2.5.2(a)].

Lipid solutions:

DPPC: Dipalmitoylphosphatidylcholine

POPS: 1-palmitoyl-2-oleoyl-sn-3-[phosphor-L-Serin]

Rb: Diacyl phosphoethanolamine-N-lissamine Rhodamine B Sulfonyl
(fluorescence-labeled lipid)

02. Take 50 μ l of lipid solution in the glass vial and evaporate the solvent using a rotary evaporator with N₂ blowing for 30 min to form a thin lipid films on the wall [Fig.2.5.2(b)].
03. Dry the lipid film in vacuum chamber for 10 h [Fig.2.5.2(c)].
04. Add 5 ml of 10mM KCl solution into the vial and incubate for 12 h at 49°C [Fig.2.5.2(d)].
The lipid concentration of the obtained suspension was 0.1 mg/ml.
05. Dialysis of the solution by using 5 μ m filter (JM Type, Millipore, Ltd.) for 1hr [Fig.2.5.2(f)].
06. For the deposition of lipid bilayer membranes, the substrate was incubated for 1 h at 50°C by hotplate [Fig.2.5.2(g)] under the buffer solution formed by mixing the 200 μ l of the vesicle suspension and 50 μ l of CaCl₂ 50mM solution.
07. The sample was washed for five times at RT by the 10 mM KCl solution.

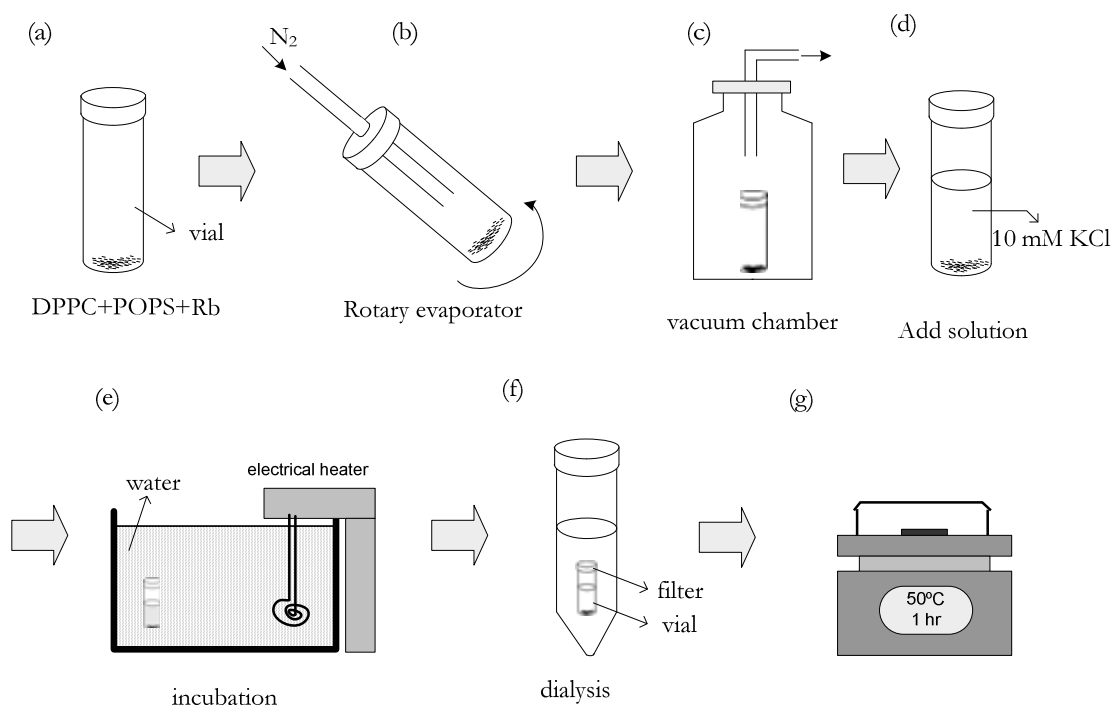


Figure 2.5.2: Protocol of unilamellar giant vesicles preparation and formation of SPLB on substrate

Figure 2.5.3(a) shows the fluorescence microscope image of a giant vesicle made by above procedure. Figure 2.5.3(b) shows the fluorescence microscope image after the rupture of the giant vesicle on SiO₂/Si substrate, The giant vesicle in this process was 150 ~ 300 μm in diameter, which is large enough to cover the electrode area (10 μm ~ 30 μm diameter) (more details in chapter 4).

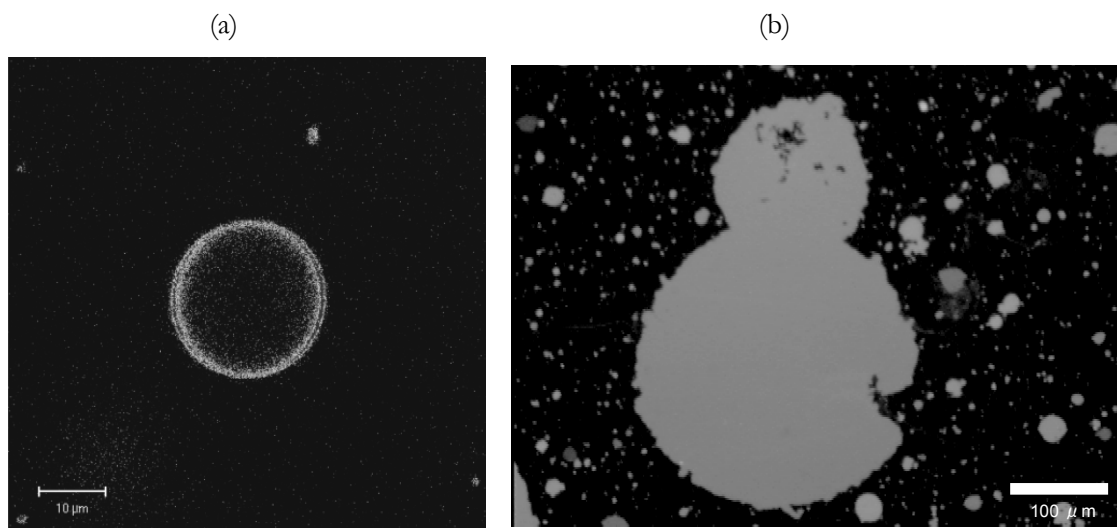


Figure 2.5.3. (a) Confocal microscopy image of a giant vesicle. (b) Fluorescence microscopy image of SPLB domains on SiO₂/Si substrate formed by the rupture of giant vesicle.

Measurement system

A patch-clamp system (CEZ-2400, Nihon-Koden Co., Japan) was used to measure the stability, electrical resistance, capacitance, and current noise of the bilayers. For data acquisition and analysis the eCell (Ver 2.12, InstruTECH Corporation) and Origin (Ver 6.0, Microcal Software Inc.) software was used. Figure 2.5.4(a) shows the schematic drawing of the system. The patch-clamp system used in the experiments is able to apply ± 200 mV.

The patch clamp technique is the central method in modern electrophysiology. [78] It allows the recording of single ion-channel currents, or alternatively currents from entire small cells. It traditionally uses a glass pipette as an "electrode" which is gently applied to a cell membrane through control by a skilled operator. The patch clamp technique was introduced to biology initially by Cole in the late 1930's and was exploited by the Hodgkin & Huxley team in the late 1940's. The technique has been applied widely since then using a variety of modifications. Recording of planar bilayers and patch clamp preparations provide the most detailed information now available concerning the biophysics of ion channels: they enable the study of single-channel conductance, opening and closing lifetimes, and opening and closing probabilities. I used a silicon based electrode instead of a glass pipette.

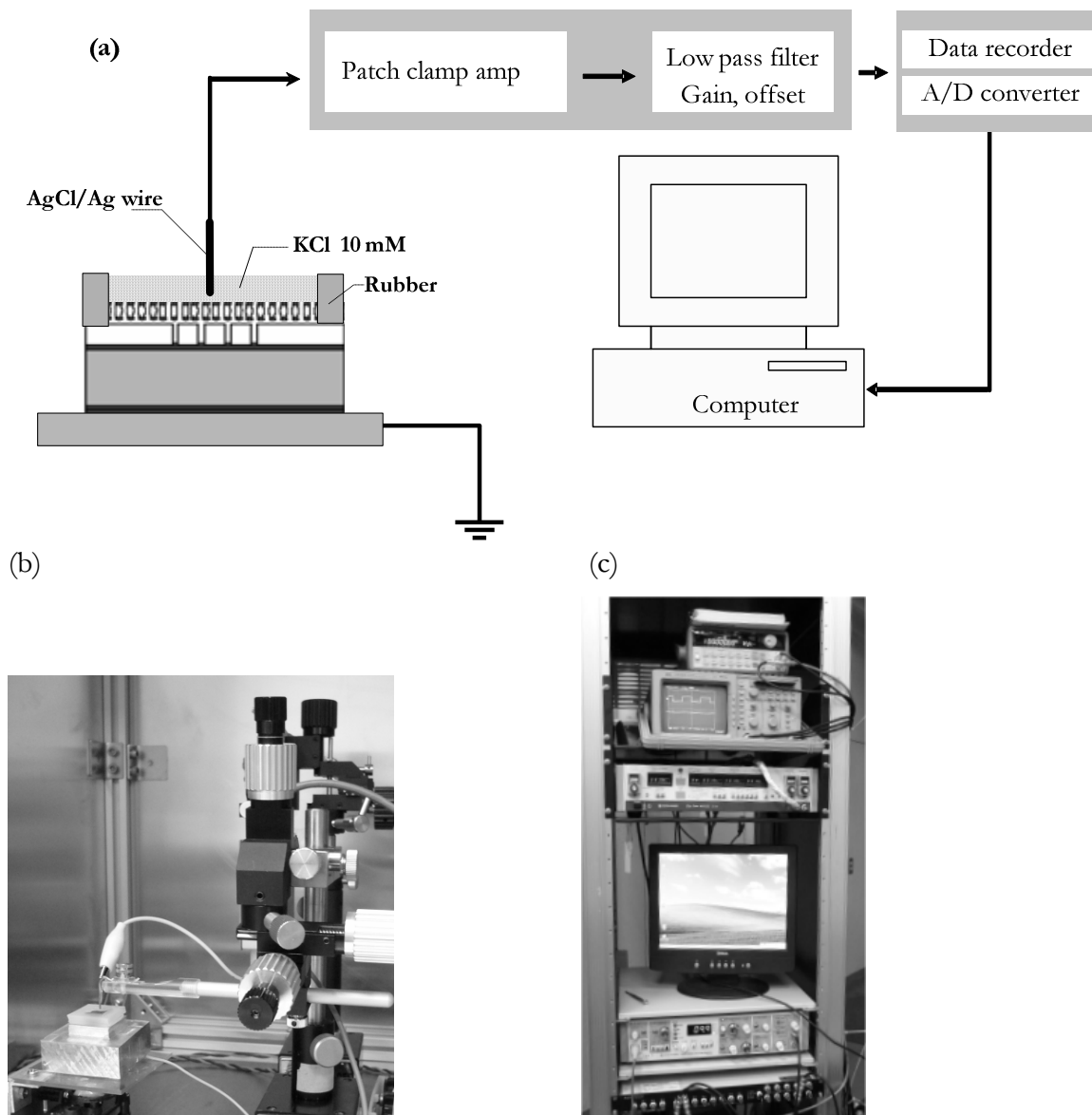


Figure 2.5.4: (a) Schematic drawing of the measurement system, (b) electrode cell chamber, and (c) measuring instruments used in the experiments.

Noise level

Usually suspended type planar bilayer experiments have some limitations[79]: (i) their noise level is higher than that in patch clamp recordings. This noise is mainly due to the large capacitance ($\gg 100$ pF) of most planar bilayers. (ii) Planar bilayer experiments are done with artificial lipid membrane in buffer solutions and are thus carried out under nonphysiological conditions. (iii) To study ion channels in planar lipid bilayers, the channels have to be reconstituted into the bilayer. [80]

I have fabricated the hole (well) with a diameter of about $1\ \mu\text{m}$ for the microelectrode on the surface of SiO_2/Si substrate, which would be desirable to reduce the capacitance across the bilayers, and to enable low-noise recordings. Figure 2.5.5 shows the output noise of the whole system measured in 10 mM KCl solution. The root mean square (RMS) value is $0.6\ \text{pA}$, which is quite low to measure the single channel current ($2 \sim 10\ \text{pA}$). The interface potential difference is $0.2\ \text{mV}$.

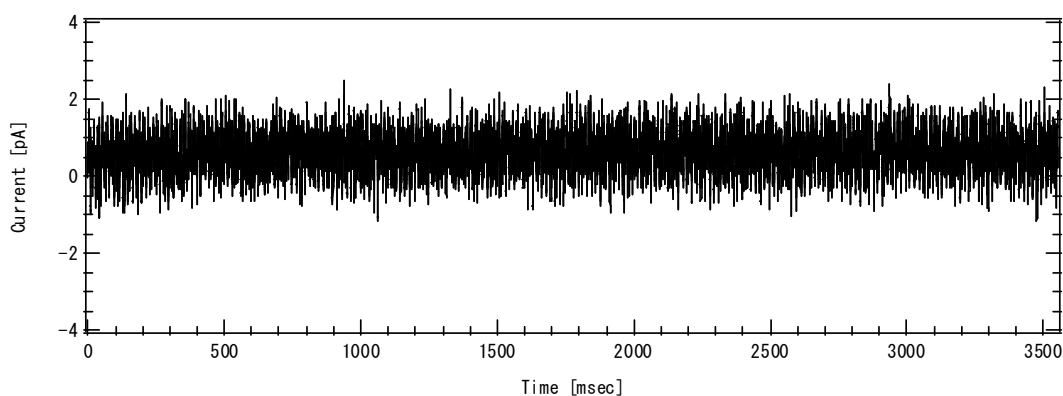


Figure 2.5.5: Output noise of the total system in 10mM KCl solution.

Reference

1. I.M. Ross, Bell Labs Technical Journal, **2** (1997) 3-14.
2. S.M. Sze, *Semiconductor Devices: Physics and Technology*. 1985: Wiley, New York.
3. K.K. Schuegraf, *Handbook of thin-film deposition processes and techniques : principles, methods, equipment, and applications*. Materials science and process technology series. Electronic materials and process technology. 1988, Park Ridge, N.J: Noyes. xvii, 413.
4. K. Wasa and S. Hayakawa, *Handbook of sputter deposition technology : principles, technology and applications*. Materials science and process technology series. Electronic materials and process technology. 1992, Park Ridge, N.J: Noyes. xii, 304.
5. B. Chapman, *Glow discharge processes : sputtering and plasma etching*. 1980, New York ; Chichester: Wiley. xv, 406.
6. A.O. Shilova, Surface Coatings International Part B-Coatings Transactions, **86** (2003) 195-202.
7. P.H. Chen, T. Chen, and H.C. Shih, Microelectronics Journal, **35** (2004) 985-987.
8. R. Osredkar, Microelectronics and Reliability, **34** (1994) 1265-1267.
9. S. Ito, Y. Homma, and E. Sasaki, Journal of Vacuum Science & Technology a-Vacuum Surfaces and Films, **9** (1991) 2696-2703.
10. S.K. Gupta, Microelectron. Testing, 10-12.
11. J. Taniguchi, K. Kanda, Y. Haruyama, S. Matsui, M. Tokunaga, and I. Miyamoto, Japanese Journal of Applied Physics Part 1-Regular Papers Short Notes & Review Papers, **41** (2002) 4304-4306.
12. P.D. Blais, International Society for Hybrid Microelectronics., Northern California Microphotomask/Masking Working Group., and Materials Research Society., *Submicron lithography*. Proceedings of SPIE--the International Society for Optical Engineering ; v. 333. 1982, Bellingham, Wash.: International Society for Optical Engineering. viii, 179.
13. J. Bondur, A.R. Reinberg, and SPIE., *Dry processing for submicrometer lithography : 12-13 October 1989, Santa Clara, California*. 1990, Bellingham, Wash: SPIE--the International Society for Optical Engineering. vii, 307.
14. J.H. Bruning, Journal of Vacuum Science & Technology, **17** (1980) 1147-1155.
15. H. Cliffe, *Lithography*. Studio Handbooks. 1965, Studio Vista., 96.
16. N.G. Einspruch and R.K. Watts, *Lithography for VLSI*. VLSI electronics microstructure science ; v. 16. 1987, Orlando ; London: Academic Press. xi, 361.
17. S.K. Ghandhi, *VLSI fabrication principles : silicon and gallium arsenide*. 2nd ed. Wiley-Interscience publication. 1994, New York ; Chichester: Wiley. xxiv, 834.
18. B. Fay, J. Trotel, and A. Frichet, Journal of Vacuum Science & Technology, **16** (1979) 1954-1958.
19. M.B. Heritage, Journal of Vacuum Science & Technology, **12** (1975) 1135-1145.
20. J.L. Mauer, H.C. Pfeiffer, and W. Stickel, Ibm Journal of Research and Development, **21** (1977) 514-521.
21. J.M. Moran and D. Maydan, Journal of Vacuum Science & Technology, **16** (1979) 1620-1624.
22. W.M. Moreau, *Semiconductor lithography : principles, practices, and materials*. Microdevices : physics and fabrication technologies. 1988, New York ; London: Plenum. xx, 931.
23. M. Parikh, Ibm Journal of Research and Development, **24** (1980) 438-457.
24. J.A. Reynolds, Solid State Technology, **22** (1979) 87-94.
25. W.C. Till and J.T. Luxon, *Integrated circuits : materials, devices, and fabrication*. 1982, Englewood Cliffs, N.J.: Prentice-Hall. xiii, 462.
26. R.K. Watts and J.H. Bruning, Solid State Technology, **24** (1981) 99-105.

27. K.A. Valiev, *The physics of submicron lithography*. Microdevices : physics and fabrication technologies. 1992, New York ; London: Plenum. xi, 493.
28. P. Weaver, *The technique of lithography*. 1964, London: Batsford. 176.
29. G. Woods, *Introducing lithography*. 1969, London New York: Batsford ;Watson-Guptill. 88.
30. M. Hatzakis, Makromolekulare Chemie-Macromolecular Symposia, **24** (1989) 169-175.
31. M. Hefher, J. Photog. Sci., **12** (1964) 181.
32. H. Moritz, Ieee Transactions on Electron Devices, **32** (1985) 672-676.
33. T. Batchelder, Proceedings of the Society of Photo-Optical Instrumentation Engineers, **275** (1981) 143-149.
34. M. Hatzakis, Journal of the Electrochemical Society, **134** (1987) C436-C436.
35. N.G. Einspruch, *VLSI electronics : microstructure science*. 1981, New York: Academic Press. v. [1 -19, 21 -24].
36. P.R. Deshmukh and W.S. Khokle, Ieee Transactions on Electron Devices, **36** (1989) 2011-2017.
37. F. Romanato, M. Tormen, L. Businaro, L. Vaccari, T. Stomeo, A. Passaseo, and E. Di Fabrizio, Microelectronic Engineering, **73-74** (2004) 870-875.
38. S.I. Kuroki, T. Kikkawa, H. Kochiya, and S. Shishiguchi, Japanese Journal of Applied Physics Part 1-Regular Papers Short Notes & Review Papers, **42** (2003) 1907-1910.
39. [Anon], Solid State Technology, **43** (2000) 18-+.
40. J.J. Degan, R.A. Colclaser, J.E. Sergent, and L. Palkuti, Ieee Transactions on Parts Hybrids and Packaging, **12** (1976) 273-275.
41. D.A. McGillis and D.L. Fehrs, Ieee Transactions on Electron Devices, **ED22** (1975) 471-477.
42. P. Vase, Y.Q. Shen, and T. Freltoft, Appl Surf Sci, **46** (1990) 61-66.
43. M.L. Gaillard, A. Quenzer, European Physical Society., European Federation for Applied Optics., SPIE., and Association nationale de la recherche technique., *High power lasers and laser machining technology : 25-28 April 1989, Paris, France : ECO2*. 1989, Bellingham, Wash: SPIE--the International Society for Optical Engineering. viii, 298.
44. A. Demmier, Aerospace Eng, **15** (1995) 42-42.
45. L. Schick, Photon Spectra, **23** (1989) 90-94.
46. B. Shen, M. Allard, S. Boughaba, R. Izquierdo, and M. Meunier, Can J Phys, **74** (1996) S54-S58.
47. E. Wiener-Avnear, Laser Focus World, **34** (1998) 105-+.
48. W. Pflöging, A. Ludwig, K. Seemann, R. Preu, H. Mackel, and S.W. Glunz, Appl Surf Sci, **154** (2000) 633-639.
49. S. Hirano, A. Yoshigoe, M. Nagasono, K. Mase, J. Ohara, Y. Nonogaki, Y. Takeda, and T. Urisu, Journal of Synchrotron Radiation, **5** (1998) 1363-1368.
50. T. Urisu, H. Kyuragi, Y. Utsumi, J. Takahashi, and M. Kitamura, Review of Scientific Instruments, **60** (1989) 2157-2159.
51. H. Akazawa, J. Takahashi, Y. Utsumi, I. Kawashima, and T. Urisu, Journal of Vacuum Science & Technology a-Vacuum Surfaces and Films, **9** (1991) 2653-2661.
52. Y.B. Park, S.W. Rhee, Y. Imaizumi, and T. Urisu, Journal of Applied Physics, **80** (1996) 1236-1238.
53. T. Urisu, J. Takahashi, Y. Utsumi, and H. Akazawa, Applied Organometallic Chemistry, **5** (1991) 229-241.
54. J. Takahashi, Y. Utsumi, H. Akazawa, I. Kawashima, and T. Urisu, Applied Physics Letters, **58** (1991) 2776-2778.
55. H. Akazawa, Y. Utsumi, J. Takahashi, and T. Urisu, Applied Physics Letters, **57** (1990) 2302-2304.
56. C.S. Wang and T. Urisu, Japanese Journal of Applied Physics Part 1-Regular Papers Short Notes & Review Papers, **42** (2003) 4016-4019.
57. T. Urisu and H. Kyuragi, Journal of Vacuum Science & Technology B, **5** (1987) 1436-1440.

58. Y. Utsumi, J. Takahashi, and T. Urisu, *Journal of Vacuum Science & Technology B*, **9** (1991) 2507-2510.
59. A.J. Bard, L.R. Faulkner, C.G. Zoski, and J. Leddy, *Electrochemical methods : fundamentals and applications*. 2nd ed. 2001, New York ; Chichester: Wiley. xxi, 833.
60. D.T. Sawyer, A. Sobkowiak, and J.L. Roberts, *Electrochemistry for chemists*. 2nd ed. 1995, New York ; Chichester: Wiley. xv, 505.
61. D.J.G. Ives and G.J. Janz, *Reference electrodes, theory and practice*. 1961, New York: Academic Press. 651.
62. J.W. Hill and D.K. Kolb, *Chemistry for changing times*. 9th ed. 2001, Upper Saddle River, NJ: Prentice Hall. xxv, 623.
63. K.B. Oldham and J.C. Myland, *Fundamentals of electrochemical science*. 1994, San Diego ; London: Academic Press. xxii, 474 .;
64. J.O.M. Bockris, N. Bonciocat, and F. Gutmann, *An introduction to electrochemical science*. 1974, London: Wykeham Publications. x, 133.
65. K.E. Langford, *Analysis of electroplating and related solutions*. 1951, Teddington, Eng.: Electroplating and metal finishing. 387.
66. E.A. Ollard, *Elementary science for electroplating students and foremen*. 1961, Teddington Eng.: Robert Draper. 99.
67. M. Schlesinger and M. Paunovic, *Modern electroplating*. 4th ed. Electrochemical Society series. 2000, New York ; Chichester: John Wiley. xiv, 868.
68. W.R. Barclay and C.H. Hainsworth, *Electroplating, by W.R. Barclay and C.H. Hainsworth*. 1912, Lond.
69. W. Blum and G.B. Hogaboom, *Principles of electroplating and electroforming : (electrotyping)*. 3d ed. 1949, New York: McGraw-Hill. xv, 455.
70. *Advances in electrochemical science and engineering*. 1990, Weinheim: VCH.
71. A.J. Bard and L.R. Faulkner, *Electrochemical methods : fundamentals and applications*. 1980, New York ; Chichester: Wiley. xviii, 718.
72. H.M. McConnell, T.H. Watts, R.M. Weis, and A.A. Brian, *Biochimica Et Biophysica Acta*, **864** (1986) 95-106.
73. R. Tero, M. Takizawa, Y.J. Li, M. Yamazaki, and T. Urisu, *Langmuir*, **20** (2004) 7526-7531.
74. T.M. Bayerl and M. Bloom, *Biophysical Journal*, **58** (1990) 357-362.
75. T.M. Bayerl and M. Bloom, *Biophys J*, **58** (1990) 357-62.
76. S.J. Johnson, T.M. Bayerl, D.C. McDermott, G.W. Adam, A.R. Rennie, R.K. Thomas, and E. Sackmann, *Biophys J*, **59** (1991) 289-94.
77. S. Krueger, B.W. Koenig, W.J. Orts, N.F. Berk, C.F. Majkrzak, and K. Gawrisch, *Basic Life Sci*, **64** (1996) 205-13.
78. E. Neher, *Neuron*, **8** (1992) 605-612.
79. M. Mayer, J.K. Kriebel, M.T. Tosteson, and G.M. Whitesides, *Biophysical Journal*, **85** (2003) 2684-2695.
80. C. Miller, *Ion channel reconstitution*. 1986, New York ; London: Plenum.

Chapter 3

3 Shrinking of Spin-on-Glass Films Induced by Synchrotron Radiation and Its Application to Three- Dimensional Microfabrications

Japanese Journal of Applied Physics

Vol. 43, No. 6B, 2004, pp. 3941-3944

Abstract

Photoinduced etching of siloxane-type spin-on-glass (SOG) by synchrotron radiation (SR) using a SF_6/O_2 etching gas and a Co contact mask has been investigated. The SOG film was etched by direct SR irradiation similarly to the case of thermally oxidized SiO_2 . I found that the indirect exposure to SR caused shrinkage of SOG under the Co mask. The shrinkage depth of SOG was attenuated by the thickness of the Co mask, but not eliminated even by a Co mask 350 nm thick, due to the high-energy photons (≥ 230 eV) being transmitted through the mask. The shrinkage phenomenon was successfully applied in the fabrication of a three-dimensional structure of the SOG thin film on Si(100). Atomic force microscopy observations showed that the surfaces were very smooth both on the completely etched Si area and on the shrunken SOG area. I investigated the mechanism of the shrinkage of SOG by Fourier-transform infrared spectroscopy.

3.1 Introduction

Spin-on-glass (SOG) is an important material in semiconductor processes and is widely used for flattening interlevel dielectrics which improve the step coverage of the upper metal level.[1] In the IC fabrication process, the curing temperature of a SOG film is usually limited to 420°C as a maximum because of the presence of aluminum interconnections. Higher-temperature annealing may improve the material properties but cannot be adopted after the incorporation of the first Al level. The properties of annealed SOG are comparable to those of SiO₂ made by chemical vapor deposition, which is widely used in very-large-scale-integrated technology.[2] To improve the material properties of SOG, several techniques such as ion implantation[3] and electron-beam curing[4] have been proposed.

Synchrotron radiation (SR) stimulated semiconductor processes have been attracting considerable attention from the viewpoint of developing new semiconductor process technologies. SR stimulated process have many advantages, such as selective cleaving of chemical bonds by exciting certain dissociative energy levels, low damage to substrates in comparison with plasma processes, and a high spatial resolution and aspect ratio because of the short wavelengths used. A large number of studies have been reported on SR etching or ablation of SiO₂. [5, 6] However, very few studies of the SR process on SOG surfaces have been performed. The SR etching experiment with SOG by Taniguchi *et al.*[7] is the only report to the best of my knowledge. They showed that the curing of SOG occurred by exposure to SR in ultra high vacuum without etching gas at room temperature (RT) and was related to the carbon concentration in SOG, whereas the etching of thermally oxidized SiO₂ under the same conditions had been reported to be negligible.[8]

In this work, I have performed experiments on the SR etching of SOG using a Co thin film as an etching mask and a mixture of SF₆ and O₂ as an etching gas. It was found that the thickness of SOG under the Co mask was also reduced by irradiation with the SR beam. The

shrinkage phenomenon is a photoinduced process caused by SR permeating through the Co mask due to the high-energy photons rather than a thermal process, because the SOG is pre-annealed at 425°C before irradiation with SR. The shrinkage of SOG was attenuated by increasing the Co thickness. An application of this phenomenon to a three-dimensional (3D) microfabrication process using Co masks of varying thickness has also been demonstrated. Atomic force microscopy (AFM) observations showed that the surface of the shrunken SOG was as flat as a mirror-polished silicon surface. I have also investigated the mechanism and the characteristics of the shrinkage process by Fourier-transform infrared spectroscopy (FT-IR).

3.2 Experimental

A Si(100) wafer (*p*-type, 0.03 Ω cm) covered by native oxide was first cleaned in acetone, ethanol and de-ionized water in an ultrasonic bath for 5 min each. Then it was immersed in a solution of concentrated H₂SO₄ and H₂O₂ (30%) (7:3 in volume ratio) at 120°C for 2 min and treated with a diluted HF solution (2.5%) for 2 min to remove the surface oxide layer. A commercial siloxane-type SOG (Accuglass 512B, Honeywell) was used in this study. It is composed primarily of siloxane which contains CH₃ (15% organic content) as illustrated in Fig. 3.1. The SOG was spin-coated onto a 14×14 mm² silicon wafer at a spin rate of 3000 rpm for 10 s. Immediately after the spin-coating, the film was subjected to three stages of soft baking on hot plates at 80°C, 150°C and 250°C for 1 min at each temperature. The final curing was performed at 425°C for 30 min under a nitrogen gas flow of 1.0 liter min⁻¹. After these curing processes, the thickness of the SOG film on the Si wafer was approximately 550 nm. Patterned Co layers were deposited on the SOG surface as an etching contact-mask by sputtering deposition combined with photolithography and the lift-off technique.[9] The Co contact-mask could be removed without damaging the

substrate by immersion into 0.1 N HNO₃ aq.[9]

The SR etching of the SOG/Si(100) substrate was carried out at beam line 4A2 of the SR facility (UVSOR) at the Institute for Molecular Science. The electron beam energy was 750 MeV. The emitted beam with horizontal acceptance angle of 11 mrad was reflected by 6° and focused on the sample surface by a bent-elliptical mirror 490 mm long. The SR light irradiated the sample directly without passing through any window because of the large pressure difference between the etching chamber and the beam line produced by a differential vacuum pumping system. Details of the apparatus for SR etching were described in an earlier article.[10] The beam diameter on the sample surface was about 9 mm, and the calculated total photon flux was 4.2×10^{16} photons s⁻¹ for the 100 mA ring current. In this study, all the SR etching processes were performed in a gas mixture of SF₆ (0.05 Torr) and O₂ (0.002 Torr) using a Co thin film contact mask at RT. The sample surface was set normal to the incident SR beam.

The surface structure of the samples was investigated using a step profile meter (Dektak3, ST), a scanning electron microscope (SEM) (JSM-5510, JEOL) and an AFM (SPI-3800N, Seiko Instruments Inc.). The AFM images were obtained in the dynamic-force mode (=tapping mode) using a Si cantilever (SI-DF40, spring constant = 43 N/m). The IR spectra were measured by a FT-IR spectrometer (FT/IR 620, JASCO) in the transmission mode under vacuum using a tri-glycine-sulfate detector (TGS) at 4 cm⁻¹ resolution for 300 scans. The Si (100) wafers with higher resistivity (40 ± 1 Ω cm) were used for the measurement of IR transmission spectrum, because the Si wafer was sufficiently transparent for IR.

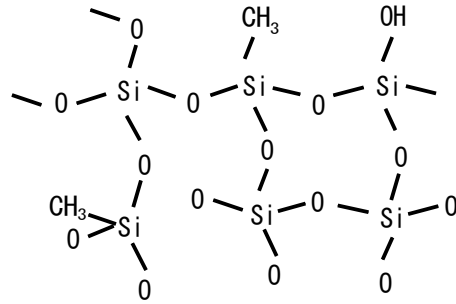


Figure 3.1: Structure of Accuglass 512B, composed mainly of siloxane.

3.3 Results and Discussion

3.3.1 SR-induced etching and shrinkage of SOG

Figure 3.2 shows the line profiles of the Co/SOG/Si surface measured by the step profile meter before and after exposure to 2.00×10^4 mA min of SR. There are three regions on the sample surface as shown in Fig. 3.2(a); (A) an open region and regions covered by (B) a thinner (230 nm) Co mask and (C) a thicker (560 nm) Co mask. The line profile of the SOG/Si surface after the removal of the Co layer with HNO₃ aq. (0.1 N) is superimposed in Fig. 3.2(b). The SOG film at the open region (A) is completely etched after exposure to SR, and the etching stops at the Si surface as reported by Urisu and Kyuragi.[11] The important point to note is that the thickness of the SOG film diminishes even in the region covered by the Co mask. At regions B and C, the SOG film shrinks by 152 nm and 10 nm, respectively.

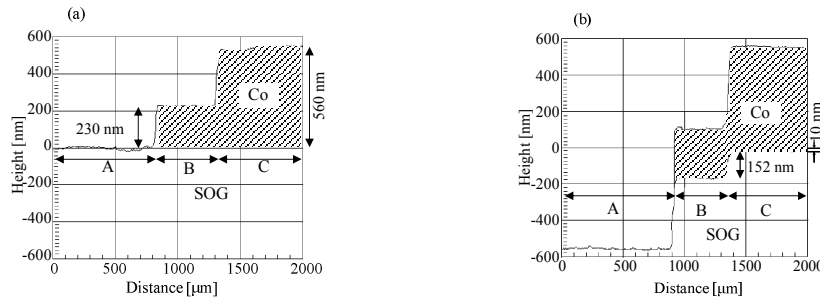


Figure 3.2: Step profiles of the Co/SOG/Si surface (a) before and (b) after SR etching. The step profile of SOG/Si after removal of the Co layer is superimposed in (b).

Figure 3.3 shows the etched depth of the SOG film induced by direct SR irradiation ranging from 2.00×10^3 to 1.80×10^4 mA min. The etched depth of SOG increases with the SR dose, but not linearly. The higher etching rate at the initial stage is probably due to the shrinkage effect, which also occurs with direct SR irradiation, as well as the etching reaction. The etching proceeds linearly at a lower rate (1.1×10^{-2} nm mA⁻¹ min⁻¹) after saturation of the shrinkage at 1.00×10^4 mA min exposure.

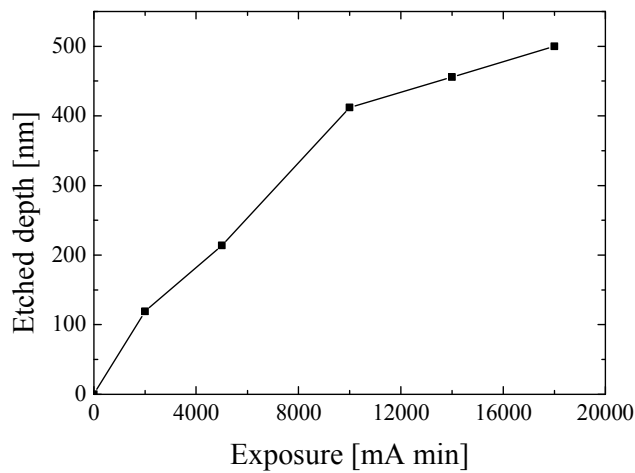


Figure 3.3: Etched depth of SOG as a function of SR exposure. The reaction gas was SF₆ (0.05 Torr) + O₂ (0.002 Torr). The original SOG film thickness was 480 nm.

Figure 3.4 shows the depth of SOG due to shrinking induced by 2.00×10^4 mA min of indirect SR irradiation as a function of the Co mask thickness. Two samples, which were cured at 200°C and 425°C in the preparation process, were investigated. The shrinkage of SOG does not completely stop even with the 350 nm thick Co mask due to the high-energy photons (≥ 230 eV) being transmitted through the Co mask. The depth is almost the same for the two samples with different curing processes. This indicates that the precuring temperature does not affect the shrinkage.

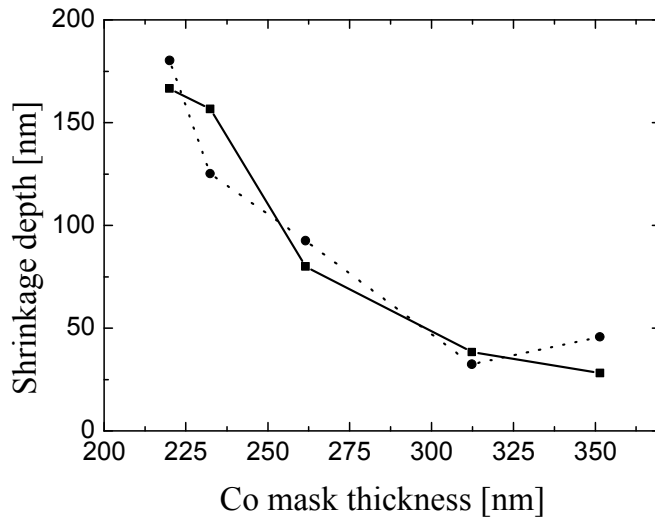


Figure 3.4: Shrinkage depth of SOG as a function of Co mask thickness. Thickness of the SOG film before exposure to SR was 480 nm, measured by a step profile meter (Dektak3, ST). Exposure was 2.00×10^4 mA min. Precuring temperatures were 425°C (■) and 200°C (●).

I have applied this shrinkage phenomenon to the fabrication of a 3D structure. The Co contact mask was deposited in two steps as shown in Fig. 3.5(a). First a line-and-space pattern was formed by photolithography and the lift-off technique (mask A). Then a rectangular Co layer was deposited using a stainless mask (mask B). The thicknesses of the former and the latter masks were

315 nm and 245 nm, respectively. Thus the SOG surface was covered with Co masks of 560, 315 and 245 nm thick which are represented by areas 1-3 in Fig. 3.5, respectively. The area without the Co mask is represented by area 4 in Fig. 3.5. Figure 3.5(b) shows the SEM image of the SOG/Si surface after exposure to 2.00×10^4 mA min of SR using the Co mask shown in Fig. 3.5(a), followed by the removal of the Co mask with HNO_3 aq. (0.1 N). The 3D structure of SOG is successfully obtained with only one time of SR exposure, because the thinner the Co mask is, the deeper the SOG shrinks. Figure 3.5(c) shows the schematic drawing of the 3D structure in Fig. 3.5(b). The height of each area has been measured using the step profile meter. The depth of each area is reasonable in comparison with Fig. 3.4.

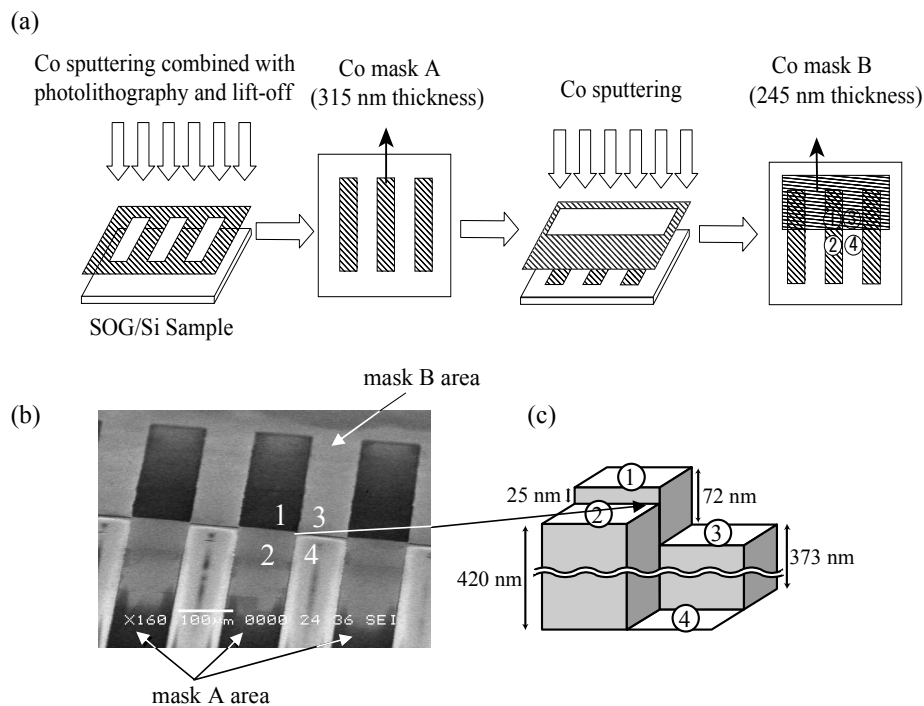


Figure 3.5: (a) Fabrication process of the Co contact mask. Mask A (315 nm thick) and mask B (245 nm thick) were overlapped. (b) SEM image of the 3D structure of SOG on Si fabricated by exposure to 2.00×10^4 mA min of SR using the Co contact mask in (a). (c) Schematic drawing of the 3D structure.

Figure 3.6 shows the surface roughness of areas 1-4 in Fig. 3.5(b) measured by AFM. The surface on area 4, where the SOG is completely etched to the Si surface, is very flat ($R_a \cong 0.40$ nm), as expected on the basis of previous results.[6,9] The Small particles visible on areas 1-3 may be contamination that adhered during the Co removal process when the samples were carried out of the clean room to the AFM apparatus. The substrate surfaces of SOG on areas 1-3 are also quite flat as a mirror-polished silicon surface, and the values of R_a are approximately 0.75, 0.65 and 0.48 nm, respectively.

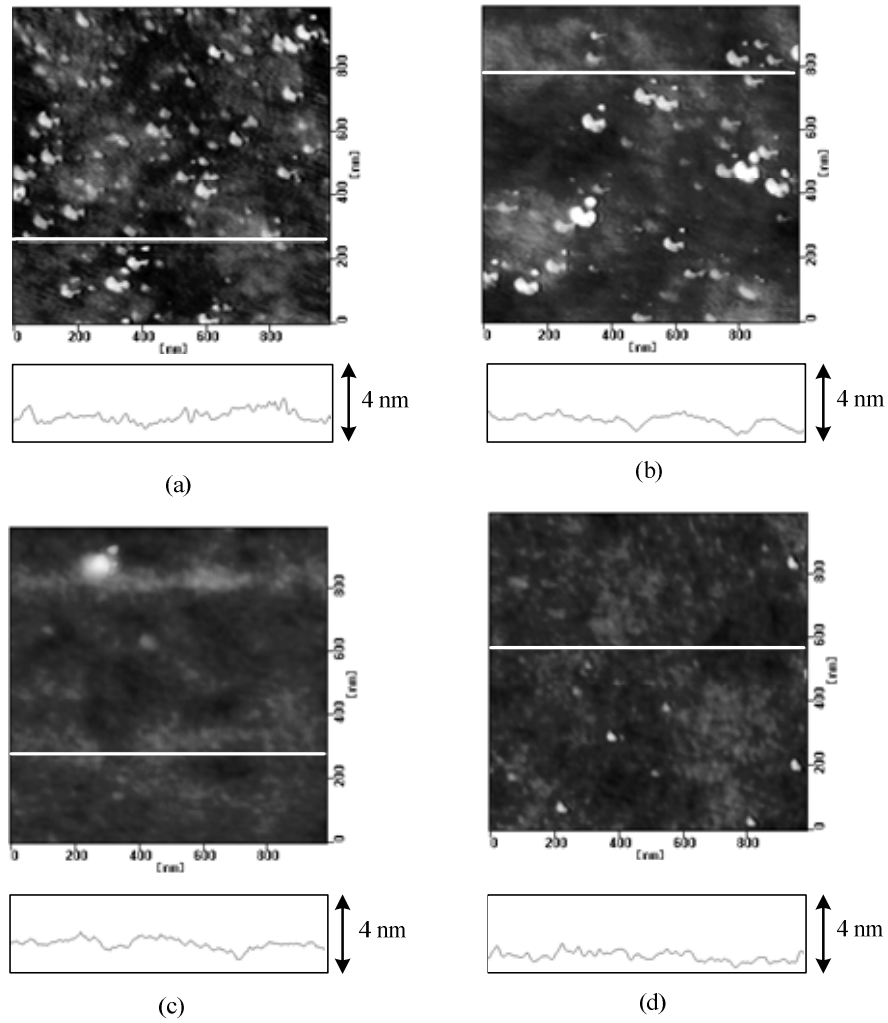


Figure 3.6: (a-d) AFM images of the areas 1-4 in Fig. 3.5(b), respectively. Surface roughness of areas 1-4 are $R_a \cong 0.75, 0.65, 0.48,$ and 0.4 nm, respectively.

3.3.2 Change in IR absorption spectrum induced by SR

I have investigated the mechanism of the SR-induced shrinkage by measuring the change in the FT-IR absorption spectrum (Fig. 3.7). To eliminate the ablation effects of direct SR irradiation, the SOG(550 nm thick)/Si sample surface was covered by a Co thin film (250 nm thick). The sample was cut into two pieces, and one was exposed to 1.00×10^4 mA min of SR at RT. The single-beam IR transmission spectra were successively measured for both the irradiated and the nonirradiated samples after removing the Co film using 0.1 N HNO₃ aq. The spectrum shown in Fig. 3.7 is given by $-\log(I/I_0)$, where I_0 and I are the observed single-beam IR transmission spectra of the nonirradiated and irradiated samples, respectively. Thus the negative and positive peaks in Fig. 3.7 show that the corresponding species have decreased and increased in response to the SR, respectively.

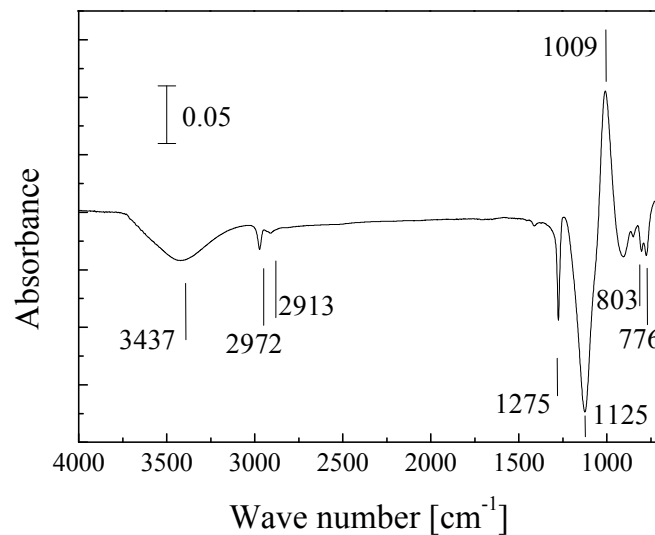


Figure 3.7: Differential spectrum of the FT-IR absorbance of the SOG films on Si(100) surfaces. The spectrum is obtained by $-\log(I/I_0)$, where I_0 and I are the single-beam IR transmission spectra of the sample before and after the exposure to 1.00×10^4 mA min of SR, respectively.

The observed band at 3437 cm^{-1} is assigned to the O-H stretching vibration of bulk H_2O .^[12] The 2972 cm^{-1} and 2913 cm^{-1} peaks are assigned to the asymmetric stretching vibrations of methyl ($-\text{CH}_3$) groups and methylene ($-\text{CH}_2$) groups, respectively.^[13] The 1275 cm^{-1} band is assigned to the Si-C stretching vibration.^[14] The 1125 cm^{-1} and 1009 cm^{-1} peaks are assigned to the Si-O stretching vibrations of SiO_x , the frequency of which is known to shift from 1075 cm^{-1} to 940 cm^{-1} as x decreases from 2 to 1.^[15] Here, the 1009 cm^{-1} peak is positive which means that SiO_2 reconstructed to denser SiO_2 , similarly to thermally oxidized SiO_2 . The 776 cm^{-1} and 803 cm^{-1} peaks are assigned to the multiple peaks of $\text{Si}(\text{O})_x\text{-CH}_3$.^[16]

The IR spectrum in Fig. 3.7 reveals that transmitting SR through the Co mask causes the reconstruction of SiO_2 along with the desorption of the organic compounds. Yamada and Takahashi have reported that the Si-O-Si bond forms in the methylsiloxane-type SOG when the substrate is cured at 450°C .^[14] In this shrinkage process, I cured the sample at 425°C before the IR experiments. The shrinkage of SOG caused by transmitting SR is a photoinduced process, which is completely different from thermal reconstruction. The result in Fig. 3.4 indicates that the final form of SiO_2 after the SR process is independent of the precuring temperature.

Based on the assignments of the peaks in Fig. 3.7 and the structural information on SOG materials, I consider the mechanism of the shrinkage phenomenon as follows. The SR excites the core and valence electrons of Si, O and C atoms and breaks the Si-C, Si-O, C-H and O-H bonds. The emission of the secondary electrons accompanying these excitations may also contribute to these bond dissociations. Some of the dissociated species may recombine with the dangling bonds in the bulk, but the significant shrinkage effect indicates that the majority of these dissociated species desorbs from the bulk to the vacuum in such forms as CO_2 , H_2O and CH_4 .^[16] Si- dangling bonds, which result from Si-C and Si-O bond breakage, are the driving force of the reconstruction to denser SiO_2 .

3.4 Conclusion

I have found that the thickness of the SOG film on the Si(100) surface is reduced by SR under a Co mask. This shrinkage phenomenon is a photoinduced process occurring due to the transmission of SR through the Co mask. A 550 nm thick SOG film shrinks by 152 nm under the Co mask that is 230 nm thick after exposure to 2.0×10^4 mA min of SR. Without the Co mask, the etching depth of SOG increased with the SR dose and the SOG film was completely removed by an exposure of 1.8×10^4 mA min. The shrinkage of SOG decreased with an increase in the Co mask thickness. Utilizing this phenomenon, I have successfully fabricated a 3D SOG structure by a one-time SR exposure. To investigate the mechanism of the shrinkage effect, I measured the FT-IR absorption spectra of SOG samples before and after the SR. The SR excites the core and valence electrons of Si, O and C atoms, and breaks the Si-C, Si-O, C-H and O-H bonds.

Reference

1. N. Oda, T. Usami, K. Kishimoto, A. Matsumoto, K. Mikagi, K. Kikuta, H. Gomi, and I. Sakai, VLSI Technology, 1997. Digest of Technical Papers., 1997 Symposium on, (1997) 79-80.
2. F. Dupuis, W.G. Oldham, and Y. Shacham-Diamand. in *IEEE 1985 Symp. VLSI Technology*. 1985. New York, 1985 p. 52.
3. Y. Shachamdiamand, E. Finkman, Y. Pinkas, and N. Moriya, Appl Phys Lett, **59** (1991) 2953-2955.
4. C.F. Lin, I.C. Tung, and M.S. Feng, Jpn J Appl Phys 1, **38** (1999) 6253-6257.
5. H. Akazawa, J. Takahashi, Y. Utsumi, I. Kawashima, and T. Urisu, Journal of Vacuum Science & Technology a-Vacuum Surfaces and Films, **9** (1991) 2653-2661.
6. Y. Nonogaki, H. Hatate, R. Oga, S. Yamamoto, Y. Fujiwara, Y. Takeda, H. Noda, and T. Urisu, Materials Science and Engineering B-Solid State Materials for Advanced Technology, **74** (2000) 7-11.
7. J. Taniguchi, K. Kanda, Y. Haruyama, S. Matsui, M. Tokunaga, and I. Miyamoto, Jpn J Appl Phys 1, **41** (2002) 4304-4306.
8. H. Akazawa, Y. Utsumi, J. Takahashi, and T. Urisu, Appl Phys Lett, **57** (1990) 2302-2304.
9. C.S. Wang, S.D. More, Z.H. Wang, S. Yamamura, Y. Nonagaki, and T. Urisu, J Vac Sci Technol B, **21** (2003) 818-822.
10. S. Hirano, A. Yoshigoe, M. Nagasono, K. Mase, J. Ohara, Y. Nonogaki, Y. Takeda, and T. Urisu, J Synchrotron Radiat, **5** (1998) 1363-1368.
11. T. Urisu and H. Kyuragi, Journal of Vacuum Science & Technology B, **5** (1987) 1436-1440.
12. S.W. Chung, J.H. Shin, N.H. Park, and J.W. Park, Jpn J Appl Phys 1, **38** (1999) 5214-5219.
13. R. Snyder, H. Strauss, and C. Elliger, J. Phys. Chem, 5145.
14. N. Yamada and T. Takahashi, Jpn J Appl Phys 1, **39** (2000) 1070-1073.
15. P.G. Pai, S.S. Chao, Y. Takagi, and G. Lucovsky, Journal of Vacuum Science & Technology a-Vacuum Surfaces and Films, **4** (1986) 689-694.
16. J.D. Romero, M. Khan, H. Fatemi, and J. Turlo, J Mater Res, **6** (1991) 1996-2003.

Chapter 4

4 Giant Vesicle Fusion on Microelectrodes Fabricated by Femtosecond Laser Ablation Followed by Synchrotron Radiation Etching

Japanese Journal of Applied Physics (Pt2 Letter, in press)

Abstract

I have developed a new technique for fabricating a hole (well) with a diameter of about 1 μm for a microelectrode on the surface of SiO_2 (600 nm)/ CoSi_2 (10 nm)/Si substrate. This process enabled the fabrication of electrode holes while maintaining the original nanolevel flatness ($R_a \sim 0.8$ nm) of the SiO_2 surface. A lipid bilayer was formed by giant vesicle fusion on these microelectrodes. Fluorescence microscope, *in situ* atomic force microscope and electrical characteristics measurements showed that a single lipid bilayer of sufficiently high resistance (gigaohm seal) was successfully fabricated.

4.1 Introduction

The preparation of protein-incorporating supported planar lipid bilayers (SPLBs) by vesicle fusion on solid supports was pioneered by the group of McConnell for studying cell-cell interaction processes.[1] The vesicle fusion method is a feasible and prevalent technique for forming supported membranes on solid surfaces.[2] A substantial body of evidence suggests that a thin layer of water approximately 1~2 nm thick is trapped between the support and the headgroups of the lower leaflet of the bilayer.[3] Since the SPLBs have the advantage of long-term and high mechanical stability compared with black lipid membranes,[4] they have been used not only in the *in vitro* basic research of cell-membrane-related phenomena such as cell-cell recognition in the immune system,[2] but also in the applied research of biosensors and biochips,[5,6] which are useful in diagnostics for many serious diseases and drug screening assays. Concerning ion channel biosensors, single ion channel recordings have been realized in suspended membranes made by the painting method on micromachined supports.[7,8] In the SPLBs made by vesicle fusion, however, single channel recordings have not yet been reported. It is considered that a major challenge is the production of tightly sealed bilayers to reduce leakage currents to the levels found in suspended membranes, and most likely, this will require the reduction of the substrate surface roughness and the elimination of edge effects.[9] In spite of the difficulty in fabrication, solid-supported membranes, especially supported membranes on microelectrodes, are extremely attractive because

of their potential of high stability and high density of integration. Therefore, efforts to attain high resistivity in supported membranes have been carried out by several groups.[5] Terrettaz *et al.* achieved a tethered lipid bilayer with a high electrical resistance of $\sim 130 \text{ M}\Omega$ and the subsequent detection of only a few synthetic ligand-gated ion channels incorporated in the tethered lipid bilayer.[5]

In the present work, I have fabricated hole (well) structures with AgCl/Ag electrodes at the bottom surface of $\text{SiO}_2/\text{CoSi}_2/\text{Si}$ substrates, while maintaining the SiO_2 surface roughness at less than 1 nm using a femtosecond laser microfabrication technique[10] and synchrotron radiation (SR) etching.[11] An SPLB membrane was formed on the surface of a microelectrode area by the fusion of giant vesicles. The measured electrical resistance was 1.2 G Ω .

4.2 Experiment

1-Palmitoyl-2-oleoyl-sn-3-[phosphor-L-serin] (POPS), and fluorescence-labeled lipid diacyl phosphoethanolamine-N-lissamine rhodamine B sulfonyl (Rb) were purchased from Avanti Polar Lipid. Dipalmitoylphosphatidylcholine (DPPC) was provided by Nippon Fine Chemical. HF, H_2O_2 , H_2SO_4 , HCl, HNO_3 solutions, CaCl_2 and KCl were of analytical grade and purchased from Sigma-Aldrich. All of the chemicals and solvents were used without further purification. The purities of Co and SiO_2 sputter targets and Ag wires (0.5 mm diameter) were 99.99%. Spin-on-glass (SOG) was purchased from Rasa Industries. Si(100) wafers (p type, B doped, 0.018 $\Omega \text{ cm}$, and 525 μm in

thickness) were purchased from Miyoshi. Water with a typical resistivity of $>18 \text{ M}\Omega \text{ cm}$ was produced using a Milli-Q purification system (Millipore, Ltd.).

Figure 4.1 shows the fabrication process for the well structures with microelectrodes. A Co thin film (10 nm thick) was sputter deposited on a mirror-polished Si(100) surface after conventional wet cleaning and Co (10 nm thick) and Ag (100 nm thick) films on the rough back surface [Fig. 4.1(b)]. After that, a SiO₂ thin film consisting of SOG (400 nm thickness) and sputtered SiO₂ (200 nm thickness) were deposited [Fig. 4.1(c)], then the sample was annealed at 540°C for 10 min. The Co layer was changed to CoSi₂ and the Co/Si interface became ohmic [Fig. 4.1(d)]. The sample was then annealed by SR irradiation to remove gas from SOG [Fig. 4.1(e)]. [12] A Co layer as an etching contact-mask was deposited on the SOG surface by sputtering [Fig. 4.1(f)], and electrode hole mask patterns were made using a femtosecond laser ($\lambda=1,560 \text{ nm}$, average power= 250 mW, frequency= 258 KHz, pulse width= 900 fs, and irradiation time= 4 ms) [Fig. 4.1(g)]. The diameter of an electrode hole was about 1 μm . SR etching of the SiO₂ layer for making the well on the electrode was carried out at beam line 4A2 of the SR facility (UVSOR) at the Institute for Molecular Science, using a mixture of SF₆ (0.05 Torr) and O₂ (0.002 Torr) as the etching gas [Fig. 4.1(h)]. The SR etching provides a vertical side wall and completely stops at the CoSi₂ surface. [11] The Co contact-mask was successfully removed without damaging the substrate by immersion into 0.1 M HNO₃ aq. [Fig. 4.1(i)]. Ag (50 nm thickness) was deposited on CoSi₂

electrode surfaces by electroplating [Fig. 4.1(j)]. Then, AgCl/Ag was formed also by electroplating

[Fig. 4.1(k)].

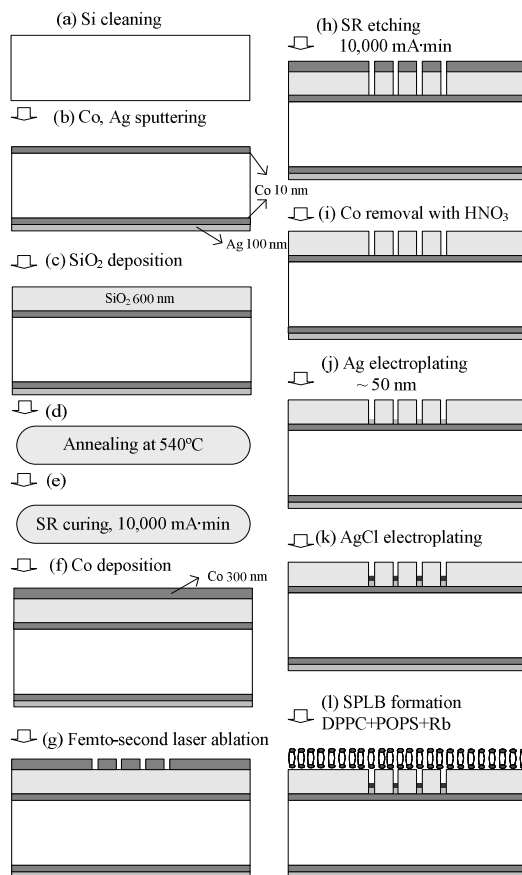


Figure 4.1: Schematics of fabrication process for supported membrane substrate with

AgCl/Ag microelectrodes and SPLB.

Unilamellar giant vesicles[13] of DPPC+POPS+Rb (89.5:10:0.5) were prepared as follows; a chloroform solution of a lipid mixture (10 mg/ml) was dried under N₂ flow using a rotary evaporator for about 30 min and subsequently vacuum-dried for 10 h to clearly remove the solvent; then a buffer solution (10 mM KCl) was added to the obtained lipid thin film and gently agitated.

The lipid concentration of the obtained suspension was 0.1 mg/ml. All the processes were carried out at room temperature (RT). Then, after incubation at 48°C for 10 h, dialysis was carried out for the suspension of giant vesicles by using a 5 μm filter for 1 h in the buffer solution (10 mM KCl, pH = 6.6) at RT. For the deposition of lipid bilayer membranes, the substrate was incubated for 1 h at 50°C under a buffer solution formed by mixing 200 μl of the vesicle suspension and 50 μl of CaCl_2 50 mM solution. Then the sample was washed five times at RT with the buffer solution [Fig. 4.1(l)]. Atomic force microscope (AFM) observations were performed using a SPI3800 scanning probe microscopy system (Seiko Instrument Inc.) in the dynamic-force mode (tapping mode) using a Si cantilever. The spring constant of the cantilever for measuring the surface roughness of the substrate in air was 43 N/m, and 1.5 N/m for the *in situ* characterization of the lipid bilayer.

4.3 Results and Discussion

Figure 4.2(a) shows the AFM topography of the substrate surface around the electrode wells made by the process shown in Fig. 4.1. The cross-sectional profile in line with X-Y is also shown in Fig. 4.2(b). These data show the surface around the electrode well is very flat ($R_a \sim 0.8$ nm). To obtain such a flat surface, it was important to control the irradiation power of the femtosecond laser such that only the Co film is removed while causing negligible damage to the SiO_2 layer beneath. If the SiO_2 layer is also sputtered by the laser, particles (composition is unknown) of 100 ~ 200 nm diameter, which are difficult to remove using the usual etching

solutions such as HF, HCl, H₂SO₄, and HNO₃, were deposited around the wells. The electric characteristics were determined using a patch clamp amplifier (CEZ-2400, Nihon-Koden Japan) through the AgCl/Ag electrode in conjunction with the eCell (Ver 2.12) software. Line (a) in Fig. 4.3 shows the current-voltage characteristics of the substrate under the buffer solution before vesicle fusion. From this data, the series resistance R_s in the equivalent circuit shown in Fig. 4.3(c) is given to be $10 \pm 3 \text{ M}\Omega$.

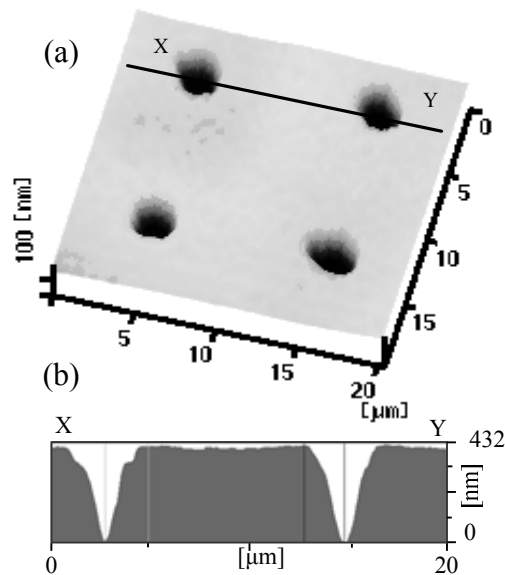


Figure 4.2: (a) Surface morphology measured by AFM around electrode holes of substrate after AgCl electroplating (step k in Fig. 4.1) and, (b) cross-sectional profile.

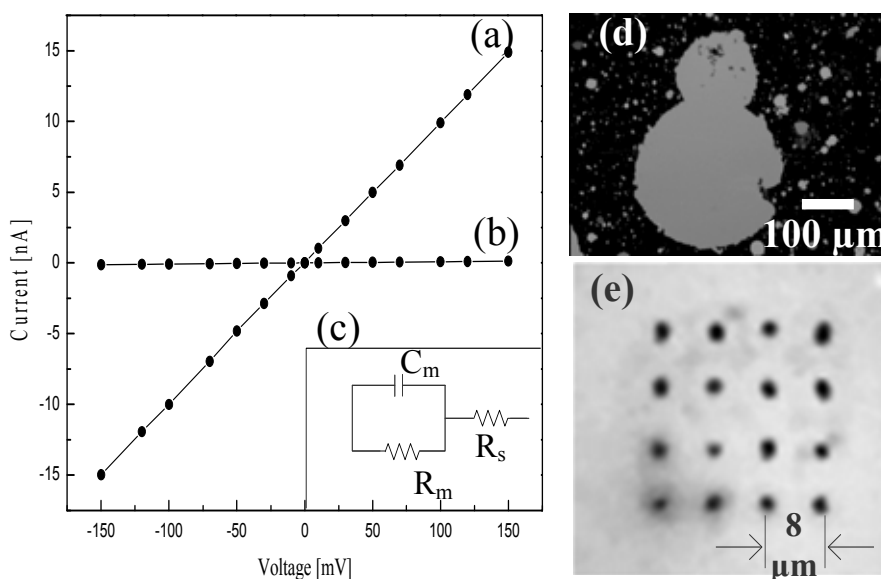


Figure 4.3: Current–voltage characteristics of substrate obtained under KCl solution (10 mM), (a) before (\square) and (b) after (\bullet) SPLB formation, and (c) equivalent circuit of system. Fluorescence microscopy image of lipid bilayer formed by rupture of giant vesicle on (d) $\text{SiO}_2/\text{CoSi}_2/\text{Si}$ surface and (e) electrode area.

Mixing of negatively charged lipid POPS with neutral lipid DPPC was essentially effective in forming unilamellar giant vesicles without aggregation. Addition of Ca^{+2} was also necessary to induce the rupture of vesicles on the SiO_2 surface.[14] Figure 4.3(d) shows a fluorescence microscopy image of a single SPLB formed on the $\text{SiO}_2/\text{Si}(100)$ surface by the rupture of the giant vesicles. The diameter of the bilayer was typically about 200 ~ 300 μm , large enough to cover the electrode area (10 ~ 30 μm diameter). Figure 4.4 shows an *in situ* AFM image under the buffer

solution (10 mM KCl) and the cross-sectional profile of a bilayer formed using the same protocol for giant vesicle fusion as in the case of Fig. 4.3(d). The observed thickness of the bilayer, 4.5 nm [Fig. 4.4(b)], corresponds to the height of the single bilayer.[4]

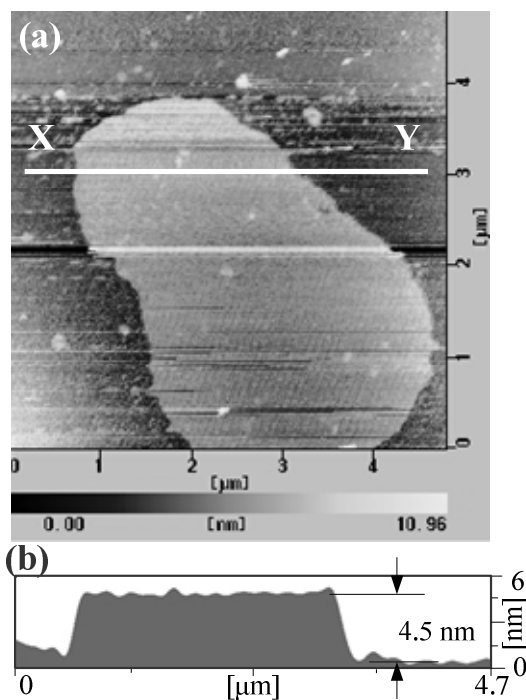


Figure 4.4: (a) AFM image of lipid bilayer formed by rapture of giant vesicle on SiO₂/Si surface, measured in tapping mode. (b) The cross-sectional profile along line X-Y is given, where the lipid bilayer height is 4.5 nm.

The lipid bilayer covering the electrode well was formed by giant vesicle fusion. A fluorescence microscopy image [Fig. 4.3(e)] after lipid bilayer formation on the microelectrode area clearly shows the existence of the homogeneous lipid thin film. Since the bilayer was formed using the same protocol as that used in the formation of the single bilayer patches shown in Figs. 4.3(d)

and 4, it is considered from the fluorescence microscope image that the single bilayer was formed on the microelectrode area. From the current-voltage characteristics of the system measured after the lipid bilayer formation (shown as line b in Fig. 4.3), the resistance of the lipid bilayer [R_m in Fig. 4.3(c)] was estimated to be 1.2 G Ω . The capacitance [C_m in Fig. 4.3(c)] of the bilayer measured using a patch clamp amplifier was 10.7 pF. These values were observed with extremely good reproducibility during my experiments for more than 5 h. From the fact that the resistance almost completely returns to the original value of 10 M Ω when the bilayer is broken by adding 5 μ l of gramicidin solution (3×10^{-6} mg/ml), the observed high resistance after the bilayer formation is considered to be not due to small vesicles clogging the electrode hole. Dark spots at the electrode holes in Fig. 4.3(e) are not due to the nonexistence of the bilayer on the well. At the region of 600-nm-thick SiO₂, the fluorescence microscopy image is very bright due to the fluorescence interference-contrast effect.[15] On the other hand, the electrode hole area, in which there is no back surface reflection, is relatively very dark.

Since the observed capacitance 10.7 pF agrees well with the calculated capacitance 10 pF due to the SiO₂ thin film (600 nm in thickness and 0.5 mm in diameter, determined using the upper electrode, were assumed), the capacitance due to the lipid bilayer formed on the well is considered to agree almost fully with the value estimated from the specific capacitance of the single bilayer, 0.8 μ F.[5,6] From these considerations, it is concluded that the gigaohm seal produced by the single

bilayer was formed on the microelectrode area.

The authors thank Nippon Fine Chemical Co., Ltd., for donating the DPPC sample. This research was supported by a Grant-in-Aid for Scientific Research from the Ministry of Education, Culture, Sports, Science and Technology (13GS0016).

Reference

1. H. M. McConnell, L. K. Tamm and R. M. Weis: Proc. Natl. Acad. Sci. USA **81** (1984) 3249.
2. H. M. McConnell, T. H. Watts, R. M. Weis and A. A. Brian: Biochim. Biophys. Acta **864** (1986) 95.
3. T. M. Bayerl and M. Bloom: Biophys. J. **58** (1990) 357.
4. Z. V. Leonenko, A. Carnini and D. T. Cramb: Biochim. Biophys. Acta **1509** (2000) 131.
5. S. Terrettaz, M. Mayer and H. Vogel: Langmuir **19** (2003) 5567.
6. B. A. Cornell, V. L. B. BraachMaksvytis, L. G. King, P. D. J. Osman, B. Raguse, L. Wiczorek and R. J. Pace: Nature **387** (1997) 580.
7. Y. Cheng, S. D. Ogier, R. J. Bushby and S. D. Evans: Mol. Biotechnol. **74** (2000) 159.
8. W. Romer and C. Steinem: Biophys. J. **86** (2004) 955.
9. H. Bayley and P. S. Cremer: Nature **413** (2001) 226.
10. Y. Li, K. Itoh, W. Watanabe, K. Yamada, D. Kuroda, J. Nishii and Y. Y. Jiang: Opt. Lett. **26** (2001) 1912.
11. T. Urisu, H. Kyuragi, Y. Utsumi, J. Takahashi and M. Kitamura: Rev. Sci. Instrum. **60** (1989) 2157.
12. M. M. Rahman, R. Tero and T. Urisu: Jpn. J. Appl. Phys. **43** (2004) 3941.
13. K. Akashi, H. Miyata, H. Itoh and K. Kinoshita: Biophys. J. **74** (1998) 2973.
14. J. Wilschut, N. Duzgunes and D. Papahadjopoulos: Biochemistry **20** (1981) 3126.
A. Lambacher and P. Fromherz: Appl. Phys. A **63** (1996) 207.

Chapter 5

5 Formation of supported planer lipid bilayer by vesicle fusion on patterned octadecyltrichlorosilane self-assembled monolayer for reducing the edge leak current

e-Journal of Surface Science and Nanotechnology (in press).

Abstract

In this work, a technique for the patterning of octadecyltrichlorosilane self assembled monolayer (OTS-SAM) has been developed. First, OTS-SAM was deposited on SiO₂/Si substrates. A negative resist pattern on the OTS-SAM layer was fabricated by photolithography technique. Then, the OTS-SAM in the open area was removed by an ultraviolet light ashing process. Finally, the negative resist was removed by a resist remover. A supported planer lipid bilayer (SPLB) was successfully formed on the patterned OTS-SAM by rupturing giant vesicles. Fluorescence microscopy image shows that the OTS-SAM plays an important role as an anchor for the formation of SPLB. The SPLB is formed as a bilayer on hydrophilic SiO₂ surfaces. Whereas, a lipid monolayer is formed on hydrophobic OTS-SAM surfaces. This anchor can be used as a guard ring to prevent leak currents from the SPLB edge.

5.1 Introduction

A supported planar lipid bilayer (SPLB) is a lipid bilayer supported on solid surfaces. SPLBs have been studied as an active medium for biosensors and as systems for mimicking plasma membranes. This is due to the fact that membrane proteins can be deposited together with a SPLB on solid surfaces, retaining the biological functions of the protein as well as controlling their respective orientations.[1-3] SPLBs on silicon based microelectrodes are extremely attractive, since small pores can be easily made on it. Thus they have the potential of high stability, high sensitivity and high integration density. It is considered that a major challenge in the fabrication of an ideal (sufficiently high resistance) supported membranes is the production of tightly sealed bilayers to reduce the leakage current to the level found in suspended membranes. For this purpose, the reduction of substrate roughness and the elimination of the edge leak current are required.

In a recent report[4], I have described a technique for the fabrication of well-structures of 1 μm diameter for microelectrodes on the surface of SiO_2/Si substrates, maintaining the surface roughness to less than 1 nm, and to deposit the SPLB membrane on the surface of a microelectrode area by rupturing the giant unilamellar vesicles. The measured electrical resistance was 1.2 $\text{G}\Omega$. Although the resistance value fulfills the condition required for the measurement of single channel measurements, even then it is much smaller than those ($> 30 \text{ G}\Omega$) realized in the planer or suspended membranes. This may be due to the edge leak current. Therefore, by

depressing the edge leak current, much higher resistance of lipid bilayer is expected to be obtained.

The octadecyltrichlorosilane self assembled monolayer (OTS-SAM) is a densely packed, highly organized monolayer film, covalently bound to the substrate. [5, 6] The reaction of OTS with SiO₂ to form SAM was first investigated by Sagiv [7] and extensively studied by many other groups. [8-10] The reaction mechanism is understood as the hydration of alkylchlorosilane to form alkylsilanol followed by dehydration, i.e., the removal of water from alkylsilanol and surface hydroxyl groups.[8] Another advantage of OTS-SAM is their high stability in air. It has been reported that the monolayer coverage does not degrade even its 18 months exposure in air.[5]

There are several common technologies used to pattern thin films on silicon, such as, microcontact printing, ink jet printing, and electron beam lithography.[11] However, there are several limitations for each of these techniques. In the case of microcontact printing, a pin damage can lead to differences in spot diameter and thickness. It uses a polydimethyl siloxane (PDMS) elastomeric stamp, whose has some limitations such as elastomer shrinkage after curing, swelling in some solvents, and an inherent elasticity that makes difficult to pattern over large areas. In the case of ink jet printing, it is difficult to achieve high resolution (below 5 μm). In electron beam lithography, OTS-SAMs might be damaged when their surface is struck with the beam and it requires a significant amount of time to pattern micron scale features over a whole wafer. Since photolithography process has no effect on OTS-SAM like the above techniques, I considered to

use it for the patterning of OTS-SAM. In the present work, I have developed a patterning method of OTS-SAM by photo-lithography and ultraviolet light (UV) ashing.

Many researchers have reported the formation of OTS-SAM on thermally grown SiO₂, but in most cases of device making process they faced difficulties in making the thermally grown SiO₂, because of some interlayers which are sensitive to high temperature. Sputtered SiO₂ is one way to solve this problem. The surface roughness of the sputtered SiO₂ is close to that of thermally oxidized SiO₂. In my technique, OTS-SAM was deposited on sputtered SiO₂. OTS-SAM patterns were successfully made by using a negative resist and UV ashing. Finally SPLB was formed on this patterned OTS-SAM area and it was found that a bilayer is formed on the bare SiO₂ area and a monolayer on the OTS-SAM area. I considered that the hydrophobic SAM around SPLB works as a “guard ring” to prevent the edge leak current of SPLB. The concept is shown in Fig. 5.1.

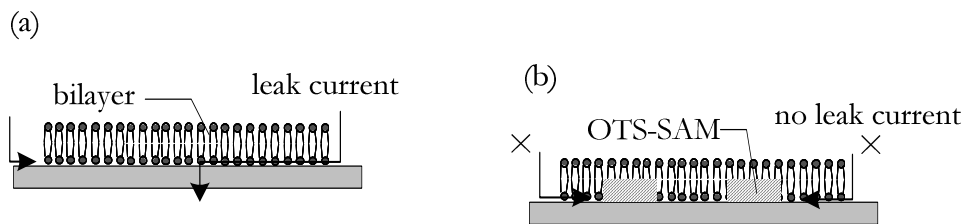


Figure 5.1: Schematic drawing of the patterned SAM to prevent the leak current of the lipid bilayer. (a) lipid bilayer on substrate without any anchor (b) lipid bilayer on patterned OTS-SAM which protects the leak current.

5.2 Experiment

5.2.1 Deposition and patterning of OTS-SAM

Figure 5.2 shows the schematic drawing of the OTS-SAM patterning process. A mirror polished Si (100) wafer covered with the native oxide was first sonicated in acetone, ethanol and Milli-Q water ($>18\text{ M}\Omega\text{cm}$; Millipore Co., Ltd) for 5 min each. Subsequently the substrate was boiled in a solution of concentrated H_2SO_4 and H_2O_2 (30%) (7:3 in volume ratio) at 120°C for 5 min to remove the organic contaminations and then immersed in a HF solution (2.5%) for 2 min to remove the surface oxide layer. After this cleaning, the SiO_2 film of 120 nm thickness was deposited on the Si(100) surface by sputtering (SMH -2304 RE, Ulvac) [Fig. 5.2(a)]. The sample was then exposed to UV light (UVL20US-60, Sen Lights) for 10 min. The distance between the sample and the lamp was 3 cm. Atomic force microscope (AFM) images show that the SiO_2/Si surface is very flat and the value of average surface roughness, $R_a = 0.22\text{ nm}$.

The OTS-SAM was deposited by immersing the $\text{SiO}_2/\text{Si}(100)$ substrate in a 10 mM solution of OTS (Sigma-Aldrich Co., Ltd) in water-saturated toluene (Sigma-Aldrich Co., Ltd) for 5 sec at room temperature (RT) [Fig. 5.2(b)]. The OTS/ SiO_2 sample was sonicated in toluene, acetone, ethanol, and pure water in order to remove the excess OTS molecules from the OTS/ SiO_2 surface. The sample treatment and the OTS deposition were done by the methods reported in my earlier work [12].

Patterned negative resist was deposited on the OTS/SiO₂ surface by photolithography [Fig. 5.2(c)]. A 50 μm line and space pattern was used as the photomask. The sample was then exposed to UV light in air for 30 min, in order to remove the OTS-SAM from the open area, where the distance between the sample and the lamp was 3 cm [Fig. 5.2(d)]. Finally, the photo-resist was removed by a negative resist remover (NS, Tokyo Ohka Kogyo) [Fig. 5.2(e)] followed by rinsing with distilled water and dried by N₂ flow. It is important to mention here that there are two kinds of resists for photolithography: positive resists and negative resists. Since the OTS-SAM surface is hydrophobic, positive resists are not suitable for coating on OTS-SAM layer. Negative resist is the stickiest and results in a very hard coating on OTS-SAM. So, the negative resist has been chosen for lithography on hydrophobic OTS-SAM.

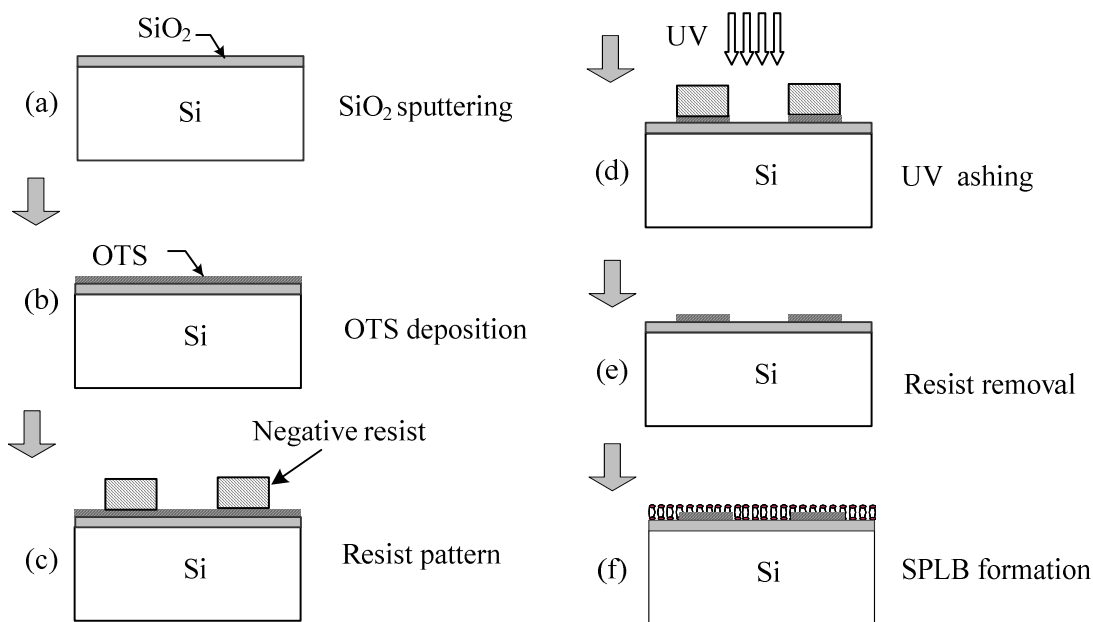


Figure 5.2: Schematic drawing of patterning process for the OTS-SAM on SiO₂

5.2.2 Preparation of giant vesicles and formation of SPLB

Lipid bilayers were deposited by the rupture of giant unilamellar vesicle [Fig. 5.2(f)]. 1-Palmitoyl-2-oleoyl-sn-3-[phosphor-L-Serin] (POPS), and fluorescence-labeled lipid (Diacyl phosphoethanolamine-N-lissamine Rhodamine B Sulfonyl, Rb) were purchased from Avanti Polar Lipid. Dipalmitoylphosphatidylcholine (DPPC) was provided by Nippon Fine Chemical. Unilamellar giant vesicles[13] of DPPC+POPS+Rb (89.5:10:0.5) were prepared as follows; a chloroform solution of a lipid mixture (10 mg/ml) was dried under N₂ flow by a rotary evaporator

for about 30 min and subsequently vacuum-dried for 10 h to remove the solvent completely. A 10 mM KCl solution was added to the obtained lipid thin film and gently agitated. The lipid concentration of the obtained suspension was 0.1 mg/ml. All the processes were carried out at room temperature (RT). Then, after incubation at 48°C for 10 h, dialysis was carried out for the suspension of giant vesicles by using a 5 μ m filter (JM Type, Millipore) for 1 h in the 10 mM KCl solution at RT. For the deposition of lipid bilayer membranes, 200 μ l of the vesicle suspension and 50 μ l of CaCl₂ 50 mM solution were mixed and the substrate was incubated in the mixed solution for 1 h at 50°C. Then the sample was washed five times at RT with the buffer solution. Mixing of negatively charged lipid POPS with neutral lipid DPPC was essentially effective in forming unilamellar giant vesicles without aggregation. Addition of Ca⁺² was necessary to induce the rupture of giant vesicles on the SiO₂ surface although the mechanism is not clear.

The surface structure of the sample was investigated using a contact mode AFM (PicoScan2500, Molecular Imaging Inc) and a dynamic-force mode (tapping mode) AFM (SPI-3800N, Seiko Instruments Inc.). The IR spectra were measured by a FT-IR spectrometer (FT/IR 620, JASCO) in the transmission mode under vacuum using a tri-glycine-sulfate detector (TGS) at 4 cm⁻¹ resolution for 300 scans. Si (100) wafers with high resistivity (40 \pm 1 Ω cm), which is sufficiently transparent for IR, were used for the measurement of IR transmission spectrum.

5.3 Results and discussion

5.3.1 Patterning of OTS-SAM

To characterize the molecular structure and chemical composition of the developed OTS-SAM on the SiO₂ surface [Fig. 5.2(b)], AFM, water contact angle (WCA) measurement, and IR spectroscopy have been used. Figure 5.3(a) shows the AFM image of OTS-SAM grown on SiO₂ surface. The measured height of OTS-SAM islands was about 2.3 nm, which is in agreement with the reported value.[14] The WCA with the substrate surface was found to be 5° and 98°, before and after the OTS-SAM formation, respectively. This confirms that after the OTS-SAM formation the surface become hydrophobic.

The UV/ozone cleaning procedure is an effective method of removing a variety of contaminants from surfaces. The low pressure mercury discharge tubes generate two wavelengths of interest, 184.5 and 253.7 nm.[15] The 184.5 nm wavelength is considered to be important, because it is absorbed by oxygen, and thus leads to the generation of ozone. The 253.7 nm radiation is not absorbed by oxygen. Therefore, it does not have any contribution to ozone generation. However, it is absorbed by most hydrocarbons and also by ozone. In this study, it is found that the OTS-SAM is completely removed by the application of UV light from 3 cm distance for 30 min. Figure 5.3(b) shows the AFM image of substrate after removal of OTS-SAM by UV light. In AFM image no OTS island was found on the SiO₂ surface. The observed value of surface

roughness, $R_a=0.25$ nm, is very much close to that of substrate before the OTS-SAM formation ($R_a=0.22$ nm). After the removal of the OTS-SAM by UV ashing, the WCA becomes 5° , which indicates that the surface became hydrophilic. This confirms that the complete removal of OTS-SAM from the SiO_2 surface by UV ashing.

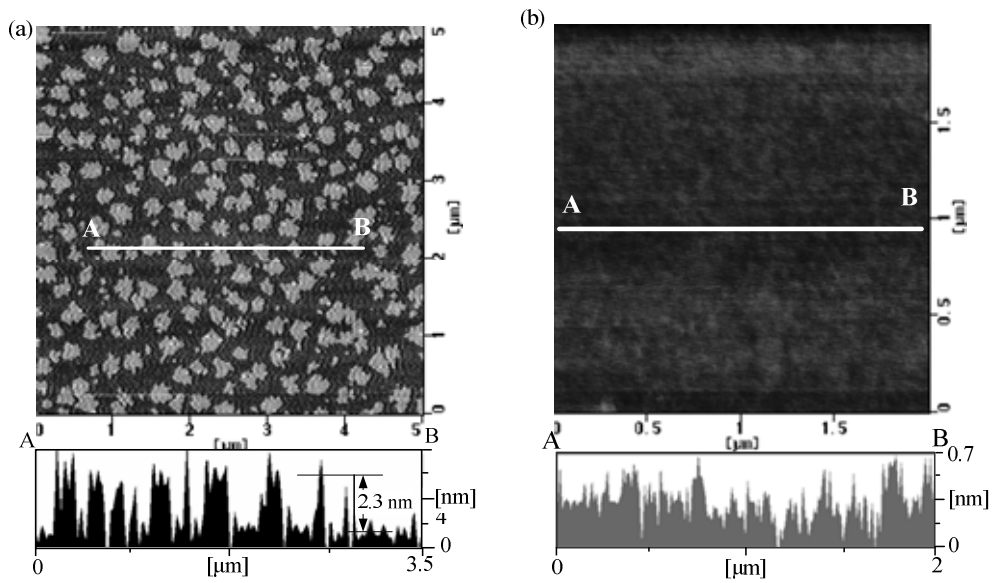


Figure 5.3: (a) AFM image after the OTS-SAM islands formation on SiO_2/Si (b) AFM image after removal of OTS-SAM from SiO_2

Figure 5.4 shows the infrared transmission spectrum in the region of CH stretching vibrations measured for the OTS-SAM deposited on SiO_2/Si surface. The spectrum shown is given by $-\log(I/I_0)$, where I_0 and I are the observed single-beam IR transmission spectra before and after the UV ashing. The peaks at 2850 cm^{-1} and 2917 cm^{-1} are assigned to the symmetric (V_s - CH_2) and asymmetric (V_a - CH_2) stretching vibrations of the methylene ($-\text{CH}_2$) groups, respectively.

These are close to the values measured for alkane crystals and far below the positions for liquid alkanes, which are at 2856 and 2928 cm^{-1} , respectively. [16, 17] This confirms that a closely packed SAM is formed on the sputtered SiO_2 .

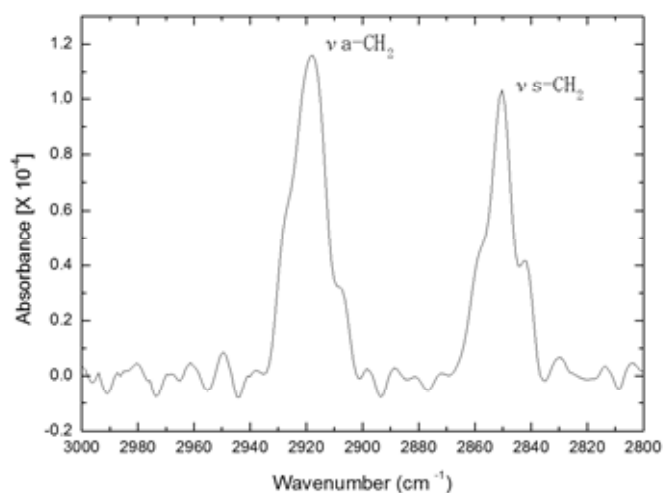


Figure 5.4: An infrared spectrum of the OTS-SAM deposited on the SiO_2 surface. The observed peaks at 2850 cm^{-1} and 2917 cm^{-1} were assigned to the symmetric and asymmetric stretching vibrations of the methylene ($-\text{CH}_2$) groups.

Figure 5.5(a) shows the AFM image of the patterned OTS-SAM on the SiO_2 surface. A line and space with 50 μm width was successfully patterned. Figure 5.5(b) shows the boundary region of OTS-SAM and bare SiO_2 . The cross sectional profile in line A and B is given in Fig. 5.5(b), where line A represents the OTS-SAM removed area and line B represents the OTS-SAM area. The value of surface roughness of the OTS-SAM removed area [line A in Fig. 5.5(b)] is $R_a=0.9$ nm and average height of OTS-SAM in covered area [line B in Fig. 5.5(b)] is 2.2 nm. This confirms that

OTS-SAM patterning is successfully achieved by this method. In the UV ashing process, ozone decomposes the OTS-SAM in the resist free area whereas the area covered with resist is not affected. After the removal of the negative resist unchanged OTS-SAM area was found.

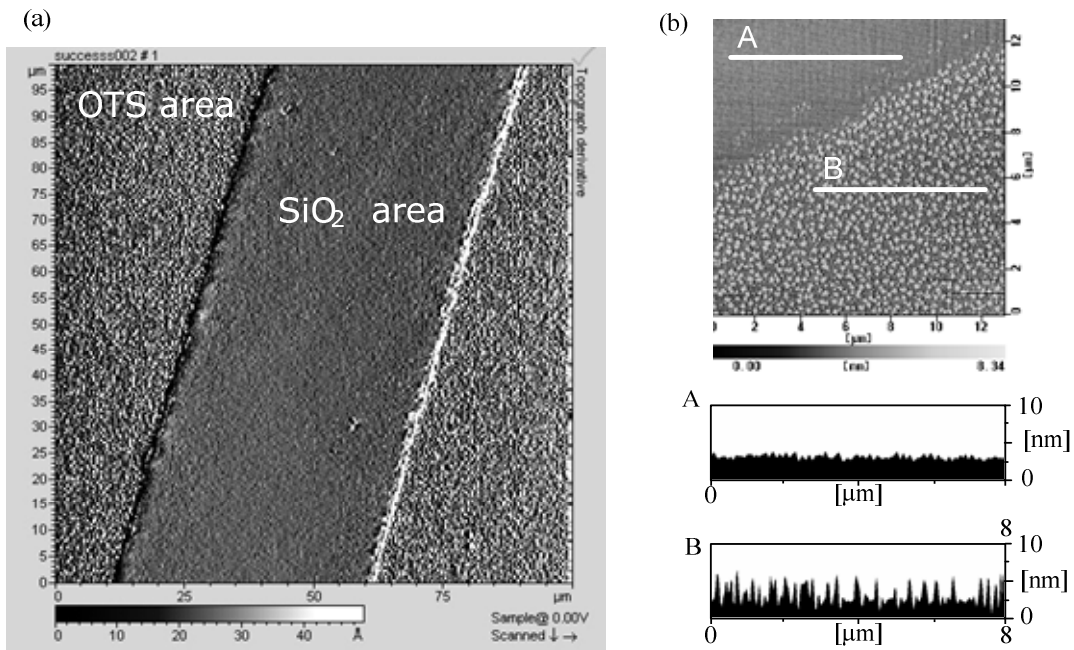


Figure 5.5: (a) AFM image after the patterning of OTS-SAM on SiO₂/Si, and (b) $\times 8$ magnification of (a).

5.3.2 Formation of lipid bilayers on patterned OTS/SiO₂ surface

Lipid bilayers were deposited on the patterned OTS-SAM area by rupturing the giant unilamellar vesicles. The vesicle fusion method is a feasible and prevalent technique for the formation of supported membrane on solid surfaces.[2] When substrates is immersed in an aqueous solution of lipid vesicles, the vesicles adhere to the surface, break up, and spread to form a bilayer on hydrophilic surfaces and a monolayer on hydrophobic surfaces.[18] Figure 5.6(a) shows the fluorescence microscopy image of the OTS-SAM patterned SiO₂ surface after immersing in the giant vesicle suspension. Figure 5.6(b) shows the intensity distribution on the A-B line in Fig. 5.6(a). An earlier study showed that after the vesicle fusion, a bilayer forms on hydrophilic SiO₂ surfaces and a monolayer forms on OTS-SAM hydrophobic surfaces.[18] In the present case, the single bilayer is formed on the hydrophobic OTS-SAM area and bilayer formed on hydrophilic SiO₂ area, so the light intensity of Rb is different in their respective areas, region (i) and region (ii). In the (iii) region, neither a bilayer nor a single layer formed on the SiO₂ surface and the light intensity of Rb is almost zero.

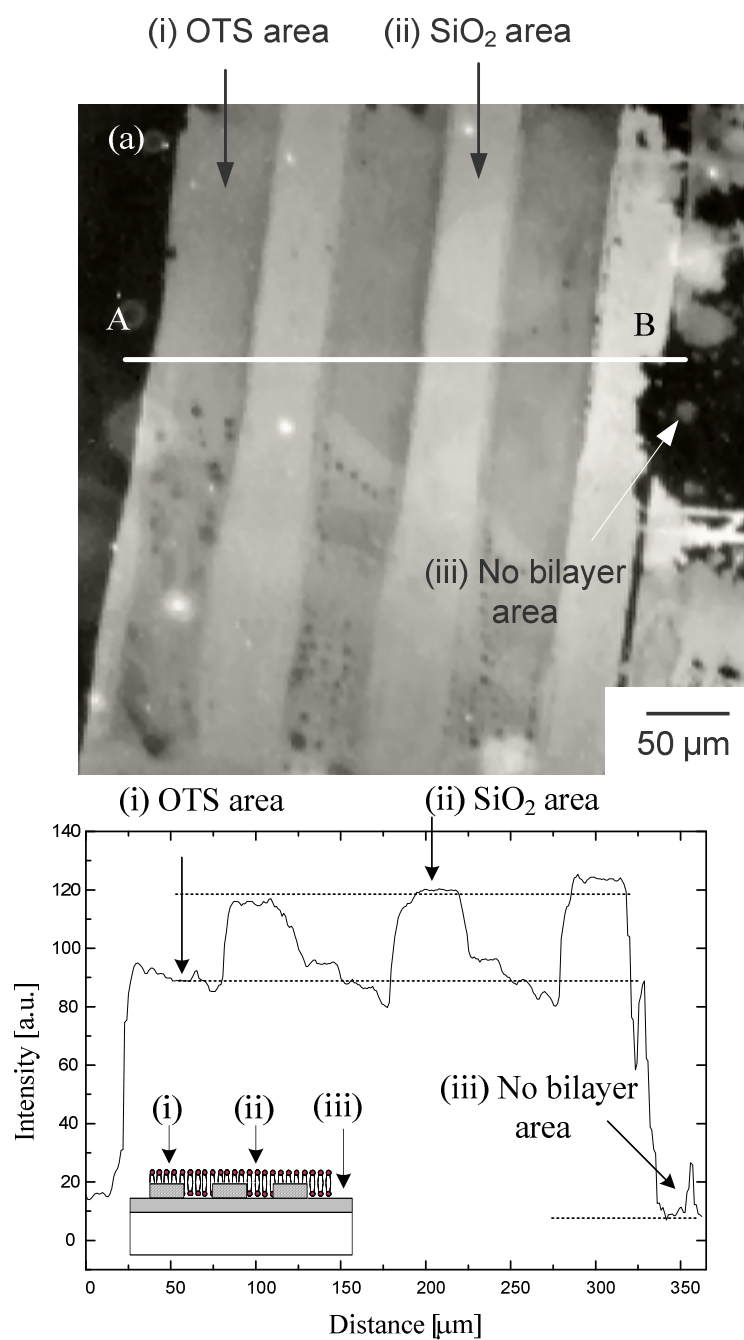


Figure 5.6: (a) Fluorescence microscope image of SPLB, and (b) intensity distribution on the A-B line in (a).

The fluorescence image confirms that the bilayer and the monolayer are successfully deposited on bare SiO₂ and on OTS/SiO₂ region, respectively. A substantial body of evidence

suggests that a thin layer of water approximately 1~2 nm thick is trapped between the support and the headgroups of the lower leaflet of the bilayer.[19] This water layer might cause the edge leak current through the SPLB. Since water does not exist at the interface between the OTS-SAM surface and the lipid monolayer (i region in Fig. 5.6) due to the hydrophobic interaction of both surfaces, this patterned OTS-SAM can be used as a guard-ring to reduce the leak current from the SPLB edge as illustrate in Fig. 5.1.

5.4 Conclusion

A new method has been developed for patterning of OTS-SAM on SiO₂ surfaces using lithography combined with UV ashing. SPLBs were deposited on these patterned OTS-SAM/SiO₂ surfaces by rupturing the giant unilamellar vesicles. The fluorescence microscopy image shows that a single bilayer formed on the bare SiO₂ regions and a monolayer formed on OTS-SAM area. This technique has been considered to use for the formation of tightly sealed bilayers to reduce leakage current of the SPLB.

Reference

1. E. Sackmann, *Science*, **271** (1996) 43-48.
2. H.M. McConnell, T.H. Watts, R.M. Weis, and A.A. Brian, *Biochimica Et Biophysica Acta*, **864** (1986) 95-106.
3. L.K. Tamm and H.M. McConnell, *Biophysical Journal*, **47** (1985) 105-113.
4. M.M. Rahman, Y. Nonogaki, R. Tero, Y.-H. Kim, H. Uno, Z.-L. Zhang, T. Yano, M. Aoyama, R. Sasaki, H. Nagai, M. Yoshida, and T. Urisu, *Japanese Journal of Applied Physics* (in press),
5. S.R. Wasserman, Y.T. Tao, and G.M. Whitesides, *Langmuir*, **5** (1989) 1074-1087.
6. D.L. Angst and G.W. Simmons, *Langmuir*, **7** (1991) 2236-2242.
7. J. Sagiv, *Journal of the American Chemical Society*, **102:1** (1980) 92-98.
8. T. Komeda, K. Namba, and Y. Nishioka, *Journal of Vacuum Science & Technology a- Vacuum Surfaces and Films*, **16** (1998) 1680-1685.
9. T.A. Witten and L.M. Sander, *Phys Rev Lett*, **47** (1981) 1400-1403.
10. R. Wang, A.N. Parikh, J.D. Beers, A.P. Shreve, and B. Swanson, *J Phys Chem B*, **103** (1999) 10149-10157.
11. R.N. Orth, J. Kameoka, W.R. Zipfel, B. Ilic, W.W. Webb, T.G. Clark, and H.G. Craighead, *Biophysical Journal*, **85** (2003) 3066-3073.
12. M. Takizawa, Y.-H. Kim, and T. Urisu, *Chemical Physics Letters*, **385** (2004) 220-224.
13. K. Akashi, H. Miyata, H. Itoh, and K. Kinoshita, *Biophysical Journal*, **74** (1998) 2973-2982.
14. C. Yuan and L.J. Johnston, *Journal of Microscopy*, **205** (2002) 136-146.
15. J.R. Vig, *J. Vac. Sci. Technol*, **A 3 (3)** (1985) 1027.
16. R. Snyder, H. Strauss, and C. Elliger, *J. Phys. Chem*, 5145.
17. A.N. Parikh, D.L. AUara, I.B. Azouz, and F. Rondelez, *J. Phys. Chem.*, **98** (1994) 7577-7590.
18. R. Tero, M. Takizawa, Y.J. Li, M. Yamazaki, and T. Urisu, *Applied Surface Science*, **238** (2004) 218-222.
19. T.M. Bayerl and M. Bloom, *Biophysical Journal*, **58** (1990) 357-362.

Chapter 6

6 Summery

In my thesis, I have developed several elementary processes to realize an ideal supported planar lipid bilayer (SPLB) with $G\Omega$ resistance on Si-based microelectrodes. Si substrates have the advantage of nano-level high controllability with the surface micro-fabrications, and provide also an easy combination with conventional Si electrical circuit devices towards a high potential for the development of new application devices.

I have developed a technique to fabricate a hole (well) with a diameter of about $1\ \mu\text{m}$ for microelectrodes on a SiO_2/Si substrate. A circular pattern was made on a Co thin film on SiO_2/Si by using femtosecond laser ablation, and the hole was made onto the SiO_2/Si surface by synchrotron radiation etching using this Co pattern as a photomask. Emphasis was put on making a very flat substrate surface, which is necessary to form a defect free membrane. This process enabled the fabrication of the electrode hole while conserving the original nano-level flatness ($R_a \sim 0.8\ \text{nm}$) of the substrate.

A single planar lipid bilayer was deposited on these microelectrodes by the rupture of giant unilamellar vesicles. Fluorescence microscopy images showed that the diameter of the SPLB formed on the $\text{SiO}_2/\text{Si}(100)$ surface by the rupture of the giant vesicles was typically about $150 \sim 300\ \mu\text{m}$, large enough to cover the electrode area ($10\ \mu\text{m} \sim 30\ \mu\text{m}$ diameter). AFM images of the bilayer showed that the thickness of the SPLB membrane was $4.5\ \text{nm}$, corresponding to the height of a single bilayer. The electric characteristics were measured by a patch clamp amplifier through AgCl/Ag electrodes. The resistances before and after the lipid bilayer formation were $10 \pm 3\ \text{M}\Omega$ and $1.2\ \text{G}\Omega$, respectively. This confirmed the $G\Omega$ seal formation of SPLB on the microelectrodes

and this high resistivity (1.2 G Ω) is necessary for the single channel recordings. The measured capacitance (10.7 pF), however, showed the existence of the edge leak current which effectively enlarge the electrode area. Depressing the edge leak current may be necessary to get much higher resistance and smaller capacitance of the SPLB on the microelectrode.

In the SR etching of SOG, I have investigated the shrinking phenomenon of SOG films. The SOG film was etched by the direct SR irradiation under the SF₆ + O₂ etching gas, similarly to the case of thermally oxidized SiO₂. I have found that the indirect exposure to SR caused shrinkage of SOG under a Co mask. The shrinkage phenomenon is a photoinduced process caused by SR permeating through the Co mask due to the high-energy photons rather than a thermal process, because the SOG has been pre-annealed at 425°C before the irradiation of SR. The shrinkage of SOG was attenuated by increasing the thickness of the Co mask, but not completely eliminated even by a Co mask of 350 nm thick, due to the high-energy photons (>230 eV) being transmitted through the mask. A 550 nm thick SOG film shrinks by 152 nm under the Co mask (230 nm thick) after exposure to 2.0×10^4 mAmin of SR. Without the Co mask, the etching depth of SOG increased with the SR dose and the SOG film was completely etched by an expose of 1.8×10^4 mAmin. For two different samples, which were cured at 200°C and 425°C in the SOG preparation process, it has been found that the pre-curing temperature does not affect the shrinkage. Atomic force microscopy observations showed that the surfaces were very smooth (surface roughness, Ra=0.4 ~ 0.75 nm) both on the completely etched Si area and on the shrunken SOG area.

To investigate the mechanism of the shrinkage effect, I measured the Fourier-transform infrared absorption spectra of SOG samples before and after the SR. The 1125 cm⁻¹ and 1009 cm⁻¹ peaks are assigned to the Si-O stretching vibrations of SiO_x, the frequency of which is known to shift from 1075 cm⁻¹ to 940 cm⁻¹ as x decreases from 2 to 1. Here, the 1009 cm⁻¹ peak is positive which means that SiO₂ reconstructed to denser SiO₂, similarly to thermally oxidized SiO₂. The IR

spectrum reveals that transmitting SR through the Co mask causes the reconstruction of SiO₂ along with the desorption of the organic compounds. Utilizing this phenomenon, I have successfully fabricated a 3D SOG structure by a one-time SR exposure.

To reduce the leak current through the SPLB, I have developed a OTS-SAM patterning technique which will work as a guard-ring around the SPLB. First, a negative resist pattern was fabricated on OTS-SAM layer by photolithography technique; then, OTS-SAM of the open area was removed by UV ashing process; and finally the negative resist was removed by a resist remover. A SPLB was successfully formed on the patterned OTS-SAM employing a giant vesicle deposition technique. Fluorescence image shows that the OTS-SAM can work as an anchor for the formation of the SPLB. The SPLB forms bilayers on hydrophilic SiO₂ surfaces and a monolayer on OTS-SAM hydrophobic surfaces. This confirms the work of previous authors. This anchor will work as a guard ring and prevent the leak current from the SPLB.

In my thesis works, I have achieved to make a giga ohm seal (1.2 Giga Ohm) on a patterned Si-based microelectrode by the rupture of giant unilamellar vesicles, which is higher than any previously reported resistance achieved with tethered lipid bilayer. I hope this thesis becomes meaningful step for the progress of ion channel biosensor in the future.

Chapter 7

7 List of publications

- **M. M. Rahman**, Y. Nonogaki, R. Tero, Y. H. Kim, H. Uno, Z. L. Zhang, T. Yano, M. Aoyama, R. Sasaki, H. Nagai, M. Yoshida, T. Urisu, "*Giant Vesicle Fusion on Microelectrodes Fabricated by Femtosecond Laser Ablation Followed by Synchrotron Radiation Etching*", Japanese Journal of Applied Physics (in press).
- **M. M. Rahman**, Y. H. Kim, R. Tero, M. M. Huque, T. Urisu, "*Formation of lipid bilayer on patterned octadecyltrichlorosilane self-assembled monolayer on SiO₂ surface*", e-Journal of Surface Science and Nanotechnology (in press).
- Y. H. Kim, **M. M. Rahman**, Z. L. Zhang, R. Tero, T. Urisu, "*Supported lipid bilayer formation by the vesicle fusion induced by the vesicle-surface electrostatic attractive interaction*", (Submitted to Chemical Physics Letters).
- **M. M. Rahman**, R. Tero, T. Urisu, "*Shrinking of Spin-on-Glass Films Induced by Synchrotron Radiation and Its Application to the Three-Dimensional Microfabrications*", Japanese Journal of Applied Physics, Vol. 43, No. 6B (2004) p.3941.

International Conference Proceedings

- **M. M. Rahman**, Y. Nonogaki, R. Tero, Y.H. Kim, H. Uno, Z. L. Zhang, T. Yano, M. Aoyama, R. Sasaki, H. Nagai, M. Yoshida, T. Urisu, "*Fabrication of well structures with electrode by synchrotron radiation etching and formation of lipid bilayer giga-ohm seals*", 52th International symposium and exhibition, American Vacuum Society AVS, 30 October – 4 November 2005, Boston, MA, **USA**. (accepted)
- **M. M. Rahman**, Y. Nonogaki, R. Tero, Y.H. Kim, H. Uno, Z. L. Zhang, T. Yano, M. Aoyama, R. Sasaki, H. Nagai, M. Yoshida, T. Urisu, "*Construction of well-structure for supported membrane biosensor by synchrotron radiation*", The International Chemical Congress of Pacific Basin Societies, 15-20 December 2005, Hawaii, **USA**. (accepted)
- R. Aoki, Y. Hadama, T. Kawanaka, N. Misawa, **M. Rahman**, R. Tero, T. Urisu, A. Takeuchi, T. Arakawa, T. Ogino, "*Immobilization of bio-materials on step- controlled sapphire substrates*", International Symposium on Surface Science and Nanotechnology, The Surface Science Society of Japan, 14 – 17 November 2005, Saitama, **Japan**. (accepted)

- **M. M. Rahman**, R. Sasaki, H. Nagai, M. Yoshida, M. Aoyama, T. Yano, H. Uno, R. Tero, Y. Nonogaki, T. Urisu, "Fabrication of electrode holes on the supported membrane biosensor substrates by femtosecond laser patterning followed by SR etching", International conference on Molecule-Based Information Transmission and Reception, Okazaki, Japan, 3-7 March 2005.
- R. Aoki, Y. Kawanaka, T. Iijima, N. Misawa, **M. Rahman**, R. Tero, T. Urisu, A. Takeuchi, T. Ogino, "Immobilization of inorganic and bio-materials on sapphire substrates", International conference on Molecule-Based Information Transmission and Reception, 3-7 March 2005, p.73.
- R. Tero, **M. M. Rahman**, Z. H. Wang, M. Sugawara, K. Nagayama, "Deposition of lipid bilayers on the silicon dioxide surfaces patterned by focused ion beam and synchrotron radiation etching", 51th International symposium and exhibition, American Vacuum Society, 14-19 November, 2004, Anaheim, CA, USA, p.75.
- **M. M. Rahman**, R. Tero, T. Urisu, "Shrinking of Spin-on-Glass Films Induced by Synchrotron Radiation and Its Application to the Three-Dimensional Microfabrications", 2003 International Microprocess and Nanotechnology Conference, 28-31 October 2003, Tokyo, Japan, p.75.
- C. Wang, **M. M. Rahman**, T. Urisu, "Synchrotron radiation stimulated etching of SiO₂ thin films with a Co contact mask for the area-selective deposition of self-assembled monolayer", 2002 International Microprocess and Nanotechnology Conference, 6-8 November 2002, Tokyo, Japan, Vol. 7P-7-65, p.240. .

Conference in Japan

- **M. M. Rahman**, R. Sasaki, H. Nagai, M. Yoshida, M. Aoyama, T. Yano, H. Uno, R. Tero, Y. Nonogaki, T. Urisu, "Fabrication of electrode holes on the supported membrane biosensor substrates by femtosecond laser patterning followed by SR etching", The 52th Spring meeting 2005, The Japan Society of Applied Physics, 29 March 2005, Saitama University, Tokyo.
- **M. M. Rahman**, H. Uno, R. Tero, Y. Nonogaki, T. Urisu, "Fabrication of substrate for supported membrane biosensor by Synchrotron Radiation process", 18th annual meeting of The Japanese Society for Synchrotron Radiation Research, Siga University, 7-9 January, 2005
- **M. M. Rahman**, T. Ryugo, N. Youichi, U. Tsuneco, "Fabrication of super-flat Si(100) substrate with buried electrode for supported membrane biosensor", The 63rd Autumn Meeting, The Japan Society of Applied Physics, Tohoku University, Japan, 24-27 September 2004.
- **M. M. Rahman**, M. Takizawa, K. Hayashi, R. Tero, T. Urisu, "Patterning of octadecyltrichlorosilane self-assembled monolayer (OTS-SAM) on sputtered SiO₂ surface", The 51th

Spring meeting 2004, The Japan Society of Applied Physics, 28-31 March 2004, Tokyo University of Technology.

- **M. M. Rahman**, C. Wang, T. Urisu, "*Synchrotron Radiation induced shrinking of SOG films and its application to the 3-D microfabrications*", The 50th Spring meeting 2003, The Japan Society of Applied Physics, Kanagawa, Japan, 27-30 March 2003, Vol. 27-p-ZL-2, p.15
- C. Wang, **M. M. Rahman**, T. Urisu, "*Synchrotron radiation stimulated etching of SiO₂ thin film at low temperatures*", The 63rd Autumn Meeting, The Japan Society of Applied Physics, Nigata University, Japan, 24-27 September 2002, Vol. 25a-W-5 P.644
- R. Tero, **M. M. Rahman**, T. Urisu, "*3-Dimensional Fine Modification on SiO₂/Si Surface by Focused Ion Beam Mask Patterning and Synchrotron Radiation Etching*", The 63rd Autumn Meeting, The Japan Society of Applied Physics, 24-27 September 2002.

Acknowledgment

All of the studies in my doctoral course were carried out under supervision of Prof. Tsuneo Urisu. I would like to express here a million of gratitude to him for the opportunity to meet this attractive theme. This thesis could not take a form without his tremendous support. He has been very patient and kind to me when I had troubles in experiments and living life.

I would like to thank Hironaga Uchida, Professor Md. Monimul Huque, Dr. Ryugo Tero and Dr. Sam More for their comments and advises on my thesis. They also taught me many skills of scientific expression for manuscript and thesis preparation.

I would like to thank all members of Urisu group, Yong-Hoon Kim, Nobuo Misawa, Zhen-long Zhang, Hidetaka Uno and Naohito Nakai for useful discussion and heartfelt encouragement. I am also grateful to past members of Urisu group, Dr. Youchi Nonogaki, Dr. Changshun Wang, Dr. Shusaku Yamamura, Dr. Morio Takizawa for teaching me the operation of apparatus within and beyond manuals. Earnest thanks go to all staff of the UVSOR facility for technical support. I would like to thank sincerely Mrs. Shimizu Atsuko, Secretary of Urisu group for helping me in several occasions to prepare important documents related to my research studies and also living in Okazaki.

I would like to thank Altamas Karim, Asif Iqbal, Mahmudul Kabir, Prano Bondhu Biswash, Golam Mustofa, Sofia Khatun, M. Saif Islam, Sarbanoo Das, Takahashi Haruo. They inspired me to learn science. At last, I fondly remember the silent contribution made by my wife and my parents. They are source of happiness, motivation and drive to achieve something worthwhile in life.